

THE UNIVERSITY OF CALGARY

EFFECT OF AGING AND OVERAGING ON FATIGUE BEHAVIOR
OF 2024-T3 AND 7075-T6 ALUMINUM ALLOYS.

by

TARSEM SINGH NIJJAR

A THESIS

SUBMITTED TO THE FACULTY OF GRADUATE STUDIES
IN PARTIAL FULFILLMENT OF THE REQUIREMENTS FOR THE
DEGREE OF MASTER OF ENGINEERING

DEPARTMENT OF MECHANICAL ENGINEERING

CALGARY, ALBERTA

DECEMBER, 1994

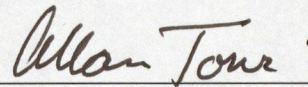
© TARSEM SINGH NIJJAR 1994

THE UNIVERSITY OF CALGARY

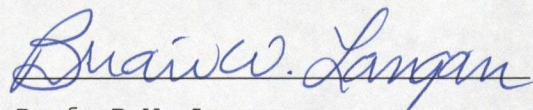
FACULTY OF GRADUATE STUDIES

The undersigned certify that they have read, and recommend to the Faculty of Graduate Studies for acceptance, a thesis entitled, "Effect of Aging And Overaging on Fatigue Behavior of 2024-T3 and 7075-T6 Aluminum Alloys", submitted by Mr. Tarsem Singh Nijjar in fulfillment of the requirements for the degree of Master of Engineering.

Dr. W.J.D. Shaw, Supervisor,
Department of Mechanical Engineering



Prof. A.A. Torvi
Department of Mechanical Engineering



Prof. B.W. Langan
Department of Civil Engineering

December 19, 1994

ABSTRACT

The object of this study was to investigate the low temperature long time aging effect of 2024-T3 and 7075-T6 on the fatigue life of the CT-114 tutor aircraft.

The alloys were artificially reaged. Mechanical properties of yield strength and ductility, material properties of hardness and electrical conductivity were measured and related to the changes in fracture toughness and microstructure as altered by the various aging conditions.

Major changes in the material and mechanical properties behavior of 7075-T6 took place at the reaging condition of 175°C for 38 hours. Similar changes in 2024-T3 alloy took place at the reaging condition of 175°C for 150 hours.

Both 2024-T3 and 7075-T6 have complex fatigue life behaviors. Initially the fatigue life of each alloy increases to peakaged conditions and thereafter decreases continuously. However, highly overaged 2024-T3 alloy provides an overall improved fatigue life. When compared to their original materials, both alloys provide better fatigue life at least up to 300 accumulated hours of operations at 175°C.

ACKNOWLEDGEMENTS

The author wishes to express his sincere gratitude to his supervisor, Dr. W.J.D. Shaw, for his very professional guidance, support, advice and encouragement throughout the program.

Thanks to Institute for Aerospace Research formally known as National Aeronautical Establishment of Ottawa for providing funds for the project, contract # 5555.31946-8-0016.

Sincere thanks to the technical staff of the Department of Mechanical Engineering for their invaluable help, especially Brent Daley for his CAD and CAM services.

Special thanks to the computer systems manager, Mr. Brad Stephens and Mr. Nick Vogt for providing help in computer graphics and drafting.

Sincere thanks to his father Captain Pritam Singh Nijjar for encouragement and support.

Finally, the author acknowledges the support and co-operation by his wife Swarnjit K. Nijjar, to Navpreet and Ramandeep K.Nijjar as a testimony of gratitude.

TABLE OF CONTENTS

	Page
Abstract	(iii)
Acknowledgements	(iv)
Table of contents	(v)
List of Tables	(xii)
List of Figures	(xiv)
Nomenclature	(xix)
CHAPTER 1	
INTRODUCTION	1
1.1 BACKGROUND	1
1.2 SCOPE OF THESIS	2
CHAPTER 2	
LITERATURE REVIEW AND BACKGROUND INFORMATION	6
2.1 FATIGUE LIFE AND MICROSTRUCTURE	6
2.1.1 GENERAL	6
2.2 FATIGUE CRACK GROWTH RATE	7
2.2.1 GENERAL	7
2.3 SECONDARY INTERMETALLIC PARTICLES	8
2.3.1 GENERAL	8
2.3.2 STRUCTURAL PROPERTIES OF INTERMETALLIC PARTICLES	9
2.4 DISPERSOIDS	10
2.4.1 GENERAL	10
2.4.2 EFFECT OF DISPERSOIDS ON STRUCTURAL PROPERTIES	11
2.4.3 EFFECT OF DISPERSOIDS ON FATIGUE PROPAGATION	11

2.5	METASTABLE PRECIPITATES	12
2.5.1	ALUMINUM-ZINC-MAGANESIUM-COPPER ALLOYS	12
2.5.2	COPPER FREE ALLOYS	12
2.5.3	7075 ALUMIUM ALLOYS	13
2.5.4	EFFECTS OF ADDITION OF COPPER TO Al-Zn-Mg-Cu ALLOYS	15
2.5.5	HETROGENEOUS NUCLEATIONn IN Al-Zn-Mg-Cu ALLOYS	17
2.5.6	GRAIN-BOUNDARY PHENOMENA	17
2.6	EVALUATION OF AGING CONDITIONS IN ALUMINUM 7xxx ALUMINUM ALLOYS	18
2.7	EFFECT OF CONDITIONS ON FRACTURE TOUGHNESS & FATIGUE RESISTANCE	21
2.8	FATIGUE CRACK GROWTH UNDER CONSTANT AMPLITUDE LOADING	23
2.8.1	AGING AND FATIGUE CRACK PROPAGTION RATE OF 7xxx ALLOYS	23
2.9	ALUMINUM -COPPER- MAGNESIUM ALLOYS	26
2.9.1	METASTABLE PRECIPITATES	26
2.10	ARTIFICIAL AGE HARDENING OR SOFTENING OF 2xxx ALUMINUM ALLOYS	28
2.11	FATIGUE CRACK GROWTH UNDER CONSTANT AMPLITUDE LOADING	40
2.11.1	INTRODUCTION TO CRACK GROWTH THROUGH 2xxx ALLOYS	40
2.11.2	GENERAL	40

2.11.3	EFFECT OF MICROSTRUCTURE OF 2xxx ALUMINUM ALLOY ON FATIGUE CRACK GROWTH	40
2.11.4	EFFECT OF INTERMETALLIC PARTICLES ON FATIGUE CRACK INITIATION	42
2.12	AGING AND FATIGUE CRACK GROWTH RATE THROUGH 2xxx ALUMINUM ALLOYS	42
2.13	SUMMARY	47
CHAPTER 3	EXPERIMENTAL TECHNIQUES AND PROCEDURES	52
3.1	GENERAL	52
3.2	MATERIAL SPECIFICATIONS AND CHEMICAL COPPOSITION OF 2024-T3 AND 7075-T6 ALUMINUM ALLOYS	52
3.3	DESIGNING, CUTTING AND PREPARATION OF TEST SPECIMENS	54
3.4	HEAT TREATMENT OF 7075-T6 AND 2024-T3 ALUMINUM ALLOYS	57
3.5	MECHANICAL PROPERTY TESTS OF AIRCRAFT ALLOYS	59
3.5.1	TENSILE TEST	59
3.6	MATERIAL PROPERTIES TESTS OF AIRCRAFT ALLOYS	61
3.6.1	MEASUREMENT OF MACRO-HARDNESS OF 7057-T6 AND 2024-T3 ALLOYS	61
3.6.2	MEASUREMENT OF MICRO-HARDNESS 2024-T3 AND .7075-T6 ALLOYS	61
3.6.3	MEASUREMENT OF ELECTRICAL CONDUCTIVITY OF 2024-T3 AND 7075-T6 ALLOYS	63

3.7	MATERIAL FATIGUE TESTS FOR 2024-T3 AND 7075-T6 ALUMINUM ALLOYS	63
3.7.1	FATIGUE CRACK GROWTH MEASUREMENTS	63
CHAPTER 4	RESULTS AND ANALYSIS	67
4.1	INTRODUCTION	67
4.2	ALUMINUM ALLOY BEHAVIOR: 7075-T6	67
4.2.1	GENERAL	67
4.3	MECHANICAL PROPERTY ANALYSIS OF 7075-T6 ALLOY	68
4.3.1	TENSILE TEST	68
4.3.2	YIELD STRESS BEHAVIOR OF 7075-T6 ALLOY	68
4.3.3	ULTIMATE TENSILE STRESS BEHAVIOR OF 7075-T6 ALLOY	73
4.3.4	DUCTILITY BEHAVIOR OF 7075-T6 ALLOY	73
4.4	REAGING AND HARDNESS BEHAVIOR: 7075-T6	80
4.4.1	GENERAL	80
4.4.2	MACRO-HARDNESS BEHAVIOR OF 7075-T6 ALLOY	80
4.4.3	MICRO-HARDNESS BEHAVIOR OF 7075-T6 ALLOY	85
4.5	ELECTRICAL CONDUCTIVITY BEHAVIOR OF 7075-T6 ALLOY	85
4.6	FATIGUE CRACK GROWTH BEHAVIOR OF 7075-T6 ALLOY	90
4.7	ALUMINUM ALLOY BEHAVIOR: 2024-T3	101
4.7.1	GENERAL	101
4.8	MECHANICAL PROPERTY ANALYSIS OF 2024-T3 ALLOY	102
4.8.1	TENSILE TEST OF 2024-T3 ALLOY	102
4.8.2	YIELD STRESS BEHAVIOR OF 2024-T3 ALLOY	102

4.8.3	ULTIMATE TENSILE STRESS BEHAVIOR OF 2024-T3 ALLOY	106
4.8.4	DUCTILITY BEHAVIOR OF 2024-T3 ALLOY	106
4.9	REAGING AND HARDNESS BEHAVIOR: 2024-T3	113
4.9.1	MACRO-HARDNESS BEHAVIOR OF 2024-T3 ALLOY	113
4.9.2	MICRO-HARDNESS BEHAVIOR OF 2024-T3 ALLOY	119
4.10	ELECTRICAL CONDUCTIVITY BEHAVIOR OF 2024-T3 ALLOY	119
4.11	FATIGUE CRACK GROWTH BEHAVIOR OF 2024-T3 ALLOY	127
CHAPTER 5	DISCUSSION OF EXPERIMENTAL RESULTS	136
5.1	INTRODUCTION	136
5.2	COMPARISON OF GROWTH OF PRECIPITATES OF 7075-T6 AND 2024-T3 ALLOYS	139
5.3	COMPARISON OF SIMILARITIES AND DISSIMILARITIES OF 7075-T6 AND 2024-T3 ALUMINUM ALLOYS	140
5.3.1	SIMILARITIES BETWEEN BEHAVIORS OF 7075-T6 2024-T3 ALUMINUM ALLOYS	140
5.3.2	DISSIMILARITIES IN BEHAVIORS OF 7075-T6 AND 2024-T3 ALLOYS	145
5.4	IDENTIFICATION OF THE UNDERAGED AND OVERAGED CONDITIONS OF 7075-T6 ALUMINUM ALLOYS	146
5.5	EFFECT OF AGING CONDITIONS ON MECHANICAL PROPERTIES OF 7075-T6 ALUMINUM ALLOY	149

5.5.1	EFFECT OF REAGING ON THE YIELD STRESS, ULTIMATE STRESS, ULTIMATE STRAIN AND FRACTURE STRAIN OF 7075-T6	149
5.6	EFFECT OF PRECIPITATE HARDENING ON FATIGUE LIFE OF 7075-T6 ALUMINUM ALLOY	152
5.6.1	GENERAL	152
5.6.2	EFFECT OF UNDERAGED 7075-T6 ALLOY ON ITS FATIGUE LIFE	153
5.6.3	EFFECT OF OVERAGED 7075-T6 ALLOY ON ITS FATIGUE LIFE	154
5.7	IDENTIFICATION OF UNDERAGED AND OVERAGED CONDITIONS OF 2024-T3 ALUMINUM ALLOY	155
5.8	EFFECT OF AGING ON THE MECHANICAL PROPERTIES OF 2024-T3 ALLOY	159
5.8.1	EFFECT OF REAGING ON THE YIELD STRESS, ULTIMATE STRESS, ULTIMATE STRAIN AND FRACTURE STRAIN	159
5.9	EFFECT OF PRECIPITATION HARDENING ON THE FATIGUE LIFE OF 2024-T3 ALUMINUM ALLOY	161
5.9.1	GENERAL	161
5.9.2	EFFECT OF UNDERAGED 2024-T3 ALLOY ON ITS FATIGUE LIFE	161
5.9.3	EFFECT OF OVERAGED 2024-T3 ALUMINUM ALLOY ON ITS FATIGUE LIFE	163

CHAPTER 6	CONCLUSIONS AND RECOMMENDATIONS	166
6.1	CONCLUSIONS	166
6.2	GENERAL	166
6.2.1	PRECIPITATION BEHAVIOR OF 7075-T6 ALUMINUM ALLOY	166
6.2.2	FATIGUE LIFE BEHAVIOR OF 7075-T6 ALUMINUM ALLOY	168
6.2.3	PRECIPITATION HARDENING BEHAVIOR OF 2024-T3 ALLOY	169
6.2.3.1	GENERAL	169
6.2.4	FATIGUE LIFE BEHAVIOR OF 2024-T3 ALLOY	171
6.3	RECOMMENDATIONS FOR FUTURE WORK	172
6.3.1	RECOMMENDATIONS FOR FUTURE WORK ON 7075-T6 ALLOY	172
6.3.2	RECOMMENDATIONS FOR FUTURE WORK ON 2024-T3 ALLOY	173
REFERENCES		174

LIST OF TABLES

	<u>Page</u>
Table 3.1 Chemical composition of aluminum alloys by wt%.	53
Table 4.1 Tensile mechanical properties of 7075-T6 aluminum alloy.	69
Table 4.2 Macro-hardness of 7075-T6 alloy measured at room temperature.	81
Table 4.3 Micro-hardness of 7075-T6 alloy measured at room temperature.	81
Table 4.4 Electrical conductivity of 7075-T6 alloy at room temperature.	86
Table 4.5 Reaging conditions and normalized fatigue life of 7075-T6.	97
Table 4.6 Tensile mechanical properties of 2024-T3 aluminum alloy.	103
Table 4.7 Macro-hardness of 2024-T3 alloy measured at room temperature.	114
Table 4.8 Micro-hardness of 2024-T3 alloy measured at room temperature.	114
Table 4.9 Electrical conductivity of 2024-T3 alloy at room temperature.	120
Table 4.10 Reaging conditions and normalized fatigue life of 2024-T3.	128

Table 5.1	Comparison of original 7075-T6 and reaged at 107°C for 300 hours.	137
Table 5.2	Comparison of original 2024-T3 and reaged at 135°C for 300 hours.	137
Table 5.3	Comparison of original 7075-T6 and reaged at 135°C for 300 hours.	138
Table 5.4	Comparison of original 2024-T3 and reaged at 207°C for 300 hours.	138

LIST OF FIGURES

	<u>Page</u>
Figure 3.1: Configurations of test specimens.	55
Figure 3.2: MTS machine with fatigue crack propagation test set-up.	62
Figure 4.1: Variation of yield stress of 7075-T6 alloy under various reaging conditions.	70
Figure 4.2: Relationship between yield stress and reaging time of 7075-T6 alloy at 175°C.	71
Figure 4.3: Relationship between yield stress and reaging temperature of 7075-T6 alloy at 300 hours.	72
Figure 4.4: Variation of ultimate stress of 7075-T6 alloy under various reaging conditions.	74
Figure 4.5: Relationship between ultimate stress and reaging time of 7075-T6 alloy at 175°C.	75
Figure 4.6: Relationship between ultimate stress and reaging temperature of 7075-T6 alloy at 300 hours.	76
Figure 4.7: Variation of fracture strain of 7075-T6 alloy under various reaging conditions.	77
Figure 4.8: Relationship between fracture strain and reaging time of 7075-T6 alloy at 175°C.	78
Figure 4.9: Relationship between fracture strain and reaging temperature of 7075-T6 alloy at 300 hours.	79
Figure 4.10: Variation of macro-hardness of 7057-T6 alloy under various reaging conditions.	82
Figure 4.11: Relationship between macro-hardness and reaging time of 7075-T6 alloy at 175°C.	83

Figure 4.12:	Relationship between macro-hardness and reaging temperature of 7075-T6 alloy at 300 hours.	84
Figure 4.13:	Variation of micro-hardness of 7075-T6 alloy under various reaging conditions.	87
Figure 4.14:	Relationship between micro-hardness and reaging time of 7075-T6 alloy at 175°C.	88
Figure 4.15:	Relationship between micro-hardness and reaging temperature of 7075-T6 alloy at 300 hours.	89
Figure 4.16:	Variation of electrical conductivity of 7075-T6 alloy under various reaging conditions.	91
Figure 4.17:	Relationship between electrical conductivity and reaging time of 7075-T6 alloy at 175°C.	92
Figure 4.18:	Relationship between electrical conductivity and reaging temperature of 7075-T6 alloy at 300 hours.	93
Figure 4.19:	Relationship between crack length and fatigue life cycles of 7075-T6 alloy; reaged at various conditions.	94
Figure 4.20:	Relationship between crack length and fatigue life cycles of 7075-T6 alloy; reaged at 175°C.	95
Figure 4.21:	Relationship between crack length and fatigue life cycles of 7075-T6 alloy; reaged at 300 hours.	96
Figure 4.22:	Variation of normalized fatigue life of 7075-T6 under various reaging conditions.	98

Figure: 4.23	Relationship between the crack growth rate and change in stress intensity factor of 7075-T6 alloy; reaged at 175°C.	99
Figure 4.24:	Relationship between the crack growth rate and change in stress intensity factor of 7075-T6 alloy; reaged for 300 hours.	100
Figure 4.25:	Variation of yield stress of 2024-T3 alloy under various conditions.	104
Figure 4.26:	Relationship between yield stress and reaging time of 2024-T3 alloy at 175°C.	105
Figure 4.27:	Relationship between yield stress and reaging temperature of 2024-T3 alloy at 300 hours.	107
Figure 4.28:	Variation of ultimate stress of 2024-T3 alloy under various reaging conditions.	108
Figure 4.29:	Relationship between ultimate stress and reaging time of 2024-T3 alloy at 175°C.	109
Figure 4.30:	Relationship between ultimate stress and reaging temperature of 2024-T3 alloy at 300 hours.	110
Figure 4.31:	Variation of fracture strain of 2024-T3 alloy under various reaging conditions.	111
Figure 4.32	Relationship between fracture strain and reaging time of 2024-T3 alloy at 175°C.	112
Figure 4.33:	Relationship between fracture strain and reaging temperature of 2024-T3 alloy at 300 hours.	115
Figure 4.34:	Variation of macro-hardness of 2024-T3 alloy under various reaging conditions.	116

Figure 4.35:	Relationship between macro-hardness and reaging time of 2024-T3 alloy at 175°C.	117
Figure 4.36:	Relationship between macro-hardness and reaging temperature of 2024-T3 alloy at 300 hours.	118
Figure 4.37:	Variation of micro-hardness of 2024-T3 alloy under various reaging conditions.	121
Figure 4.38:	Relationship between micro-hardness and reaging time of 2024-T3 alloy at 175°C.	122
Figure 4.39:	Relationship between micro-hardness and reaging temperature of 2024-T3 alloy at 300 hours.	123
Figure 4.40:	Variation of electrical conductivity of 2024-T3 under various reaging conditions.	124
Figure 4.41:	Relationship between electrical conductivity and reaging time of 2024-T3 alloy at 175°C.	125
Figure 4.42:	Relationship between electrical conductivity and reaging temperature of 2024-T3 alloy at 300 hours.	126
Figure 4.43:	Relationship between crack length and fatigue life cycles of 2024-T3 alloy; reaged at various conditions.	129
Figure 4.44:	Relationship between crack length and fatigue life cycles of 2024-T3 alloy, reaged at 175°C.	130
Figure 4.45:	Relationship between crack length and fatigue life cycles of 2024-T3 alloy; reaged for 300 hours.	131

Figure 4.46:	Variation of normalized fatigue life of 2024-T3 alloy under various reaging conditions.	132
Figure 4.47:	Relationship between the crack growth rate and change in stress intensity factor of 2024-T3; reaged at 175°C.	133
Figure 4.48:	Relationship between the crack growth rate and change in stress intensity factor of 2024-T3 alloy; reaged for 300 hours.	134
Figure 5.1	Relationship between hardness and electrical conductivity of 2219 alloy by Chihoski (23)	141
Figure 5.2	Relationship between hardness and electrical conductivity of 7075-T6 alloy under various reaging conditions.	143
Figure 5.3	Relationship between hardness and electrical conductivity of 2024-T3 alloy under various reaging conditions.	144

NOMENCLATURE

Symbol	Description
G.P. zones	Copper precipitates (metastable precipitates)
G.P1. zones	Early phase of metastable precipitate.
G.P2. zones	η'' or Θ'' phase precipitates.
η''	Coherent precipitates in 7075-T6 alloy.
η'	Semi coherent or Incoherent metastable precipitates.
Θ''	Coherent precipitates in 2024-T3 alloy.
Θ'	Semicoherent or Incoherent precipitates in 2024-T3 alloy.
θ	Stable particles both in 2024-T3 and 7075-T6 alloys.
α	Aluminum concentration in Aluminum alloy's matrix.
ΔC_p	Differential specific heat.
ΔH	Change in enthalpy.
h	Distance of crack plane from the centre of loading.
W	Width of test specimen at the test section.
A	Preexponential constant.

Q	Activation energy.
MTS	Mechanical Testing System.
T.M.	Testing Machine.
IACS	International Annealed Copper Standards unit to measure electrical conductivity.
P	Load
a	Crack length
B	Thickness of test section.
σ_y	Yield stress.
σ_u	Ultimate stress.
ϵ_f	Fracture strain.
VHN	Vickers Hardness Number.
Rockwell B	Macro-hardness measurement unit.
N	Number of cycles
da/dN	Fatigue crack growth rate.
ΔK	Stress intensity factor range.
K_{IC}	Stress intensity factor range.
f(a/W)	Compliance factor for SEN specimen.

C Electrical conductivity.

N_f Number of fatigue life cycles to failure.

SCC Stress corrosion cracking.

CHAPTER 1

INTRODUCTION

1.1 BACKGROUND

Aluminum alloys have comparatively high strength to weight ratios, therefore these are preferred in the aircraft industry. Two precipitate hardening aluminum alloys used to design and fabricate the CT-114 aircraft (Tutor) are 2024-T3 and 7075-T6. During a precipitate hardening process an aluminum alloy starts with an underaged condition and as a result of some microstructural changes in the size, shape, and nature of precipitates the aging condition progressively moves towards peakaged and thereafter overaged conditions. The degree of precipitation depends upon the original temper, reaging temperature and the reaging time. Most Previous researchers are quite consistent in their findings that precipitate hardening of underaged aluminum 7xxx and 2xxx series alloys progresses to peakaged conditions followed by continuous precipitate softening during overaged conditions. However when it comes to fatigue life behavior, some claim that underaged 7xxx and 2xxx series alloys have better fatigue life while others have concluded that overaged aluminum alloys provide superior fatigue life.

2024-T3 aluminum alloy is originally solution treated at 495°C, quenched, cold worked and finally aged at room temperature for two weeks providing -T3 temper of the alloy. While 7075-T6 aluminum alloy is solution treated at 490°C, quenched and then artificially aged at 120°C for 24 hours to provide -T6 temper of the alloy.

Presently, the CT-114 aircraft is used in high speed operations at different levels of assignments. During the high speed flights, some of the parts of the aircraft such as aircraft skin and supporting panels undergo pressure cyclic loading and mechanical vibration loading thus causing material fatigue. After a flight mission, like any other aircraft, CT-114 is ported on a tarmac base. It has been

observed that throughout the year the fuselage temperature at shutdown conditions varies from 95°C to 177°C. Therefore considering the fact that 2024-T3 and 7075-T6 are precipitate hardening alloys and at times the aircraft skin is exposed to quite a high temperature of 177°C, the question arises whether or not further precipitate hardening has any detrimental effect on the fatigue life of the aircraft. It is also of interest to know if further precipitate hardening below the temperatures of original tempers has any marked effect on the fatigue life or not.

In order to find the solution to this problem, a project was setup that would provide experimental information regarding the effects of reaging and overaging on the fatigue life of the 2024-T3 and 7075-T6 aluminum alloys.

1.2 SCOPE OF THESIS

The purpose of this project was to investigate through experimental analysis the effects of precipitate hardening (reaging and overaging) on the fatigue life of 2024-T3 and 7075-T6 aluminum alloys. The whole project was investigated by accomplishing different objectives such as:

- (i) to review the previous research work on 2024-T3 and 7075-T6 alloys as regards to their precipitate hardening behavior, material properties behavior, and fatigue life behavior with respect to aging conditions and microstructural change with aging and overaging conditions, and other related areas.
- (ii) to decide about different tests, techniques, and specimen designs.
- (iii) to have each of the two alloys in underaged and overaged conditions such that each alloy should have at least two underaged and likewise two overaged conditions.
- (iv) to identify the aging conditions.
- (v) to determine the strength and ductility behavior of each alloy under different aging conditions.

- (vi) to predict the fatigue behavior of each alloy, based on material properties under different aging conditions.
- (vii) to experimentally measure the actual fatigue response of each alloy under different aging conditions.
- (viii) to discuss the fatigue life behavior of each alloy on the basis of metastable precipitates.

All these objectives were accomplished in steps to complete the project. The approaches, techniques and procedures to find the solution of these objectives are briefly given as:

The literature review was focused on certain key areas such as:

- (i) the nature of metastable precipitates and their nucleation, growth, and transformations.
- (ii) evaluation of aging conditions of 2xxx and 7xxx series aluminum alloys.
- (iii) the sequence of precipitates in a progressive aging and overaging conditions.
- (iv) effect of precipitate hardening or softening on mechanical and material properties.
- (v) relationship between aging conditions and time-temperature control.
- (vi) relationship between material properties and aging conditions (underaged and overaged conditions)
- (vii) effect of aging and overaging on the fatigue crack growth rates, da/dN , tests. This literature review is covered in Chapter 2.

The next most challenging work was to decide on different tests, techniques, and procedures to successfully and safely conduct the research work. Considering the fact that the aluminum alloys sheets were quite thin, therefore designing of the test specimens especially for the tensile test and the fatigue tests required careful considerations. The techniques and the procedures of the experimental work are covered in Chapter 3.

In order to know the precipitate hardening behavior of 2024-T3 and 7075-T6 aluminum alloys with respect to the metastable precipitates, it was most essential to select suitable heat treatment schedules for both the alloys. The literature review of the previous research work, the processing of the original 2024-T3 and 7075-T6 and their

respective tempers were certainly major factors in deciding the artificial reaging schedules. After coding all the test specimens for different tests, both the alloys were reaged under fixed temperatures and for a predicted reaging time to provide each alloy with both the underaged, peakaged and overaged conditions. The heat treatment program for 2024-T3 was decided at 175°C for 150, 300, 600 effective hours respectively and at 95°C, 135°C, and 207°C for 300 effective hours. While 7075-T6 was reaged at 107°C and 135°C for 300 effective hours and at 175°C for 38, 150, and 300 effective hours. The techniques and procedures of the project work for both the alloys are covered in Chapter 3.

The aging condition of each alloy was determined through the combined analysis of material hardness, H, and electrical conductivity C. After every heat treatment each alloy was tested for macro-hardness, micro-hardness, and eddy-current electrical conductivity. The experimental data was statistically analyzed. H-C relationships were used to identify underaged, peakaged and overaged condition of 2024-T3 and 7075-T6 alloys. These tests were also useful in knowing the microstructural behavior of each alloy under different aging conditions. The test results of the macro-hardness, the micro-hardness, and the electrical conductivity are recorded and analyzed in Chapter 4 and further discussed in Chapter 5.

In order to know the material strength and ductility behavior of both 2024-T3 and 7075-T6 alloys under different aging conditions, tensile tests were conducted. These tensile tests provided statistical behavior of strength and ductility related through mechanical properties such as yield strength, ultimate strength, ultimate strain, and the fracture strain of each alloy. These mechanical properties provided some indication of relative fatigue life behavior of each alloy under different precipitate hardening conditions. The mechanical properties test results and analysis for both 2024-T3 and 7075-T6 alloys are posted in Chapter 4 and followed by discussions in Chapter 5

The actual fatigue was decided on the basis that aircraft skin cracks grow under varying air pressure (thrust) mostly during the flights. Therefore stress intensity ranges from low stress intensity to high stress intensity factors. However, since our main objective was to compare fatigue behavior of different aging and overaging conditions, therefore a more simplified approach was followed that would serve the same purpose. The fatigue test specimen used for da/dN fatigue test were single edge notch, SEN, tested under constant amplitude loadings. In order to collect data under steady crack growth covering possible stress intensity range a set of three specimens were used. Three specimens were used to cover sequence in the order of low stress intensity, intermediate stress intensity, and high stress intensity factor ranges respectively. The actual technique and procedure used is given in Chapter 3.

The fatigue crack growth behavior under each aging condition was analyzed through a computer program. The graphical analysis of the actual fatigue tests is presented in Chapter 4. Two sets of graphs plotted are (i) crack growth verses fatigue life and (ii) fatigue crack growth rates verses stress intensity factors. The fatigue behaviors of both the alloys are then further discussed separately and on the basis of metastable precipitates and posted in Chapter 5.

CHAPTER 2

Literature Review And Background Information

2.1 FATIGUE LIFE AND MICROSTRUCTURE

2.1.1 GENERAL

This chapter covers the literature review and background information illustrating how particular microstructural features influence fatigue characteristics. Aging and overaging of a material brings microstructural changes even before these are physically evident. Effects of large intermetallic secondary phases, intermediate size dispersoid particles and fine precipitate effect on toughness and resistance to fatigue life/crack growth rates are briefly discussed. The phenomenon of age hardening in aluminum alloys has been pursued over years of extensive research. This research has had two main aims : (i) understanding the nucleation and growth kinetics of precipitates that are formed during the decomposition of a supersaturated solid solution, and (ii) relating the morphology of these precipitates and the coarser intermetallic particles to properties and physical characteristics of aluminum alloys. The industrial goal of most research programs for the last fifty years has been to develop superior high strength commercial alloy products. As a result of research and development investigations, many aluminum alloys with a high strength to weight ratio and having wide applications in the aircraft industry, have been produced. Notably, 7075 and 2024 alloys have been established as base aluminum alloys in this area. These are recognized within the research and development community as the standards with which new alloys are normally compared (1) (In order to develop improved materials). During the 1970's considerable effort was expended particularly with respect to understanding how microstructures affect the material's response to cyclic deformation either in the presence or absence of a flaw. Different investigations have indicated that the features of relatively coarse secondary intermediate particles, smaller high temperature precipitates (dispersoids), and fine metastable hardening precipitates influence fatigue response in ways that strongly depends

upon loading conditions, specimen design and environment. The microstructural changes described above all occur during reaging and can be investigated by using identical test specimens under identical loading conditions but reaged at different conditions. The main common experimental methods used to investigate fatigue characteristics are : S-N tests, strain controlled fatigue tests, and the crack growth rate method. In order to have a broad understanding of age hardening effects, all three types of particles such as secondary intermetallic particles, dispersoids and metastable precipitates are discussed but the main focus is on metastable precipitates.

2.2 FATIGUE CRACK GROWTH RATE

2.2.1 GENERAL

The fatigue crack growth rate approach started getting more and more attention during the 1970's. Most airplanes are now designed with the assumption that a flaw dimensionally below the limits of detection by nondestructive testing is present. The rate of growth of this crack before it reaches an unstable length, if catastrophic fracture is to be used, determines the inspection period of the aircraft which must be prevented. Materials with improved resistance to fatigue crack growth allow either longer intervals between inspection periods or the ability to design to higher stress and reduced weights.

To evaluate the fatigue crack growth rate, precracked specimens are cycled about some mean stress and crack length is monitored as a function of normalized cycles to failure during the test. The relative performance of materials tested with test specimens of identical configurations can be evaluated by comparing the curves of crack length versus number of cycles. More commonly, performance of materials tested using different dimensions of same configuration are normalized by applying the concepts of linear elastic stress intensity analysis. The stress intensity range, ΔK , at the crack tip is calculated along with the slope of the curve for crack length, a , versus number of cycles, N . The data is usually presented as

$\log(da/dN)$ versus $\log(\Delta K)$. Also the fatigue life of an aluminum alloy when reaged to different conditions can be compared to the original alloy using the crack growth rate approach.

In 1976, Truckner (2) from U.S. Airforce material laboratory along with his associates investigated the effects of microstructure on fatigue crack growth of high strength aluminum alloys. They examined crack growth rates within different crack propagation regions. It was observed that at high growth rate, cracks apparently were formed by coalescence of voids. The voids were initiated at smaller dispersoids. High stress intensity directed the crack tip along the separation between intermetallic particles and the matrix. Physical appearance of the fracture was compared to tensile failure. During the intermediate crack growth rate, the crack tip advanced at a definite and steady rate and formed striations along the crack plane. The physical size of striations depend upon the composition, the microstructure, and the environmental conditions. The most interesting observation regarding the low crack growth rate was advancement of crack tip in a complex erratic manner. Depending upon the environmental conditions, the advancement of the crack tip was characterized by slip plane decohesion along (111) or possibly (100) planes (1,2). The underlining conclusion was that metallurgical factors appear to control both the crack growth rate and the metastable precipitates. However in the mid seventies, there was much more work needed to be done in order to define the contributions of microstructural feature and substructure in this low ΔK region. The role of secondary intermetallic particles and metastable precipitates seems to be of paramount importance in this fracture region and are discussed in the following sections.

2.3 SECONDARY INTERMETALLIC PARTICLES

2.3.1 GENERAL

When liquid alloys of a uniform composition solidify, two levels of segregation result: (i) macro segregation in which fluctuation in composition on the scale of centimeters exist across the ingot. (ii)

micro-segregation in which fluctuation in composition on the scale of micrometers exist across the dendrite arms (3,4).

The microsegregation of the major solute elements arise in two ways:(i) Coring of the solid solution by retarding diffusing elements such as Zinc, magnesium and Copper.(ii) Formation of secondary intermetallic phase particles by eutectic decomposition of the liquid solution. The impurity elements, iron and silicon, combine with other elements and separate as intermetallic phase particles during solidification forming Al_7Cu_2Fe and Mg_2Si . While the peritectic element chromium concentrates at the center of the dendrite and forms $Al_{12}Mg_2Cr$ dispersoids during the pre-heat at temperatures above approximately $423^{\circ}C$ (1,5).

2.3.2 STRUCTURAL PROPERTIES OF INTERMETALLIC PARTICLES

The coarse secondary intermetallic particles do not contribute to the strength. Because they are brittle, they either fracture or separate from the matrix when the local strain exceeds some critical value. Consequently, they provide preferential crack paths ahead of a crack tip and promote the development of a high value of stress intensity factor. When this high cyclic stress intensity factor occurs, these preferential crack paths decrease the energy needed to propagate the advancing crack tip. Hence, by decreasing the volume fraction of secondary particles below the level found in most commercially developed aluminum alloys increases the fracture toughness and resistance to propagation of fatigue cracks under constant amplitude loading (6).

In April, 1979, Staley (6) published his research work on the influence of microstructure on fatigue and fracture of aluminum alloys" and showed that decreasing the percentage of iron and silicon resulted in improvement of K_{IC} for the 7475 alloy and consequently improvement in fatigue crack growth rate at high ΔK under constant amplitude loading conditions.

Secondary particles appear to have an effect on fatigue crack initiation at low stress levels, even though they may not fracture or separate from the matrix. In 1978, Kung (7), through his research work on fatigue crack initiation and growth of micro-cracks in commercial precipitation hardening of Al-Cu-Mg and Al-Zn-Mg-Cu alloys under constant loading, demonstrated the phenomenon that under high stress level, fatigue cracks initiate along slip bands and were not associated with intermetallic particles. However, at low stress levels, the particles had an effect that was alloy dependent. In 2024-T4, which had a lower volume fraction of intermetallic particles and a larger grain size, fewer than 50% of the cracks were associated with the particles. Furthermore, 95% of the initial cracks were associated either with the particles or with pits that developed during electropolishing. Size of the particles had also an effect. The probability of a secondary particle being associated with an initial crack increased as particle size increased to 6 μm . The effect of secondary particles was attributed to their ability to increase the local stress, which thereby increases the probability of introducing coarse, persistent slip bands, PSB.

2.4 DISPERSOIDS

2.4.1 GENERAL

Dispersoids are intermetallic particles formed by solid state precipitation. Metals such as chromium, manganese or zirconium are of high melting points and are added to high strength aluminum alloys to modify their dynamic recovery process and thus control static recrystallization in hot worked products. The dispersoids also serve to maintain fine grain size in products cold worked prior to solution heat treatment. The amounts added (Mn 0.8%, Zr 0.15%, Cr 0.25%) are retained in supersaturated solid solution but they precipitate during subsequent thermal treatments as $\text{Al}_{12}\text{Mg}_2\text{Cr}$, $\text{Al}_{20}\text{Mn}_3\text{Cu}_2$ or Al_3Zr . The first two dispersoids are 0.02 to 0.5 μm in longest dimension and develop an incoherent interface with the matrix while Al_3Zr is comparatively much smaller (less than 0.01 μm in longest dimension) and forms a coherent particle. These dispersoid

particles are formed by solid-state precipitation of chromium, copper, and zirconium at temperatures above 425°C (1,3).

2.4.2 EFFECT OF DISPERSOIDS ON STRUCTURAL PROPERTIES

Staley (8) presented effects of dispersoids in 1975 for Al-Zn-Mg-Cu alloys, containing approximately 0.1% Zr, or 0.2% Cr, or 0.4% Mn. One interesting observation was noticed that the particles provided insignificant dispersoid strengthening. However, dispersoids do have some indirect influence on material strength, particularly in extrusions. Addition of these particles of high melting points created a complicating effect called suppression of recrystallization phenomenon, the explicit effect of these particles on toughness is difficult to assess. In general, for monotonic loading, an alloy containing Al₃Zr dispersoids develops higher resistance to the stable propagation of a crack but the stress intensity at which unstable crack propagation begins is the same for Al₃Zr and Al₁₂Mg₂Cr. Alloys containing Al₂₀Mn₃Cu₂ are generally inferior in both respects. The energy to propagate a crack increases as volume fraction decreases and as dispersoid spacing increases (1,8).

2.4.3 EFFECT OF DISPERSOIDS ON FATIGUE PROPAGATION

In 1973 El-Soudani (9) from U.S. Airforce laboratories and in 1976 Truckner (2) also from U.S. Airforce conducted crack propagation tests under constant amplitude loading at intermediate levels of ΔK ranging from 10 MPa \sqrt{m} to 16 MPa \sqrt{m} and have shown no effect of volume fraction of type of dispersoids. Dispersoid spacing in 7075 alloy, however was shown to have an effect in constant amplitude loading at ΔK of 18 MPa \sqrt{m} and at higher ΔK levels. Decreasing the volume fraction of dispersoid provided higher fracture toughness and consequently higher resistance to fatigue crack propagation rate (1,9).

In 1979, Sanders, et al (10) published their research work on that included the effect of various types of dispersoids in Al-Zn-Mg-Cu

alloys. Despite the higher toughness in the alloys containing Zirconium, alloys with either Al_3Zr , or $\text{Al}_{12}\text{Mg}_2\text{Cr}$ dispersoids showed similar fatigue behaviour at the short and intermediate crack lengths. According to their further investigations, the secondary cracks formed at the secondary intermetallic particles at the lower stress intensity. In addition the average crack growth rate decreases, consequently the crack growth during subsequent constant amplitude cycles are substantially retarded. At longer cracks (higher ΔK), the effect of the type of dispersoid was more predominant in alloys with the higher volume fraction of secondary particles. In the alloys containing chromium (which had lower toughness), the crack began to accelerate at a short crack length (1).

2.5 METASTABLE PRECIPITATES

2.5.1 ALUMINUM-ZINC-MAGNESIUM-COPPER ALLOYS

2.5.2 COPPER FREE ALLOYS

Metastable precipitates (0.002 to 0.01 μm) are the smallest type of second phase particles and they contain the major solute elements zinc, magnesium, and copper. The precipitates develop in an uncontrolled manner during quenching and in a controlled manner during aging. When the alloy is quenched from above the solvus temperature and held at room temperature in case of natural aging or held at some elevated temperature (in case of artificial aging) but below a critical temperature, when precipitation forms these precipitates produce a transition structure called Guinier-Preston, G.P, zones. G.P. zones are initially spherical in Al-Zn-Mg alloys and increase both in size and number as aging progresses (1,5). In 1960, Polmear (11) related the growth of G.P. zones to increase in material strength of the alloy. With a continuous reaging of alloys relatively high zinc to magnesium ratio transforms into η' precipitates. The structure η' has the lattice parameters:

$$a = b = 4.97 \text{ \AA} , c = 5.54 \text{ \AA} \text{ and } \gamma = 120^\circ$$

The orientation of the monoclinic cell is related to the matrix by:

$$(001)_{\eta'} \parallel (\bar{1}\bar{1}\bar{1})_{Al}; (100)_{\eta'} \parallel (110)_{Al}$$

The precipitates are partly coherent along the basal planes but incoherent along the c direction of the precipitates, and the misfit of precipitates is approximately 7%. The structure of η' is alternate layers of zinc and magnesium with an atomic ratio of zinc to magnesium of 2 to 1. If the metallurgy of aluminum alloys is such that the atomic ratio $N_{Mg} \neq 0.5 N_{Zn}$, the species in excess will precipitate forming clusters of zinc and contribute to the overall hardening (1,12). Earlier in 1968, Thackery (13) found that persistent aging produces incoherent η precipitates at the expense of η' precipitates and ultimately form stable $MgZn_2$ compounds. The reduction in partial coherency between the main matrix and the precipitate results in a drop in strength. Furthermore over the extended period of aging the produced structure η is on {111} planes of primary α . Therefore, the decomposition reaction on aging and overaging can be summed up as:

Supersaturated solid solution \rightarrow G.P. zones $\rightarrow \eta' \rightarrow \eta$

The precipitates grow with time, and there is a progressive change in the relative amount of G.P. zones, η' and η precipitates. Sanders, while completing his PhD in 1974 and thereafter in 1976 along with Starke (14) through his investigations presented the time related growth of metastable precipitates in an Al-Zn-Mg alloy and 7075 aged at 120°C, and 150°C using the X-ray small angle scattering technique. In general the relative proportion of metastable precipitates depends both on the aging temperature and aging time period. Mechanical properties of aluminum alloys depend upon the precipitation hardening condition.

2.5.3 7075 ALUMINUM ALLOYS

Different phases of metastable particles, their formation, growth, and dissolution as related to aging and overaging conditions of 7075 alloys were identified through DSC and TEM techniques. DeIasi and Adler (15) used differential scanning calorimetry, DSC, in conjunction with transmission electron microscopy, TEM, to characterize precipitat-

es in 7075 aluminum as well as 7xxx series aluminum alloys. They considered one high strength 7075-T651 alloy and another overaged 7075-T7351 alloy for characterization of the solid state reactions accompanying heating (precipitate hardening). 7075-T7351 was overaged at 175°C for a period of 9 hours. DSC analysis was conducted at an average rate of 10.3°C/min. Differential capacity of each alloy was measured as a function of temperature and aging time and was analyzed graphically. Each of the observed endothermic and exothermic reactions that occurred over the 20°C to 500°C range was ascribed to the dissolution or formation of a specific precipitate. The dissolution of each matrix phase i.e G.P. zones, η' , and η was characterized by distinguishable dissolution temperature, dissolution enthalpy, activation energy and activation entropy. In fact the DSC technique was used to characterize the solid state reactions accompanying the dissolution as well as formation of additional precipitates. DSC analysis results were correlated to the TEM observations. It was observed that the matrix microstructure of the highest strength (T651) of 7075 alloy before heating consisted primarily of G.P. zones ($<75\text{\AA}$), with small concentration (5%) of semicoherent η' ($<100\text{\AA}$) phase, where as the over aged temper contains a mixture of η' and the stable incoherent η phase. The DC technique used and the typical results of differential heat capacity and the corresponding aging temperatures were graphically analyzed. DSC analysis within the temperature range 113°C to 217°C showed that in the early aging time, dissolution of G.P. zones was the predominant reaction along with formation, growth, and dissolution of η' precipitates. It was observed that 7075-T651 when aged at 151°C for 15 minutes still had predominantly G.P. zones and appreciable dissolution had not yet occurred. Aging at 190°C for 18 minutes showed an increase in volume fraction of η' phase and the size of preexisting η' phase was greater than observed at lower temperature. Above 217°C the reaction was rather complex involving formation of η' , growth, and dissolution of η' precipitates along with formation and growth of η precipitates. As aging at 234°C for 25 minutes provided microstructure showing significant amount of η (300 to 400 Å). η appears to have nucleated and have grown from the existing η' phase.

Later in 1982 Papazian (16) also published his work extended to identification of various phases during precipitate hardening and the relative amount of the various phases present, the particle sizes and distribution. His publication also included the study of reaction kinetics and thermodynamic equilibrium associated with the dissolution of precipitates in 7075 alloys. One underlying fact emerged out of this study that DSC endotherms and exotherms represent kinetic phenomena rather than equilibrium heat effects. By using DSC analysis at different heating rates, it was found that the precipitates and dissolution rate of metastable precipitate (G.P. zones and η') phases in 7075 are dominated by their reaction kinetics during DSC scans. In contrast, the dissolution rates of the stable precipitate phase η is dominated by thermodynamic equilibrium. These results were perhaps not surprising since it is generally accepted that the metastable transition phases occur primarily because of their more rapid nucleation kinetics. For the stable precipitates such as η in 7075, these can remain in equilibrium with the matrix at heating rates up to 10°C per minute in the temperature range of 300°C to 500°C .

Analysis of the shape of the G.P. zone dissolution peak in 7075 and its dependence upon heating rate showed that its behavior can most accurately be described by a kinetic relationship originally derived from a three dimensional diffusion controlled reaction in spherical particles. This is more of an approximation, therefore a more accurate analysis would be desirable.

2.5.4 EFFECTS OF ADDITION OF COPPER TO Al-Zn-Mg-Cu ALLOYS

Sanders and associates (1) reviewed some of the previous experimental work about effects of addition of copper to high strength 7xxx alloys covering the period from 1943 to 1969. They presented some of the noteworthy generalities concerning the microstructural effects.

- (i) Copper has a profound effect on the precipitation process of 7xxx alloys. It stimulates precipitation throughout the matrix, thereby reduces the size of precipitation free zones, PFZ, at the

- grain boundaries. Smaller size PFZ decrease the potential difference between the grains and the free boundaries while the copper precipitation increases with higher reaging temperatures.
- (ii) The quenched strength is greater in copper-containing alloys than in the simpler aluminum-zinc-magnesium ternary alloys.
 - (iii) The onset of hardening below 50°C is delayed when copper is present compared to the onset of hardening in the simple Al-Zn-Mg alloys.
 - (iv) The presence of copper does not seem to alter the number of stages that occur during the aging of the simpler ternary Al-Zn-Mg alloys.
 - (v) Alloys containing more than 2% copper develops peak strength over a wide range of aging temperatures extending from below 125°C to above 175°C.
 - (vi) Crystallographic arguments and some experimental observations suggest that copper and aluminum both enter into the hardening precipitates to form $Mg(CuAl, Zn)_2$.

Sanders (14) also conducted experimental analysis for the effect of change of copper content in Al-Zn-Mg-Cu alloys on fracture toughness and fatigue resistance. Adjustment of copper content modifies η' precipitate to the extent that depends upon the type of loading. Change in copper content from 1.4% to 2.3% showed no effect on the fracture toughness however there was a progressive increase in the resistance to strain controlled fatigue loading (1,14).

In 1978, Fu-shiong Lin (17) from Georgia Institute of Technology, while completing his work on "Low cycle corrosion fatigue and corrosion fatigue crack propagation of high strength 7xxx aluminum alloys" related the improved fracture resistance to an increased tendency for dislocation looping (in case of η' precipitates), as these oppose the precipitate shearing (in case of G.P. zones and η'' precipitates). Under constant amplitude loading, an increase in crack growth resistance with increase in copper content is attributed to resistance of copper to degradation from moisture in the environment. Truckner, et al (2) and also Sanders (14) separately conducted

experiments to observe the effect of change in copper content on crack growth rate both in low and high humidity air. According to Truckner, et al (2), a higher fatigue crack resistance was observed due to increase in copper content in a high humidity air. Sanders (14) also supported this fact.

2.5.5 HETEROGENEOUS NUCLEATION IN Al-Zn-Mg-Cu ALLOYS

As already mentioned, the sequence of precipitation in Al-Zn-Mg-Cu alloys follows the general scheme:

Supersaturated solid solution \rightarrow G.P. zones $\rightarrow \eta'$ $\rightarrow \eta$

G.P. zones nucleate homogeneously, and the different precipitates develop sequentially within the matrix. The presence of high-angle boundaries, subgrain boundaries and dislocations alter the free energy such that significant heterogeneous nucleation may occur (18). In going from G.P. zones to η , coherency between the matrix and precipitate progressively changes. G.P. zones are coherent, where as η' are semi-coherent while η are incoherent. Since η' and η are not coherent, these can be formed directly during quenching and aging by heterogeneous nucleation. In regards to the nucleation of η' , these being semicoherent, therefore can nucleate and grow directly on dislocations and subgrain boundaries. Likewise, η can nucleate and grow directly on grain boundaries and other incoherent boundaries such as those existing between the matrix and $\text{Al}_{12}\text{Mg}_2\text{Cr}$ (dispersoids).

Strength of 7xxx alloys can be reduced by introducing heterogeneous precipitation sites. The existence of heterogeneous sites can alter the relative proportions of G.P. zones, η' and η precipitates. Depending upon the aging treatment, the net effect can be lower strength. Overaging of 7075-T7 at 150°C or higher temperature progressively reduced its strength.

2.5.6 GRAIN-BOUNDARY PHENOMENA

In 1970, Starke (19) published his work regarding the precipitati-

on process at and near grain boundaries. According to Starke; because of the nature of grain boundaries, the incoherent η' can precipitate directly at these interfaces. Grain boundaries are sinks for vacancies and therefore, precipitates can upset the vacancy distribution in the vicinity of the boundaries.

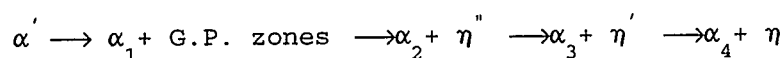
To a limited extent, the precipitation of η' on the grain boundaries can be controlled by the quench rate. Rapid quench rates tend to minimize the amount of grain boundary precipitation. Because of the high temperature of solution heat treatment and the rapid quenching rate, there can be an excess number of vacancies within the matrix. During aging, consideration of two important temperatures is very important. The first, a higher temperature of about 175°C is the G.P. zone solvus temperature. Below the G.P. zone solvus temperature, G.P. zones can nucleate, grow and eventually transform into η' and η precipitates with continued aging. The second critical temperature (about 125°C) defines whether homogeneous nucleation of G.P. zones can occur with or without excess vacancies. Above this temperature excess vacancies are required in order to nucleate G.P. zones while below this temperature excess vacancies are not necessary. Consequently, if artificial aging is carried out below the second critical temperature wide precipitation free zones will not occur. Thus with controlled quench rate and artificial aging condition, it is possible to produce commercially a material with narrow precipitate free zones, a small volume fraction of grain boundary precipitates, and a high volume fraction of matrix precipitates (1,19).

2.6 EVALUATION OF AGING CONDITIONS IN ALUMINUM 7xxx SERIES ALUMINUM ALLOYS

A number of different measurement techniques have been tried in evaluating the extent of aging in precipitation hardening aluminum alloys. Shercliff and Ashby (20) through their experimental work on 7xxx series aluminum alloys, measured Vickers hardness and yield stress of the alloys as a function of aging time and temperature. The alloys were reaged under different isothermal conditions at various

temperatures ranging from 130°C to 220°C. Graphical analysis for the relationship between yield strength and reaging time as well as between Vickers hardness and reaging time was presented. At each isothermal condition a line graph shows a continuous increase to a peak aged condition followed by a continuous and gradual decrease in the material properties. These results were consistent with the process of under aging, optimum aging and overaging. As the reaging temperature is increased to a higher isothermal condition, peak values of both yield stress and hardness shifted to lower values at shorter reaging time periods. A continuous increase in the material properties has been attributed to the formation and growth of coherent and shearable precipitates up to peakaged conditions while a continuous decrease has been associated with formation and coarsening of incoherent and nonshearable precipitates during overaging of the alloys.

Another technique used by Kenaway, et al (21) to evaluate the aging conditions was by measuring the electrical resistivity. This allowed following the precipitation process resulting from isothermal treatments of Al-2.5 wt% Cu. Increase in electrical resistivity during earlier aging time has been related to formation of a coherent phase of G.P. zones. While its decrease relates to the formation of semicoherent η' and or incoherent η phase. The contribution of clusters to the electrical resistivity was larger when they reach a "critical size and spacing" which must be smaller than the mean free path of conduction electrons. When they reach a size and spacing of the order of magnitude of the wavelength of conduction electrons, clusters contribute to an extra scattering of conduction electrons and provide a maximum electrical resistivity. However the use of this method is limited to small diameter wire and not easily applied to larger structures. A modification of this method using an eddy current decay technique for determination of electrical resistivity has been applied by Hull, et al (22). In this method a single crystal of Al-1.5 at% Cu was investigated for electrical resistivity, and supplemented with an exact determination of the precipitation sequence as:



where α' is referred to supersaturated solution, α_1 is the matrix concentration in equilibrium with G.P. zones and so on. The equilibrium state consists of the principally pure α -Al matrix (α_4) and the equilibrium η precipitates of composition CuAl_2 .

The eddy-current decay technique was used to monitor changes in the bulk-sample electrical resistivity, thus enabling the determination of the matrix Cu concentration as a function of aging time at 210°C . Small angle neutron scatterings, SANS, experiments were performed on the aged single-crystal sample, with the beam parallel to the [100] crystallographic direction. The scattering spectra was analyzed for characteristic streaks parallel to the [010] and [001] planes associated with the plate-like shape of the η' particles and their preferred orientation on the three {100} planes of the α -Al matrix. Finally, in order to correlate the yield stress of the alloy with the growth of the η precipitates, Vickers hardness measurements were performed on the surface of the sample throughout the aging process. The analysis of SANS in conjunction with the resistivity data gave information about the size, volume fraction, number density and chemical composition of precipitates. This technique was found to give accurate determination of aging conditions.

Chihoski (23), and thereafter Chihoski & Natan (24) have done some of the best research work on measurement of the condition of material due to aging. Their work indicates that the combined use of measurement of hardness and conductivity can be used to accurately establish the microstructure that is present during aging or overaging of the aluminum alloys. The H-C relationship between hardness and conductivity during aging and overaging depends upon both the quenching time and the aging time. A sail shaped envelope that is formed graphically indicates that during underaging as the aging progresses, first hardness increases drastically whereas the corresponding increase in conductivity is very small. During overaging conditions for a smaller change in hardness there is a very large increase in the conductivity. TEM work reveals that changes in conductivity coincide with the disappearance of η'' and formation and

growth of η' precipitates.

2.7 EFFECT OF AGING CONDITIONS ON FRACTURE TOUGHNESS & FATIGUE RESISTANCE

In 1978, Staley (6) presented his work at an international symposium on fracture mechanics. The main focus was on "How microstructure affects fatigue and fracture toughness of aluminum alloys". In his presentation he mentioned that when the fracture is transgranular, the types of precipitates due to aging or overaging has little effect on the combination of strength and fracture toughness developed. Lower strength tempers provide higher toughness. Quenching or aging treatments that increase the amount of intergranular fracture decrease the toughness with no effect on strength or tensile elongation. He further claimed that cold work soon after quenching has negligible effect on properties of the -T6 type temper, but it decreases the strength of the material aged to -T7 temper without any increase in fracture toughness (6). As mentioned before, both the structure and composition of precipitates have a direct effect on strength and resistance of 7xxx alloys to the environment. In the case of -T6 tempers, the maximum strength occurs in the peakaged condition when the alloy has the greatest volume fraction of closely spaced particles. In this condition, dislocations caused by stressing tend to shear the particles. During overaging, the size of precipitates increases and at high stress, the larger particles tend to be looped by dislocations rather than sheared. Overaging also improves fatigue crack growth resistance to degradation by an environment (10).

There are a variety of artificial aging and cold work treatments that can provide an ability to increase the strength of the material with little sacrifice in the fracture toughness. However another study indicates that these treatments do not provide a combination of strength and toughness. Superior crack growth resistance is obtained by increasing the Zn and Mg contents which in turn increases the volume fraction of η' precipitates (6).

In 1979, Sanders (10) and associate published their work on the effect of microstructure on fatigue resistance of 7xxx aluminum alloys that included fatigue crack growth under strain and stress controls. Their findings showed that alloys in overaged tempers have longer fatigue lives. Furthermore, precipitates are more or less effective in retarding dislocation movement because of differences in coherency, stacking fault energy, lattice parameters, and specific volume between the matrix and the second phase particles. The strength of a precipitation hardening alloy would thus depend upon factors such as coherency, size, spacing and uniformity in the distribution of precipitates. The microdeformation mode depends upon these factors which are controlled by both the degree of aging and the applied stress. In the case of 7xxx alloys dense slip bands develop in materials aged in the region of peak strength, these alloys are strained a few percent. With additional stress the slip bands may widen, intersect or alternatively cross slip with interaction between the bands. In case of any of these, the microdeformation at high strains becomes more homogeneous. The tendency to form slip bands at low plastic strains is altered by either underaging or overaging. However the actual mechanism associated with their formation is not thoroughly understood. During cyclic loading strain localization occurs at small (low) plastic strain amplitudes, whereas the deformation is more homogeneous at high strains.

The presence or absence of a localized deformation band is significant due to two reasons: (i) the band can act as initiation sites for fracture, and (ii) the magnitude of microplastic strain can not be accurately measured by a conventional extensometer. The conventional extensometer measures the average strain rather than the localized strain in deformation bands. According to Sanders and associates, analysis based on total strain showed that higher strength -T6 provides higher fatigue resistance at low total strain amplitude, whereas the higher ductility -T7 temper provides higher fatigue resistance at high total strain amplitude.

2.8 FATIGUE CRACK GROWTH UNDER CONSTANT AMPLITUDE LOADING

2.8.1 AGING & FATIGUE CRACK PROPAGATION RATE OF 7xxx ALLOYS

The degree of precipitation has a potential effect on fatigue crack growth under constant amplitude loading; this effect is attributed to the relative abilities of different types of precipitates to resist degradation from the environment. In 1979, Sanders (10) published his experimental work on "Microstructure and Fatigue Resistance of 7xxx P-M Aluminum Alloys", by measuring fatigue crack growth under constant and spectrum loading. In this experiment precracked specimens of 7075 and 7050 alloys aged to a peak strength, T6 type temper, and to overage tempers were tested at an intermediate ΔK in high humidity air. It was observed that resistance to fatigue crack growth increases with degree of precipitation (decreasing yield stress). A couple of years before in 1976, Truckner experimentally established that fatigue performance depends upon the type of precipitates rather than on the yield strength (2).

Some studies on 7xxx Al alloy in various treatment and reaging conditions have shown that the fatigue crack propagation rate is lowest in the underaged condition and highest in the overaged condition for low values of change in stress intensity factor (14,25,26).

Lindigkeit, et al (26) related the lower crack propagation rate to an increased resistance against crack propagation of microstructure containing shearable precipitates in comparison to the structure with nonshearable precipitates. It can therefore be explained based upon a higher degree of reversed slip within the plastic zone for underaged conditions. They also studied the fractured surface which showed that high slip steps are related to the microstructures containing shearable precipitates, while much finer slip steps were found for the condition with nonshearable precipitates.

Carter, et al (27) found similar results while testing 7475 aluminum alloy for the effect of slip character and grain size. The

alloy was tested in the underaged and overaged conditions with grain sizes of 18 μm and 80 μm respectively. Underaged 7475 aluminum alloy with grain size 80 μm provided an increased resistance to fatigue crack growth. The fracture surface exhibited increased irregularity and planar facet formation. While overaged 7475 aluminum alloy of 18 μm grain size exhibited relatively poor resistance to fatigue crack growth. Apart from the idea of increased slip reversibility during underaged conditions, Carter and associates (27) also related fatigue crack closure to fatigue crack resistance. Fatigue crack closure is considered a plane stress phenomenon if caused by the restraint of elastic material surrounding permanent plastic deformation and is termed plasticity-induced crack closure. If crack closure occurs under plane strain conditions and is attributed to crack branching it is termed as roughness-induced crack closure. When induced due to the aggressiveness of the environment, the crack closure is termed as oxide-induced crack closure. Planar slip and large grain size 7475 aluminum alloy provides improved fatigue crack growth rates and have been attributed to (i) slip being more reversible (ii) tortuosity of the crack path (iii) ΔK of zigzag and branched cracks (iv) enhanced closure associated with increased surface roughness. While a reduction in grain size, overaging, and an air environment reduces the reversibility of slip and crack tortuosity reducing the fatigue crack resistance. At high values of change in stress intensity factor (ΔK) the fatigue crack propagation rates are nearly the same for the different conditions.

Other studies on 7xxx Al alloy have found that the fatigue crack propagation rate decreases considerably with overaging (10). Forsyth, et al (28) conducted a crack propagation rate, da/dN test on 7178 aluminum alloy under various aging conditions and another supplementary test called reflectivity test for microscopic observations of the fracture surface. Forsyth and Bowen related the superior resistance to crack growth of overaged aluminum alloy that they derived from the greater crack tip irregularity that the microstructure imposes compared to poor crack growth resistance of the alloy aged to peak hardness and was observed to be associated with a relatively

flat fracture surface. The reflectivity test observations were correlated to the da/dN test results. The da/dN test curve has two very contrasting slopes meeting at the knee of the curve. The first steep part of the curve being associated with fracture flattening i.e, achievement of maximum coherence and short crack front length. The second part beyond the knee which had a lower slope that has been associated with increasing effective plastic zone size. From the microscopic examination it was observed that, crack starter was a narrow spark machined slot, a number of fatigue origins occurred at different levels creating facets which further interacted with one another and joined by the formation of steeper facets forming a relatively rough surface and hence poor crack growth rate. These results are consistent with the findings of Ramusat and Vidal (29) on overaged 7075-T6 alloy for diminished crack growth rate. Wei, et al (30) explained the improved fatigue life of overaged 7xxx series alloys on the basis of the role of magnesium in corrosion fatigue, CF, and stress corrosion cracking, SCC, in the peakaged and overaged conditions. An improvement in CF and SCC susceptibility of the overaged alloy was observed. Auger electron spectroscopic studies showed a significant amount of segregation of magnesium over regions on the surface for the 7075-T651 alloy during peakaged conditions and no apparent segregation in the overaged conditions. These observations suggested the commonly acknowledged environmental susceptibility of 7xxx series alloys in the peakaged conditions and might be attributed to further reaction of water vapours with segregated magnesium or magnesium in enriched regions forming $Mg(OH)_2$ and MgO , since the amount and nature of precipitates affect the slip system at the crack tip of the alloys. Therefore segregation of magnesium during peakaged conditions affect the susceptibility and in turn affect the slip system and consequently the fatigue crack growth rate. The general trend in these studies is towards a more pronounced decrease in the fatigue crack propagation rate with higher values of change in stress intensity value.

Another study conducted by Duboust, et al (31) shows that changes in fatigue crack propagation rates do not occur with variation in

overaging of 7075 alloy. However there is significant improvement that occurs in the fatigue strength on the onset of overaging. This is attributed to the decrease in fatigue crack initiation sites following extensive dissolution of coarse and brittle constituent particles.

2.9 Aluminum-Copper-Magnesium Alloys

2.9.1 METASTABLE PRECIPITATES

Precipitation in the Al-Cu-Mg system with copper to magnesium atomic ratio between 4:1 and 2:1 occurs in the following sequence:

Supersaturated solid solution \rightarrow G.P. zones $\rightarrow \Theta'' \rightarrow \Theta' \rightarrow \Theta$ (Al_2Cu)
 where the G.P. zones consist of Cu and Mg atoms on the {210} planes of the matrix.

In 1970, Kelly and Nicholson (32) through their research work on Al-Cu alloys put forth the results of their investigation into the order of reaction and the structure of precipitates. According to them Θ'' remains coherent with the aluminum lattice. According to work by Silcock (33);

Θ' is orthorhombic with following parameters:

$$a_{\Theta'} = 4.05 \times 10^{-10} \text{ m}, \quad b_{\Theta'} = 9.06 \times 10^{-10} \text{ m}, \quad \text{and} \quad c_{\Theta'} = 7.2 \times 10^{-10} \text{ m}$$

The orientation relationship of Θ' and the matrix is

$$(100)_{\Theta'} \quad (\bar{2}10)_{\text{Al}} ; \{010\}_{\Theta'} \quad \{120\}_{\text{Al}}$$

Peak strength is associated with the Θ' precipitates. Eventually Θ' loses coherency, and metallic Θ (CuAl_2) develops. In general there is an increase in the yield strength of Al-Cu-Mg alloys when the materials are cold worked after quenching or prior to either natural aging (-T3 type) or an artificial aging (-T8 type). After cold work, there is an increase in the number of nucleation sites, consequently this produces a higher volume fraction of hardening precipitates.

Kenawy et al (21) while investigating the effect of precipitate hardening on the electrical resistivity in Al-2.5 wt% Cu introduced the subdivision of G.P. zones into G.P1. zones and G.P2. zones. Thus the equivalent form of the four stages precipitation process followed as:

solid solution \rightarrow G.P1. zones \rightarrow G.P2. zones \rightarrow Θ' (semi coherent)
 \rightarrow Θ (incoherent) \rightarrow α -phase (solid solution)

In 1981, while presenting their research work on the precipitation hardening process in aluminum 2219 alloy, Rosen and associates very briefly reviewed some of the previous work on the metastable precipitates and stable particles formed during different stages of artificial aging of 2xxx aluminum alloys (34). This literature review follows as:

G.P. zones:

Guinier and Preston determined independently the nature of the precipitates through the application of X-ray diffraction techniques (34,35). Through the X-ray studies they observed that at the early stages of the aging process, segregation of clusters of copper atoms (G.P. Zones) on {100} planes of the aluminum lattice occur. These G.P. zones have a thickness of a few atomic planes and are structurally coherent with the aluminum solid solution matrix; they are formed rapidly and homogeneously by an enhanced diffusion process driven by the excess of vacancies in quenched alloys. The rapid migration of copper in the aluminum matrix, preceding zone formation is due to vacancy solute coupling (22,34).

Θ'' Particles:

The Θ'' particles in Al-Cu alloys are coherent intermediate precipitates, they have a definite crystallographic structure (32). The thickness of the Θ'' was measured to be 100 Å and having a diameter approximately 1500 Å (34). The aluminum matrix planes that are parallel to Θ'' platelet were found to be distorted by elastic coherency strains.

⊖' Precipitates:

The ⊖' precipitates were observed to be a tetragonal structure with c axis parallel to the Al [100] direction (33). Structural dislocations were observed near ⊖' precipitates, thus producing a quasi-coherent interface. The dislocation rings formed cause the relaxation of strains near the precipitates and consequently contribute to reduction in hardness and strength. It has been observed that under suitable conditions G.P. zones, ⊖'', and ⊖' can nucleate independently (34).

⊖ Equilibrium precipitates:

The equilibrium CuAl_2 incoherent ⊖ precipitates are also tetragonal structure. The nucleation of ⊖ precipitates are heterogeneous and occur at planar grain boundaries in the aluminum matrix or at metastable ⊖' precipitates which can be observed in the overaged condition.

⊖'' and ⊖' particles being coherent or quasi-coherent, contribute strongly to hardness depending upon the size and the distribution of the precipitates in the matrix. As the ⊖'' and ⊖' precipitates grow, their adjacent strain fields become larger and at peak hardness these extend from one precipitate to the next (⊖'' → ⊖') (34). However as ⊖'' and ⊖' precipitates are transformed to form ⊖ particles, the strain fields are reduced to localized fields. The alloy is softened to comparatively much lower hardness values and tends to remain steady thereafter.

2.10 ARTIFICIAL AGE HARDENING OR SOFTENING OF ~~2xxx~~ ALUMINUM ALLOYS

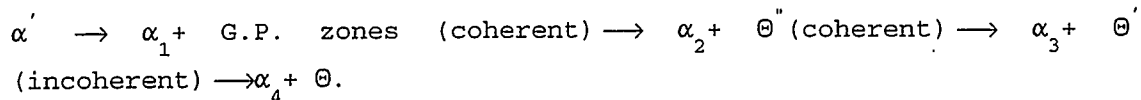
The age hardening process involves atomic rearrangements accompanying the breakdown of the supersaturated solid solution. A condition for hardening to occur is the precipitation of particles from an aluminum base supersaturated solid solution. The basic requirement for precipitation hardening of an alloy system is that the

solid solubility limit decreases with decreasing temperature. In aluminum base alloys the rapid cooling suppresses the separation of the β phase so that the alloys exist at the lower temperature in an unstable supersaturated state. If the alloy is allowed to age at temperature within an interval specific to each alloy system, the second phase precipitates out. The formation of precipitates contribute to the strengthening of the alloy. The increase in yield strength and hardness of an aluminum alloy depends largely on the structure, spacing, size, and distribution of precipitated particles. Both the yield strength and the hardness of the alloy also depends upon the degree of structural and crystallographic coherency of precipitates with the matrix. The age hardening in aluminum alloys occurs through a diffusional nucleation and growth process. The rate of growth of the nuclei is controlled by the rate of atomic migration in the alloy; thus the temperature of aging has a pronounced effect. While softening of an alloy is primarily due to formation of incoherent precipitates or transformation of Θ'' precipitates to Θ' precipitates (32). The sequence of precipitates associated with age hardening effects in 2xxx series alloys are as:

Supersaturated solid solution \rightarrow G.P. zones (coherent) $\rightarrow \Theta''$ (coherent)
 $\rightarrow \Theta'$ (incoherent) $\rightarrow \Theta$ (CuAl_2) $\rightarrow \alpha$ -phase (solid solution)

The sequence of artificial age hardening precipitates in 2xxx aluminum alloys observed by Kelly et al (32), Kenawy et al (21), Rosen et al (34) were found similar to the one above and provided similar age hardening effects. The most common age hardening effects were related to the precipitation and dissolution of coherent and incoherent precipitates. Precipitation and growth of coherent particles tend to harden the 2xxx aluminum alloys while dissolution of coherent particles or precipitation and growth of incoherent particles tend to soften the 2xxx alloys. It has also been observed that the age hardening process in 2xxx aluminum alloys is complex and the relative proportions of different particles at any aging condition dictate the resultant effect (21,34).

Hull et al (22) while studying Θ' metastable precipitates in an Al-1.56 at% Cu introduced a relationship of variation of Al concentration in the main matrix of the Al-Cu alloy during the precipitation hardening process. The precipitate sequence during the process was established by using X-ray diffraction, and electron microscopy and followed:



where $\alpha', \alpha_1, \alpha_2, \alpha_3, \alpha_4$ are the Al concentrations in the main matrix of Al-Cu alloy associated with each of the four stages of the precipitation process.

Formation and growth of coherent precipitates harden an aluminum alloy while dissolution of coherent precipitates and or formation and growth of incoherent precipitates soften the alloy. However the precipitation hardening processes in most of the alloys are some what more complex and sometimes involve formation and growth of one phase along with the dissolution of another phase simultaneously. The overall effect in such cases depends upon the relative densities of different precipitates, their distribution both along the grain boundaries and throughout the main matrix of the alloy. Sizes and shapes of precipitates also play an important role in age hardening of Al-Cu alloy and each stage of the process was also related to the types of precipitates in the process of progressive aging. In order to correlate the material properties to the type, size, nature and distribution of particles, Hull and associates used SANS technique (22).

Hull et al (22) measured the electrical resistivity, and material hardness of Al-1.56 at% Cu single crystals to correlate the precipitation process in Al-Cu aluminum alloys to the corresponding age hardening effects. The alloy was artificially aged at 210°C and the material properties were measured as a function of aging time. At each stage of the aging process, Vicker indication hardness number was measured and the corresponding yield stress was calculated. SANS

provided the microstructure analysis with respect to the metastable precipitates associated with each aging condition. Electrical resistivity of the Al-Cu alloy was then measured as a function of aging time. The electrical resistivity measured after 10 min. of aging was pretty close to its original value indicating the G.P. zones had dissolved and no significant nucleation of Θ'' phase had taken place. It was further observed that the yield stress of the alloy increased with increasing time and reached a peak after 200 minutes of aging time and then subsequently decreased. The yield stress calculated from SANS information was found to be in agreement with the experimentally measured values. However, the experimentally observed peak in yield stress was not quite consistent with the value predicted by calculation. From SANS analysis peak hardness was in close agreement with the change in the particle-matrix interface from coherent to incoherent where the strain field becomes localized around the precipitate.

In 1981, Rosen et al (34) published a research paper on the precipitation hardening process in 2219 aluminum alloy. The experimental work related to the investigation of the precipitation hardening process involved dynamic measurement of sound wave velocity, ultrasonic attenuation, and hardness as a function of aging time at constant temperatures such as 150°C, 175°C, and 220°C. Measurement of these properties was found to exhibit prominent changes and the anomalies were then related to the formation of Θ'' and Θ' precipitates in the alloy. The absorption of sound waves technique measured the degree of coherency of precipitates while the attenuation of ultrasonic waves were used to record the change in precipitate structure occurring during the aging process. From the temperature dependence of the sound velocity and ultrasonic attenuation, the activation energies for formation of Θ'' and Θ' precipitates were found to be 4.7 kcal mol⁻¹ and 9.9 kcal mol⁻¹ respectively. The activation energy of 26.6 kcal mol⁻¹ was apparently responsible for the loss coherency of Θ' precipitates and resulting decrease in hardness. This assumption was supported by experimental measurement of peak values of hardness and ultrasonic attenuation. According to their publicati-

on, some of the findings and material science behind the findings have been correlated as:

(i) Sound wave velocity measurements indicate that the elasticity of aluminum alloy 2219 depends upon the aging temperature. The elastic moduli increase with increasing temperature was attributed to a relatively large volume fraction of precipitates of intrinsically higher elastic moduli than the matrix, that resulted from aging at increased temperature (34). Growth of Θ'' and Θ' precipitates were recorded as a function of aging time at 150°C . After two hours aging time, Θ' precipitates having disk like structure were 300 \AA in diameter. As the aging time was extended to 42 hours, the Θ' precipitates grew in size to about 1000 \AA diameter indicating that as the aging time increases, the Θ' structure coarsens. It was also observed that the higher the aging temperature, the smaller the aging time required to produce quantitatively the same aging effect.

(ii) The increase in hardness of an aged alloy depends upon the variation in stress field in the vicinity of the precipitate. The contribution to hardness depends upon the coherency of the precipitate with the matrix, size, and distribution of the precipitates and proximity of a mean free path between the particles.

(iii) Large semicoherent or incoherent particles regardless of their hardness or elasticity cause softening of the matrix. The alloy begins to overage or to soften when the degree of coherency between the precipitates and the matrix decreases. As the aging temperature is increased the peak hardness decreases. Thus peak hardness at 175°C was recorded lower than the peak hardness at 150°C . Also the initial slopes of the hardness curves are steeper for higher aging temperatures. This behavior at increased temperature was explained by considering the enhanced mobility of the species which diffuse during the formation of semicoherent Θ'' and Θ' as the temperature increased. During aging at 220°C , the volume fraction of Θ'' was relatively insignificant. The main contribution to hardness thus had arisen from Θ' particles in the semi coherent state.

(iv) In 2219 aluminum alloy, the peak hardness followed by a softening process indicates loss of coherency of Θ' precipitates. At peak hardness, Θ' precipitates that were initially semicoherent might

have grown to dimensions necessitating some form of relaxation of elastic strains. The notion was supported by the fact that dislocation rings have been observed to form around θ' precipitates in Al-Cu alloy (34). The strain field is then localized around the particles rather than around the matrix. Thus as the elastic strains between the precipitate and the matrix become relaxed the strength and hardness of the alloy decreases. The above techniques were found inaccurate and the inaccuracy seems to stem primarily from the inability to uniquely describe conditions of aging as multivalued measurement conditions occur.

Another technique to observe the precipitation hardening of Aluminum alloys was the use of DSC in conjunction with TEM by Papazian (16). Papazian published his research work on calorimetric study of precipitation in Aluminum 2219 alloy in 1980, and thereafter about the calorimetric studies of precipitation and dissolution kinetics in Aluminum 2219 and 7075 alloys in 1982. The main focus of his research work was to observe the different types of thermal reactions associated with different aging conditions. Differential scanning calorimetry provided analysis regarding the type of reactions while transmission electron microscopy provided identification of various precipitates, the particle sizes, and distribution of the particles associated with each thermal reaction.

All the DSC runs were started at room temperature and ended at 575°C with a constant heating rate of 10°C/minute. In order to study the microstructure of a sample under constantly changing temperature during the DSC scan, the entire aging sequence was seen as one thermograph (relationship between differential heat capacity & aging temperature).

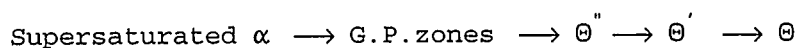
DSC arrangement was connected to a mini computer with a suitable interface, and the data from each run were continuously stored. After a run was completed, the data were converted to heat capacity vs temperature using a previously established calibration for the DSC cell. Differential heat capacity, ΔC_p that represents the heat

associated with solid state reactions which occurred during the DSC run was calculated. The reaction peaks in the ΔC_p vs T curves were characterized by a reaction enthalpy, ΔH , the area under the peak is proportional to the molar heat of dissolution or formation of a precipitate and its concentration. Differential scanning calorimetry provided exothermic (precipitation) and endothermic (dissolution) reactions as the alloy was heat treated from room temperature conditions to 550°C. The microstructural changes were accompanied by exothermic, endothermic, multiple endothermic and superimposed exothermic reactions shown by representative thermograms that provided characteristic reaction regions. The reaction region depended upon the temperature ranges during the DSC runs. Within each reaction region precipitation and or dissolution of particles, their relative sizes, and distribution densities were analyzed. It was also observed that the age hardening effect was consistent with the nature of the precipitates observed such as G.P. zones, Θ'' , Θ' , and Θ particles. The research report was extended to the transformation of one type of precipitate into other types so as to study both the age hardening and age softening effects. DSC analysis covering the thermogram showed four characteristic reaction regions as:

- (i) An endothermic (dissolution) reaction between 50°C and 200°C.
- (ii) An exothermic (precipitation) reaction between 200°C and 300°C.
- (iii) A multiple endothermic (precipitation) reactions between 300°C and 550°C.
- (iv) Superimposed exothermic (precipitation) reactions between 400°C and 575°C.

The above reactions show that under certain aging conditions, both precipitation and dissolution of precipitates could occur simultaneously.

Artificial aging of Aluminum 2219 conducted at 130°C and 190°C provided DSC response and precipitate sequence similar to the one previously found in pure binary Al-Cu system as:



Aging of Aluminum 2219-T42 alloy at 130°C for 53 hours provided G.P. zones about 10.0 nm diameter. In order to study the transformation of G.P. zones into Θ'' precipitates in the alloy, a series of samples were aged at 130°C. The characteristics of the thermograms were compared to TEM analysis. At the same time, relationships between hardness (Rockwell B) and the corresponding aging time were studied. The microscopy of this series of samples showed continuous $(100)_{Al}$ streaks through $\{200\}_{Al}$ for all samples up to and including aging for 53 hours and after 113 hours where a second maxima occurred. Thus the second rise in the hardness curve corresponds to transformation to Θ'' . Likewise Θ' formation peak was found. As the aging time progressed the Θ' formation peak reduces significantly while the hardness of the alloy fell continuously.

Reaging of Aluminum 2219-T42 alloy at 190°C, reduced the aging time periods quite drastically. It took only 15 minutes to cause initiation of transformation of G.P. zones to Θ'' at which both the thermal capacity and the hardness started to increase rather sharply. After 4 hours this transformation was found to have been completed and having only Θ'' phase present. During this aging time hardness of the alloy was found to increase to its maximum value of 76 Rockwell B. After 8 hours of reaging at 190°C Θ' began to form and the transformation took only 36 hours to complete at which time the microstructure was found to be entirely of Θ' phase. After the onset of the formation of Θ' particles, a gradual and continuous decrease in the hardness of the alloy was observed.

This publication also included the study of reaction kinetics and thermodynamic equilibrium associated with the dissolution of precipitates of 2219 alloy. The one underlying fact that emerged from this study was that DSC endotherms and exotherms represent kinetic phenomena rather than equilibrium heat effects. From the DSC scans analysis, it was found that the precipitation and dissolution rates of metastable precipitate phases in 2219 alloy are dominated by their reaction kinetics. In contrast the dissolution rates of the stable precipitate phase Θ is dominated by thermodynamic equilibrium.

Analysis of the shape of the G.P. zone dissolution peak in 2219 and its dependence on heating rate showed a behavior that can be described approximately by a three dimensional diffusion controlled reaction of spherical precipitates. Papazian and associates also obtained DSC scans at different heating rates which resulted in different temperatures for peak values of precipitation and dissolution for each case (16).

In order to make an accurate assessment of the microstructure of age hardenable aluminum alloy 2219, Papazian and associates compared it with Al-Cu alloy, for which experimental information regarding the sequence of precipitates had been accurately established with an extended research program. The comparison made was supported as occurring since 1930 especially with review of early work by Hardy (36), and more recent studies by Hirano et al (37) and Zahra et al (38). All these previous investigators observed and had also analyzed the relationship between heat capacity and temperature. Their results were in agreement with each other, but there was some disagreement on specific points, particularly the distinction between the G.P. zones dissolution peak and the Θ dissolution peak.

Kenawy, et al (21) conducted research work to measure the change in electrical resistivity of Al-2.5 wt% Cu alloy resulting from different isothermal aging conditions. They also reviewed the research work of previous investigators and considered it as guide lines for their own research work. This literature review correlated the appearance of coherent G.P. zones to increase in electrical resistivity of Al-Cu alloys while the formation of semicoherent Θ' and incoherent Θ phases showed a decrease in electrical resistivity. Size and spacing of G.P. zones have also a considerable effect on electrical resistivity. The electrical resistivity of the alloy was found to be larger when the G.P. zones reached a "Critical Size And Spacing" which must be smaller than the mean free path between the G.P. zones. When the G.P. zones reached the size and spacing of the magnitude of the wave length of the conduction electron, the clusters then contribute to an extra scattering of conducting electrons and as

a consequence provide maximum electrical resistivity (21).

Kenawy and associates (21) conducted the experiment by taking 10 cm long and 2.0×10^{-2} cm in diameter wire samples, annealed at 500°C for one hour and then cooled at a rate of $(8.9 \times 10^{-2})^\circ\text{C/s}$. One of these samples was immediately clamped in the electrical circuit and measured for electrical resistivity. These samples were then aged at temperatures from 100°C to 485°C and were tested for their respective electrical resistivities. The change in electrical resistivity was taken as a measure of precipitation hardening or softening effect during the following four stages of precipitation of the alloy given as:

G.P1. zones (coherent) \rightarrow G.P2. zones \rightarrow Θ' (semicoherent) \rightarrow Θ
 (CuAl_2) \rightarrow α phase (solid solution)

The first and the second stages were identified as stages of formation of G.P1. zones and G.P2. zones and an increase in change of electrical resistivity was observed. As the aging time and temperature were raised, internal strains increased and more G.P1 & G.P2. zones were formed. According to Kenawy and associates, the G.P. zones being clusters of Cu atoms in the Al matrix, acted as isolated scattering centers for the conducting electrons. This scattering of conducting electrons increased spontaneously with the increase of the amount of tiny G.P. zones during stage 1. While a decrease in resistivity was observed with an increase in size of G.P. zones (beyond certain limit). Scattering power of tiny G.P. zones decreases as their size and distribution increases in the matrix during stage 1 and stage 2. It was further observed that as the size and spacing of tiny G.P. zones became much larger than the electronic mean free path, the resistivity tends to decrease.

The third stage was identified as coalescence of semicoherent Θ' phase and a slight decrease in electrical resistivity was observed after a short aging time. When the linear dimension of the Θ' phase became larger than the mean free path of conducting electrons, these Θ' precipitates can then be treated as isolated scattering centers.

At aging stage 4 an increase in resistivity was associated with the dissolution of the tetragonal Θ phase. Increase in the electrical resistivity change was also correlated to the lattice parameter of the tetragonal Θ phase as a function of increasing aging temperature which implied that the concentration of vacancies increases the dissolution temperature of the Θ phase providing higher electrical resistivity.

Another study by Hillel and Edward correlated the increase in electrical conductivity to the appearance of coherent G.P. zones (39), and decrease in the electrical conductivity to the formation of semicoherent and or incoherent phases as Θ' and Θ phases.

The best work that has been done regarding the measurement of aging condition of aluminum 2xxx alloy was presented by Chihoski in 1983 (23) and also by Chihoski and Natan (24). Both these publications reveal artificial aging conditions of aluminum 2219 alloy as a function of its hardness, H, measured in Rockwell B and the corresponding electrical conductivity, C, measured in % IACS. H-C graphical analysis showed that a "sail" shaped H-C relationship envelope occurs which described the aging condition of the material. This approach of combined use of H-C measurements accurately established the microstructure present at each aging condition.

According to Chihoski, when a solutionized aluminum 2219 alloy is quenched quickly it freezes the solute atoms into a solid solution state. Subsequently, during an artificial aging at an elevated temperature, the solute atoms form finely dispersed precipitates in the aluminum matrix. During the initial stage of aging as these precipitates grow both in size and number, consequently the strength and hardness of the alloy increases. It was further observed that if the temperature of descent was lower and the quenching rate was low or the quenched alloy was aged at higher temperature, it resulted in coarse precipitates producing a comparatively smaller hardening effect in the alloy. A poor quench provides lower hardness and generally higher conductivity.

Chihoski related thermal history of aluminum 2219 alloy to its hardness, electrical conductivity, quenching time and aging time. The alloy was solution treated at 530°C, and then quenched at seven different quenching rates varying from 0.55 seconds up to 720 seconds.

During this time the quenching temperature fell from 410°C to 190°C. Based on the quenching times, Chihoski made seven metallurgically different panels by extending the quenching time for each subsequent panel. The test samples for each of the seven panels were then artificially aged. Hardness and conductivity of test samples were measured as a function of aging times varying from 10 minutes up to 3 days. The measured values of hardness and conductivity for each quenching time were then graphically analyzed. All the results for different quenching times were found to have different H-C relationships in the underaged, peak aged, and over aged conditions. However all had similar "sail" shaped relationship between H & C. Transmission electron microscopy was then used to relate microstructure of the aged alloy to the corresponding hardness and electrical conductivity for each aging condition.

It was observed that neither hardness nor electrical conductivity by themselves were sufficient to determine the state of aging of the alloy. Rather a combination of both H & C was needed to be used to accurately establish the aging condition. During the early stage of aging at 190°C, Rockwell B hardness of 2219 alloy had risen sharply while its electrical conductivity measured in % IACS had hardly changed. Then almost at a point where hardness stopped rising, its electrical conductivity virtually leaped forward, thus forming a sail shaped envelope. Like very many previous investigators, Chihoski also presented the sequence of precipitates as:

Supersaturated solid solution α \rightarrow G.P. zones \rightarrow Θ'' \rightarrow Θ' \rightarrow Θ (CuAl_2)

According to Chihoski, G.P. zones are finely dispersed sites of copper concentration and strain nodes of precipitates formed during the initial stage of age hardening of quenched supersaturated solid solution. G.P. zones are coherent with the main matrix of aluminum in the alloy, therefore as the G.P. zone precipitates grow in size and

number, they provide higher strength and hardness to the alloy. As the aging progresses, G.P. zones are then transformed into Θ'' metastable precipitates (CuAl_2). During the next stage of this continuous aging process, incoherent Θ' precipitates are formed either due to the transformation of Θ'' particles or direct nucleation of Θ' precipitates and as a consequence of these reactions the alloy loses its strength and hardness.

Aging temperature seems to have a very pronounced effect on successive transformations of metastable particles. Aluminum alloy when aged at a slightly elevated temperature of 200°C , took a very short time to start transformation of Θ'' precipitates into Θ' particles. At a higher aging temperature of 350°C a direct nucleation of Θ' precipitates seems to have occurred (24).

2.11. FATIGUE CRACK GROWTH UNDER CONSTANT AMPLITUDE LOADING

2.11.1. INTRODUCTION TO CRACK GROWTH THROUGH 2xxx ALLOYS

2.11.2. GENERAL

Crack growth through an aircraft frame depends upon strength, corrosion resistance and fracture toughness of the aluminum alloys used. The fatigue characteristic now receiving the greatest attention by the airframe industry is the rate of growth of a fatigue crack. Most airframes are now being designed with the assumption that a flaw dimensionally below the limits of detection by nondestructive testing is present. In the stable crack growth region, the rate of crack growth determines the intervals between the inspection periods or the ability to design to higher stress and reduced weights.

2.11.3 EFFECT OF MICROSTRUCTURE OF 2xxx ALUMINUM ALLOY ON FATIGUE CRACK GROWTH

W.G.Truckner, et al (2) measured the crack growth rate of high strength aluminum alloys by selecting precracked specimens and cycled about some mean stress. The crack length was monitored during the

test. The relative performance of materials tested using identical specimens was evaluated by comparing the curves for crack length versus number of cycles. The stress intensity range at the crack tip was calculated along with the slope of the curve for a crack length versus number of cycles providing crack growth per cycle. A transmission electron microscopic analysis provided microstructural features of the tested specimens.

Fractographic examinations revealed that cracks propagated in different ways in the region of high, intermediate and low growth rate. It was observed that for a high crack growth rate the fracture was similar in appearance to a tensile failure. The microstructural analysis showed that separation occurred between the large intermetallic particles and the matrix. These smaller cracks then grew by the coalescence of voids that were initiated at dispersoids. At intermediate crack growth rates, the crack grew by advancing a definite amount per stress cycle and it left evidence of striations. The magnitude of the crack advance and the character of the striations depended on composition, microstructure and environment. At the low crack growth rate, the crack did not advance a definite amount per cycle rather it advanced in a complex manner along (111) or (100) slip-planes, depending upon the environment. The major metallurgical factors controlling the crack growth rate at low ΔK appeared to be the elements that controlled the metastable precipitates.

J.T.Staley's research work of 1975 shows an improvement in fatigue crack growth rates at higher ΔK due to improvement in the fracture toughness of aluminum alloys (8). There after in the year 1979, Staley (6) reported the effect of volume fraction of coarse intermetallic particles on the fatigue crack growth rate under constant amplitude loading depends upon temper as well as on the level of ΔK . At higher ΔK , decrease in volume fraction of intermetallic particles showed increase in the fatigue crack growth resistance for higher strength -T86 temper while negligible effect occurred for the fatigue resistance of lower strength -T31 temper. While at lower ΔK , the volume fraction of intermetallics was found to have negligible effect

among the different tempers.

2.11.4 EFFECT OF INTERMETALLIC PARTICLES ON FATIGUE CRACK INITIATION

In 1978, C.Y. Kung (7) conducted an experimental analysis into the initiation and growth of microcracks in commercial precipitation hardening aluminum 2024-T4 and 2124-T4 alloys. Under constant loading the results demonstrated that when the stress level was high, fatigue cracks initiated along slip bands and were not associated with intermetallic particles. However at low stress level intermetallic particles have considerable effect on fatigue crack initiation of 2xxx alloys. In 2024-T4, more than 95% of the initial cracks were associated with the intermetallic particles. This effect was attributed to the ability of particles to increase the local stress, therefore increase the probability of introducing persistent slip bands, PSB.

2.12 AGING AND FATIGUE CRACK GROWTH RATE THROUGH 2XXX ALUMINUM ALLOYS

Precipitation hardening has a marked effect on the fatigue crack growth under constant amplitude loading. This effect is attributed to the relative abilities of different precipitates to resist degradation from the environment and improve the fatigue crack resistance of the precipitation hardening alloy. The higher the fatigue crack resistance then the slower is the crack growth rate and thus a higher fatigue life results.

W.G. Truckner et al (2) performed fatigue tests using underaged and overaged specimens under the same loading conditions and established that a specific type of precipitate controls the fatigue performance of aluminum alloys. Resistance to fatigue crack propagation increased progressively as the degree of precipitation increased. Structure containing G.P. zones formed during underaged conditions had the lowest resistance, while incoherent θ' formed

during overaged conditions had higher fatigue crack resistance than the underaged (G.P. zones) alloy.

Sanders and associates (10,14) conducted strain controlled fatigue on aluminum 2024 alloys and found the results were similar to those established by W.G. Truckner (2). T.H. Sanders also demonstrated that 2024 alloys can either strain harden or soften depending on the temper. While comparing an underaged aluminum 2024-T351 alloy (G.P. zones) to an overaged 2024-T851 alloy (Θ' precipitates) tested under constant strain amplitude established that despite its considerably lower yield strength, underaged 2024-T351 developed a much higher cyclic flow stress. While the overaged 2024-T851 had lower monotonic yield strength and lower cyclic flow stress.

Another study conducted by Park et al (40) showed a complex fatigue behavior of an aluminum Al-3.0 wt% Cu alloy. Both the polycrystalline and single crystal specimens of the alloy were tested under constant amplitude loading. The aging treatments were performed for various aging times at 160, 220, 300, and 350°C. The tensile stress, and fatigue response were measured and analyzed. The precipitate morphologies, and measurement of size and average interparticle distance of the particles were analyzed by using a transmission electron microscope, TEM.

TEM analysis showed that the microstructure produced by the aging condition at 160°C for 5 hrs contained Θ'' precipitates where as at 220°C for 2 hrs contained semicoherent Θ' and at 300°C for 48 hrs had only Θ precipitates. During overaging conditions, the interparticle distance increased with aging due to both overaging and dissolution of metastable precipitates. Park and associates then related interparticle distance to the yield stress and fatigue life of Al-3.0% Wt.Cu alloy.

The yield stress and fatigue life of the underaged Al-3.0% Wt.Cu specimens increased progressively up to an aging condition of 220°C for 2 hrs at which an interparticle distance of 1500Å^o was observed between Θ' particles. At an aging condition of 220°C for 5 hrs, for

the microstructure containing Θ' particles, the yield stress reached its maximum value while a drastic decline in the fatigue life of the alloy was observed. This decline in fatigue life was attributed to quite pronounced misorientation between adjacent cells as a result of dislocation loops between the twisted and plastically deformed Θ' precipitates. Fatigue life of overaged alloy continuously declined with dissolution of Θ' precipitates and increase in interparticle distance. The specimens when aged to 350°C for 48 hrs showed a large increase in fatigue life compared to the original alloy. This increase in fatigue life was a result of Θ equilibrium particles produced and dislocations generated on cycling. Microstructural analysis of the alloy contained Θ particles and had an induced dislocation structure in the matrix with regular cell boundaries that provided higher fatigue life.

Another study by Hidayetoglu et al (41) looking at the effect of aging on the Bauschinger effect in aluminum 2024 indicates that the alloy when overaged at an elevated temperature showed an improved fatigue life. However, strongly overaged 2024-T4 alloy had a fatigue life comparable to the original alloy.

Hidayetoglu and associates reviewed some of the previous work on aging and inflected loops in aluminum 2024-T4 alloy. They pointed out that aluminum alloy 2024 initially in the -T4 (naturally aged) condition and subjected to additional aging at an elevated temperature may exhibit inflected stress-strain hysteresis loops when it is subsequently fatigue cycled at room temperature. Inflected loops are absent in -T4 condition and appear during the first fatigue cycle in underaged material and are strongly developed after aging to peak strength and somewhat beyond. In all cases, the inflections disappear rapidly with continued cycling. Coincident with the appearance of inflected loops there is a dramatic increase in Bauschinger effect and the fatigue response shifts rapidly from cyclic hardening to moderate cyclic softening.

The aluminum 2024-T4 alloy specimens were artificially aged at

temperatures of 190°C and 300°C respectively for aging time periods ranging up to 336 hours. Some of the tests conducted were S-N fatigue tests, yield tests as a function of aging time, microstructural analysis and optical metallography tests (41).

Aging at 190°C for first half an hour caused the yield stress to fall below the -T4 condition value. The yield stress then rose rapidly to its maximum value after aging for about 10 hours. Thereafter the yield stress gradually fell with aging time as was recorded up to 336 hours.

The underaged alloy from -T4 condition up to aging for 2 hours exhibited normal hysteresis loops with no visible inflections. The metallographic examination showed fairly straight well defined slip bands. When the strain direction was reversed, cutting of G.P. zones occurred in the reverse direction at a stress level comparable with the forward yield stress. The slip remained predominantly planar and the stress/strain hysteresis loop exhibited a normal Bauschinger effect.

A dramatic change in behavior of the alloy occurred between aging times of approximately 2 and 10 hours at 190°C and was attributed to the development of strong nonshearable precipitates (presumably θ') that dominated the mechanical response of the material at longer aging times. The looping process stored populations of mobile dislocations around each nonshearable precipitate. When the stress direction was reversed, these dislocations provided a limited amount of strain in the reverse direction at a relatively low stress. In contrast to the underaged conditions, the material aged sufficiently to develop a strongly inflected hysteresis loop and therefore higher fatigue life (41).

The behavior of the strongly overaged 2024-T4 alloy was rationalized in terms of the further development of nonshearable precipitates during aging. The strengthening particles were relatively smaller in number (dissolution of nonshearable θ' precipitates). Wide space

between the particles made it possible for dislocations to move easily in the forward direction on initial loading and provided low yield stress. Because of the large spacing between the particles, only a relatively small fraction of the mobile dislocation density were stored, that resulted in a smaller Bauschinger effect and consequently a relatively lower fatigue life.

While investigating optimization of thermomechanical processing of Al-Cu-Mg alloys so as to increase strength without sacrificing fatigue resistance or fracture toughness, Thompson and Levy (42) literature reviewed the associated areas. The review indicated that fatigue crack growth rate in aluminum 2024-T3 (room temperature aged) was superior to 2024-T8 (elevated temperature aged). This was attributed to difference in microstructures. The aluminum alloy of -T3 temper contained only extremely fine G.P. zones which can more effectively block localized irreversible slip at the crack tip, which is necessary for crack extension. While aging at an elevated temperature -T8, prior to deformation results in coarse precipitates which are undesirable from toughness and fatigue considerations. These coarse precipitates promote intergranular fracture.

Contrary to the claims by previous researchers, Thompson and Levy (42) could not conclusively demonstrate that the thermomechanical processing treatments affected the fatigue crack propagations. It can be seen that a wide variety of results have been found on the effect of aging on fatigue behavior of 2xxx and 7xxx series of aircraft alloys. Some claim that overaging improves the fatigue life of 2024 and 7075 aircraft alloys while others found the results otherwise. Therefore, as desired by "National Aeronautical Establishment Ottawa", a research project has been set to evaluate the effect of aging and overaging on the fatigue life of 2024-T3 and 7075-T6 alloys. The main focus of the project was to evaluate the effect of aging on material properties, fatigue crack propagation and microstructural analysis.

2.13 SUMMARY

Main focus in the summary is on those items that are directly or indirectly applicable to the present research work.

The three major types of particles formed during processing, and thermal reaging are intermetallic secondary particles, dispersoids, and metastable particles. During solidification above 423°C, 7xxx and 2xxx series aluminum alloys, zinc, magnesium and copper elements combine with the impurity elements such as iron, silicon, and chromium to form secondary intermetallic particles. The coarse intermetallic particles are brittle. During cyclic loadings as the local strain exceed some critical value, these secondary intermetallic particles provide preferential crack paths ahead of the crack tip. Secondary particles of size 6 μm or greater have the ability to increase local stress thereby increase the probability of formation of PSB's (1,2,5).

Dispersoids are 0.01 μm to 0.5 μm size particles. Fine grains of high melting point elements such as chromium, and manganese are retained in the supersaturated solid solution but they precipitate during subsequent thermal treatments at temperatures above 425°C. Dispersoids in general provide very insignificant strengthening effect. However alloys containing Al₃Zr dispersoids develop higher resistance to stable crack propagation. Decreasing the volume fraction of dispersoids provides higher fracture toughness (6).

Metastable precipitates (0.002 to 0.01 μm) are the smallest of second phase particles and contain the major solute elements zinc, magnesium and copper. Both 7xxx and 2xxx series alloys have identical sequences of precipitate in the process of precipitate hardening or softening. The precipitates of 7xxx series alloys contain the major solute elements zinc, magnesium, and copper while the precipitates of 2xxx have copper and magnesium as major solute elements (14,32).

Different phases of metastable particles of 7075 aluminum alloy and their sequence is as:

Supersaturated solid solution \longrightarrow G.P. zones $\longrightarrow \eta'' \longrightarrow \eta' \longrightarrow \eta$

G.P. zones and η'' are shearable, coherent precipitates and develop in an uncontrolled manner during quenching of the solid solution (5). When the atomic ratio $N_{Mg} \neq N_{Zn}$ the excess species form clusters of Zn and contribute to overall hardening of the alloy. These nucleate homogeneously throughout the alloy. Growth rate of G.P. zones and η'' precipitates depends upon the initial quenching rate and reaging conditions of temperature and time. As the coherent precipitates grow, strength and hardness of the 7075 alloy increases. 7075 alloy has its highest strength when it consists primarily of G.P. zones ($75 A^\circ$) with 5% semicoherent η'' phase (15). G.P. zones and η'' precipitates have the ability to provide planer reversible slip and in doing so they improve the fatigue resistance to the crack propagation and higher fatigue life. During overaging η' semicoherent or incoherent precipitates (i) nucleate independently along the grain boundaries and (ii) are formed at the expense of η'' . The nonshearable η' precipitates, as they grow provide higher dislocation density and soften the alloy (1,19). Microstructure changes within the alloy can be monitored through an electrical resistivity measurement. Increase in the electrical resistivity can be related to formation of G.P. zones and η'' precipitates while decrease in the electrical conductivity are due to formation and coarsening of η' and η particles (21).

Formation of η' precipitates is accompanied by depletion of zinc from the matrix of the alloy. Decrease in the yield strength and its hardness are associated with formation and coarsening of incoherent, nonshearable η' and η particles (20).

Reaging and overaging conditions effect the fracture toughness and resistance to crack propagation and stress corrosion cracking. During underaged conditions fracture is transgranular caused by shearing of precipitates by dislocation movements. 7xxx aluminum alloy reaged to peakaged condition can develop dense slip bands and with additional

stress these bands may widen (10).

Resistance to fatigue crack is affected by the nature of the precipitates and resistance to degradation from the environment. Fatigue performance depends upon the type of precipitates rather than on the yield stress (2).

Lower crack propagation rate during underaged conditions can be related to reversible slip within the plastic zone (26). While during the overaged conditions, precipitates having high stacking energy can be associated to cross slip that can retard the fatigue growth rate thereby provides improved fatigue life. Aggressiveness of environment induces oxide induced crack closure that also improves the fatigue life of the alloy (27). Superior resistance to crack growth of overaged aluminum alloy can be derived from the greater crack tip irregularity. Corrosion fatigue and stress corrosion cracking of peakaged alloy can be associated to segregation of magnesium over the regions on the surface of 7xxx alloy while no apparent segregation in the overaged conditions. The environmental susceptibility of 7xxx alloys in the peakaged condition can be attributed to formation of $Mg(OH)_2$ and MgO (30).

Precipitate hardening process of 2xxx series aluminum alloys has a sequence of precipitates very similar to ones for 7xxx series aluminum alloys and can be expressed as:

Supersaturated solid solution \longrightarrow G.P. zones \longrightarrow Θ'' (coherent) \longrightarrow Θ' (semicoherent and incoherent) \longrightarrow Θ (Al_2Cu).

where the stable Θ has the chemical composition Al_2Cu .

Precipitate hardening process in 2xxx aluminum alloys is complex and in any reaged condition, the relative proportion of different particles dictate the resultant effect (21,34). Some times the complex process involves formation and growth of one phase along with dissolution of an other phase simultaneously and the most predominant phase (precipitates) controls the behavior of the alloy (22).

Increase in hardness of reaged alloy depends upon the variation in

stress field in the vicinity of the precipitates, coherency of Θ' precipitates with the matrix, size and distribution of precipitates while loss in coherency of Θ' precipitates results in softening of 2xxx alloys. During progressive reaging transformation of Θ'' precipitates to form Θ' along the grain boundaries results in depletion of copper from the matrix of the alloy and can be related to increase in the electrical conductivity of the 2219 alloy (21,34).

During the reaging process, formation and dissolution of precipitates can be observed through a thermogram by recording change in heat capacity of precipitates. Analysis of exothermic and endothermic reactions provide formation and dissolution of precipitates of different chemistries and can be identified from the exothermic and endothermic peaks of the thermogram (16).

Aging condition of 2219 alloy was identified through H-C sail diagram. Material hardness and its electrical conductivity depend upon the quenching rate and reaging condition. During underaged conditions, there is a large increase in the material hardness for the corresponding increase in the electrical conductivity. While during overaged conditions there is a gradual decrease in the hardness for a much larger increase in the corresponding electrical conductivity (23,24).

Reaging condition of 2xxx series aluminum alloy can be fully explained by using the H-C sail diagram. However neither H nor C alone can define the state of reaging condition. A complex fatigue behavior of 2xxx series aluminum alloy can be associated to the nature and size of the precipitates.

The yield stress and fatigue life of an underaged Al-3% wt Cu increases progressively up to an aging condition at which the interpretable distance of 1500 A^o was observed. While decline in the fatigue life was associated to an increase in misfit of Θ' incoherent precipitates (40). Another study associated increase in fatigue life of an overaged 2024 alloy to Bauehinger effect (41).

Improved fatigue life of overaged 2xxx series aluminum alloy can be related to development of cross slip due to incoherent precipitates.

Electrical resistivity behavior provides higher resistivity of 2xxx alloy when the size and spacing between the precipitates is comparable to the wavelength of conducting electrons. There is sharp drop off in the electrical resistivity near the peakaged condition indicating onset of overaging condition to form incoherent θ' precipitates (21,34).

The present work requires study of the effects reaging and overaging on the fatigue life of 7075-T6 and 2024-T3 aluminum alloys. Some of the key areas of this literature review can be applied to the project work. These include identification of reaged conditions by using H-C sail diagram, and material hardening and softening during underaged and overaged conditions respectively. The relative hardening and or softening will be analyzed on the basis of metastable precipitates. Fatigue behavior will be analyzed on the basis of fatigue crack propagation rates. Interaction between the dislocation movement and the nature of precipitates of the reaged condition will provide the answers for a particular type of fatigue behavior. Comparison of fatigue crack growth rates will provide the comparison of their fatigue lives.

CHAPTER 3**EXPERIMENTAL TECHNIQUES AND PROCEDURES****3.1 GENERAL**

This project on the effect of precipitate hardening on the fatigue lives of aircraft alloys 2024-T3 and 7075-T6 was investigated by using several different types of tests such as: mechanical property tests, electrical conductivity tests, material hardness tests, and fatigue crack propagation tests. The different types of tests require different testing facilities, therefore the test specimens were designed accordingly. The test specimens were then heat treated at pre-decided temperatures and corresponding time periods. Some of the tests were conducted to study the general material properties (strength/ductility) of the two alloys while other tests were conducted to determine fatigue behavior under the types of loading consistent with aircraft operating conditions. All the different tests were conducted on the original as well as on the heat treated alloys. The project was completed in the sequences described in this Chapter.

3.2 MATERIAL SPECIFICATIONS AND CHEMICAL COMPOSITION OF 2024-T3 AND 7075-T6 ALUMINUM ALLOYS

The test specimens for the tensile tests, and the material fatigue test were designed and were cut from a 0.1016 cm metal sheets which are used to fabricate CT-114 bodies, normally in the form of aircraft skin. The chemical compositions of the original 2024-T3 and 7075-T6 differ. The chemical compositions of the "mil specs" by weight% for both 2024-T3 and 7075-T6 was supplied by the material suppliers and is recorded in Table 3.1

Table 3.1: Chemical composition of aluminum alloys by weigh %.

METAL	2024-T3		7075-T6	
	Min.	Max.	Min.	Max.
SILICON		0.50		0.40
IRON		0.50		0.50
COPPER	3.80*	4.90	1.20*	2.00
MANGANESE	0.30	0.90		0.30
MAGNESIUM	1.20*	1.80	2.10*	2.90
CHROMIUM		0.10	0.18	0.28
ZINC		0.25*	5.10	6.10*
TITANIUM		0.15		0.20
OTHERS		0.15		0.15
ALUMINUM	REMAINDER		REMAINDER	

* major differences.

3.3 DESIGNING, CUTTING AND PREPARATION OF TEST SPECIMENS

In order to conduct safe and successful tests on such thin sheets careful consideration was given to some of the critical factors involved in both testing and handling the specimens.

Physical dimensions of both the tensile test specimens and fatigue test specimens are as shown in Figure 3.1. The design calculations for the tensile test specimens were based upon the material properties of 7075-T6 and 2024-T3 aluminum alloys. Literature values of mechanical properties of wrought aluminum alloys were used initially in choosing the operating ranges of the materials testing machine. Tests were conducted using a servo controlled hydraulic testing machine, MTS model 810 as shown in Figure 3.2.

The overall length of the designed specimens for both the alloys was 33.02 cm with 10.16x10.16 cm square holding ends. The stress concentration between the test section and the holding ends was reduced by modifying the shape of the ends. In order to hold the thin test specimens on the MTS machine, specially designed holding grips were used. A torque wrench was used to apply uniform bolt pressure on the holding grips so as to avoid any torque or rotational friction between the bolts and the test specimen.

The physical dimensions of the fatigue test specimen were based on design parameters such as : (i) a single edge notch, SEN, configuration specimen for the fatigue test under constant end displacement loading. (ii) the ratio of height, h , to width, W , $\frac{h}{W} = 1.5$ was maintained, where h is the distance of crack plane from the centre of loading. This allowed use of a specific known compliance function for a single edge notch conditions. It is worth mentioning that under constant displacement loading tests, the compliance function $f(a/W)$ for a restrained end condition SEN configuration depends upon the ratio of $\frac{h}{W}$ (46).

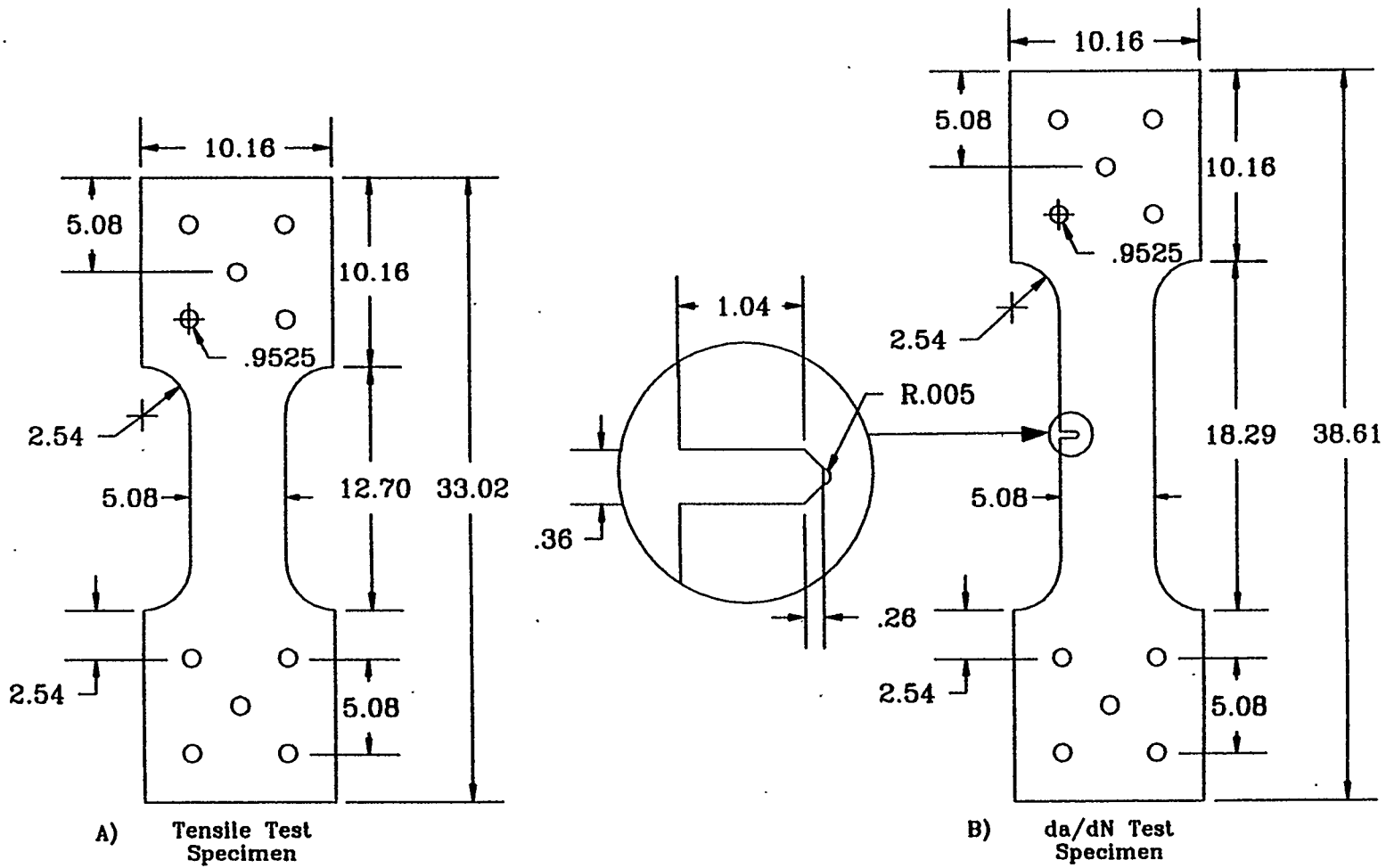


Figure 3.1: Configurations of the Test Specimens

All fatigue test specimens were notched by using a sharp wedge shear machine. The specimens were notched by taking few specimens at a time and resulted in overall variation of notch length (depth) from 10 mm to 12 mm. The notches were cut out sharp enough to reduce the crack initiation fatigue cycles by a large factor.

The total specimen requirement for both the tensile tests and the fatigue tests was worked out by considering a test sample size that could provide a relatively high reliability factor for a reasonable amount of testing. After initial tensile tests on both the original alloys, it was decided to use a sample size of four specimens for each heat treatment as well as for the original alloys.

The material hardness and electrical conductivity tests were conducted with small rectangular pieces of the aluminum alloys. The size of the rectangular pieces were 7.62 cm x 10.16 cm for each heat treatment and this was decided simply on the basis of an approximate requirement for both the hardness and the electrical conductivity tests equipment. In order to conduct micro-hardness and electrical conductivity tests keeping within the restraints of the testing machines, the test specimens were then cut from these heat treated sheets to much smaller sizes of 2.5 cm x 3.81 cm, and 5.08 cm x 3.81 cm respectively.

For a superior and high precision cutting of both the tensile test specimens and the fatigue test specimens, a CIM cutting & machining system "Matsuura Machinery Center" was used to cut a stacked arrangement of specimens. The assignment of cutting the specimens was handled by CAD and CAM section (the manufacturing division) of the Department of Mechanical Engineering, U F C. All the test specimen were then identified for each heat treatment before starting the reaging treatment.

3.4 HEAT TREATMENT OF 7075-T6 AND 2024-T3 ALUMINUM ALLOYS

Reaging (artificial aging) of each of these alloys has invariably been considered a function of both the temperature and the reaging time. The heat treatment schedule for each of the two alloys was carefully decided so that each alloy was reaged to specific conditions. Knowledge of processing of original 7075-T6 and 2024-T3 was an important factor in finalizing the heat treatment schedules.

The processing of the original 2024-T3 alloy involves solutionizing the alloy followed by quenching, cold working and finally natural aging at room temperature providing the -T3 condition. In contrast to 2024-T3, the original 7075-T6 alloy was processed by solutionizing followed by quenching and an artificial aging at 120°C for a period of 24 hours. Therefore, considering the tempering conditions of the alloys, it is expected that both alloys are slightly under aged. However since 7075-T6 alloy was initially aged at a higher temperature (120°C) compared to naturally aged 2024-T3, therefore the level of the aging condition of 7075-T6 is expected to be higher than that of 2024-T3. Thus it was desired to setup two different heat treatment schedules for the two alloys. These schedules were carefully worked out so that each alloy could be reaged to under aged, peak aged, and over aged conditions respectively. The time and temperatures in the heat treatment schedules were controlled by using the Arrhenius rate equation. According to which diffusion (nucleation and growth) of precipitates in metals alloys is governed by

$$\text{rate} = Ae^{-Q/RT} \quad (1)$$

Where A is preexponential constant (independent of temperature), Q is the activation energy, R is the universal gas constant and T the absolute temperature.

The two alloys differ in their chemical composition, original tempers, and precipitation mechanisms. However it is possible to set rough time and temperature reaging conditions to obtain comparable

precipitation conditions for each alloy by using the above Arrhenius rate equation.

The heat treatments of the alloys were conducted in an automatic temperature controlled (Power-O-Matic 60 System) oven. Before starting each of the heat treatments, the oven temperature was stabilized to a predecided temperature. It is worth mentioning that the temperature of the oven was controlled by using a built-in rotating cam that could change the temperature by 0.1°C . In order to study the initial temperature distribution inside the oven, a set of as many as nine thermocouples were arranged on dummy masses of the same alloys held on a set of vertical stands. These thermocouples were hooked up to a time-temperature recorder that was capable of sensing and recording temperature up to 0.01°C at any desired time. Once the temperature of the oven had stabilized, the dummy loads were then replaced by bundles of actual test specimens of the two alloys in case of common reaging condition and or by a bundle of test specimens of any one of the alloys for a separate reaging condition. The temperature distribution throughout the oven was not uniform and there was temperature fluctuation that occurred at a given point inside the oven during the heat treatment process. However the temperature fluctuations were within an acceptable level of $\pm 3.0^{\circ}\text{C}$ and the whole oven was successfully maintained within $\pm 1.5^{\circ}\text{C}$ of any required heat treatment temperature.

Measurement of an effective aging time for a given heat treatment temperature was another critical factor. Once the oven temperature had stabilized, the dummy loads were replaced by bundles of actual test specimens. During the replacement time of about two minutes, the oven door was open which caused the oven temperature to drop by about 50°C . After replacement of test specimens the oven door was immediately closed to start the reaging process. However it took a certain time for the oven to get back to the stabilized temperature. Therefore, it became essential to correct the recorded aging time. This time correction was calculated from the time-temperature

relationship during the specimen replacement period. This aging time correction when applied to the aging time recorder provided an effective reaging time. Time- temperature relationships during specimen replacement were different for different heat treatment conditions, therefore for each reaging condition the recorded time was corrected for an effective aging time. The heat treatment conditions for each alloy are given separately as:

- (a) Heat treatment conditions for 7075-T6 alloy:
 - (i) Reaged at 107°C for 150 effective hours.
 - (ii) Reaged at 135°C for 150 effective hours.
 - (iii) Reaged at 175°C for 38 effective hours.
 - (iv) Reaged at 175°C for 150 effective hours.
 - (v) Reaged at 175°C for 300 effective hours.
- (b) Heat treatment conditions for 2024-T3 alloy:
 - (i) Reaged at 95°C for 150 effective hours.
 - (ii) Reaged at 135°C for 150 effective hours.
 - (iii) Reaged at 175°C for 150 effective hours.
 - (iv) Reaged at 175°C for 300 effective hours.
 - (v) Reaged at 175°C for 600 effective hours.
 - (vi) Reaged at 207°C for 300 effective hours.

According to the Arrhenius rate equation, the following conditions between the two alloys should be comparable:

1. 7075-T3 alloy reaged at 107°C for 300 hours and 2024-T3 alloy reaged at 135°C for 300 hours.
2. 7075-T6 alloy reaged at 135°C for 300 hours and 2024-T3 alloy reaged at 207°C for 300 hours.

3.5 MECHANICAL PROPERTY TESTS OF AIRCRAFT ALLOYS

3.5.1 TENSILE TEST

The tensile tests for test samples of the original alloys as well as for the heat treated samples were conducted using an MTS machine. A specially designed specimen holder was used to apply uniformly distributed loading. The experimental test conditions were decided on

the basis of dimensions of test specimens and literature values of their material properties. The test conditions were kept the same for all tests. The tensile test was conducted by using a strain clip gauge mounted on the specimen. The MTS machine was operated under stroke control. In order to apply a uniformly changing load, a RAMP step function was used at a frequency as dictated by ASTM E-8 material testing procedures. These operating conditions were kept the same through out the tensile testing of both alloys. A sample of four specimens was tested for each aged and reaged conditions.

Two chart recorders were used in parallel for the tensile tests. One of the recorders was adjusted for a calibration value of the clip gauge (strain gauge) attached to the test specimen and the other recorder was used for the load-extension relationship of both the test specimen and the specimen holders. This experimental set up provided a graphical approach for actual relationship between load and extension of the test specimens.

Before running each tensile test, initial load and clip gauge output were adjusted to zero. All the loading conditions were rechecked, clip gauge pin was released and the recorder for the load-extension calibration was re-adjusted to zero. As a precautionary measure during each test operation, the moment the recording pen crossed the loading corresponding to ultimate stress, the clip gauge was taken off the test specimen.

From the graphical analysis provided by the two chart recorders, the material properties such as tensile yield stress (σ_y), tensile ultimate stress (σ_u), and fracture strain (ϵ_f) were determined for each specimen and then averaged for the each sample size. Statistical variation for each test sample was also determined.

3.6 MATERIAL PROPERTIES TESTS OF THE AIRCRAFT ALLOYS

3.6.1 MEASUREMENT OF MACRO-HARDNESS 7075-T6 AND 2024-T3 ALLOYS

The purpose of the macro-hardness tests was two fold (i) to establish the state of precipitate hardening of underaged, peakaged, and overaged conditions developed during artificial reaging and (ii) to study the relative changes in the material hardness with respect to the reaging temperature and the reaging time periods respectively.

The macro-hardness test was conducted using the T.M. All Scale hardness testing machine for standard and superficial "Rockwell Testing". The test specimens for the macro-hardness tests were cut to 3.81 cm x 5.08 cm sizes. In order to be consistent, Rockwell B scale was used for the measurement of all the macro-hardness tests. The testing machine provided direct measurement of macro-hardness of the alloys. A set of ten or more readings were taken for each aging condition providing both the statistical average and the corresponding standard deviation.

3.6.2 MEASUREMENT OF MICRO-HARDNESS 2024-T3 AND 7075-T6 ALLOYS

The micro-hardness tests were conducted using the "Micromet Tester" and the hardness of the alloys was measured in Vicker's hardness number. The test specimens were cut approximately to 2.54 cm x 3.81 cm and were tested under a square diamond tip using 200g operating load. The square diamond causes an indentation. The two diagonals of the indentation were measured to within 0.001 mm. The mean value of the diagonal of indentation was then used in conjunction with D.P.H hardness tables to find the corresponding Vicker's hardness (HV). A set of more than ten readings of micro-hardness were taken for each aging condition that provided an average value of micro-hardness and its corresponding standard deviation for the each case.

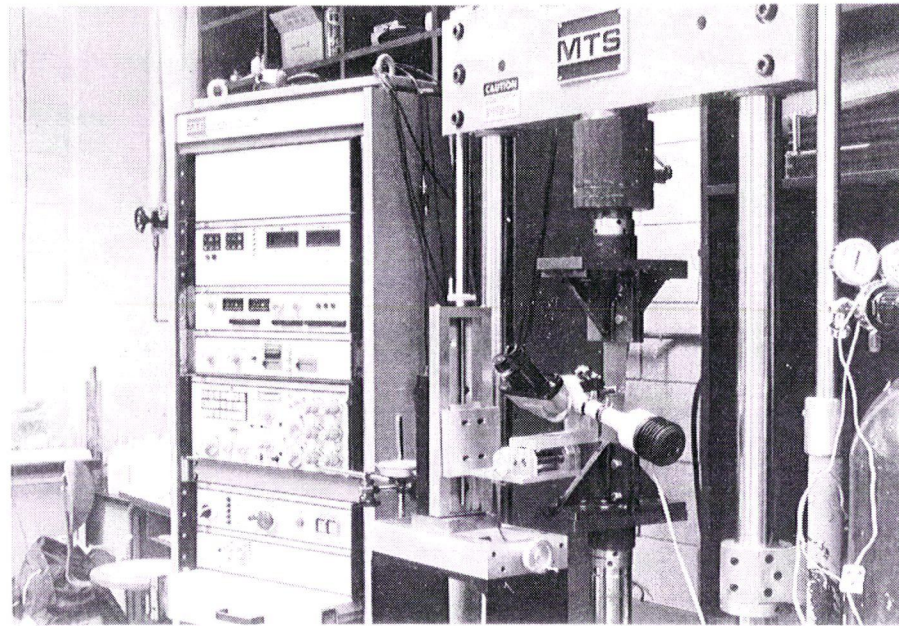


Figure 3.2: MTS machine with fatigue crack propagation test set-up.

3.6.3 MEASUREMENT OF ELECTRICAL CONDUCTIVITY OF 2024-T3 AND 7075-T6 ALLOYS

The purpose of the electrical conductivity test was two fold: (i) to verify the relative changes in the electrical conductivity of each alloy during progressive reaging of the underaged, peakaged, and the overaged stages of precipitation. (ii) to establish a qualitative relationship between depletion of copper from the main matrix of each alloy to the reaging condition, consequently formation of copper precipitates or intermetallic particles along the grain boundaries of the alloys.

A digital conductivity meter (FM-140) of Magma Flux corporation at NAE Ottawa was used to measure the electrical conductivities of the original as well as heat treated 7075-T6 and 2024-T3 alloys. This induced current electrical conductivity was measured in % IACS units. The instrument was calibrated at the beginning and end of each set of readings. In order to have a higher level of reliability in the test results, a set of more than fifteen readings were taken for each condition providing an average and standard deviation value of the induced current electrical conductivity.

3.7 MATERIAL FATIGUE TESTS FOR 2024-T3 AND 7075-T6 ALUMINUM ALLOYS

3.7.1 FATIGUE CRACK GROWTH MEASUREMENTS

The material fatigue test was designed to compare crack propagation rates of each alloy under different heat treatment conditions. This fatigue test was designed and setup to compare the crack propagation rates at low stress, intermediate and high stress intensity factors. The growth of the fatigue crack was measured using a high power optical microscope, and a dial gauge micrometer shown in Figure 3.2. Design and dimensions of da/dN test specimens are as shown in Figure 3.1. The fatigue test specimens were mechanically notched. Width and thickness of each specimen was measured by using a Vernier caliper to calculate the design loading for a given initial stress intensity

factor for a single edge notch (SEN) as:

$$\Delta K = \frac{\Delta P}{B \times W} \sqrt{a \pi} \times f(a/w) \quad (2)$$

$$f(a/w) = 1.1417 - 0.1634(a/w) + 3.1695(a/w)^2 - 4.5418(a/w)^3 + 3.5(a/w)^4 \quad (3)$$

where $f(a/w)$ is the compliance function polynomial for the SEN

$$\text{configuration with the ratio } \frac{h}{W} = 1.5 \quad (4)$$

$$A = B \times W \quad (5)$$

A, B, and W are the area of crosssection, thickness and the width of the test section of the specimen respectively. While a is the notch length and ΔP is the cyclic loading for the crack propagation rate test.

MTS machine provided cyclic loading to the test specimen while both the optical microscope and the dial micrometer were used for observing the crack tip and recording the growth of the crack respectively. This test was conducted under constant amplitude loading by using a Haversine wave function at a frequency of 5 Hz. MTS machine was operated under 50% load control and the operating conditions were kept the same through out the fatigue test.

Before turning the hydraulic system of the MTS machine on, the machine's electronic counsel was properly warmed up. The hydraulic system of the MTS machine was then turned on and all preliminary adjustments such as load range %, stroke range %, and D.C. error from the controller, remote control, counter input (frequency and type of wave function), counter multiplier, and preset counter from the digital functional generator were made. All these adjustments were checked on the digital indicator that displays input conditions, modes, over range and under range conditions. Initial load and displacement adjustments were made with set point potentiometer.

The test specimen was then fixed on the specimen holders fitted on the MTS machine and the loading was reset for zero static loading.

Initial crack length (notch) was measured by using both the optical microscope and the dial gauge. The load cycle operates between a minimum and a maximum, therefore to avoid measurement and control of minimum load during the test, it was adjusted and controlled to zero by using the main load/displacement set point potentiometer. The experimental data were collected for fatigue cycles verses crack lengths. Now by using initial crack length, load, specimen width, and thickness the change in stress intensity factor was determined as follows:

$$\Delta K = \frac{\Delta P}{B \times W} \sqrt{a\pi} \times f(a/W)$$

$$\Delta P = P_{\max} - P_{\min} \quad (6)$$

where $P_{\max} = \Delta P$, and $P_{\min} = 0.00$ (adjusted)

The loading conditions for all the three stress intensity ranges were calculated. Three test specimens, one for each stress intensity range to start with were considered for each aging condition.

Before starting the fatigue test, initial adjustments of both the optical microscope and the dial gauge micrometer were made. Cross hairs of the optical microscope was focused and adjusted at the notch (crack tip) and the position of the crack tip was recorded from the dial micrometer (Fig. 3.2).

The fatigue test was started at a low stress intensity range and the machine was run for 1000 cycles between crack length readings. A relationship between the number of fatigue cycles (N) and corresponding crack length (a) was measured and recorded. The same procedure was adopted for all of the fatigue testing conditions.

Fatigue testing was conducted at a low initial stress intensity, at intermediate and at high stress intensity factors such that about 4 MPa \sqrt{m} stress intensity factor overlapping occurred between the

successive stages. For the low stress intensity factor (6 MPa√m), a crack was initiated at 10 MPa√m followed by crack sharpening at 8 MPa√m and finally the stabilized crack growth due to cyclic loading was set at 6 MPa√m. Similarly for the intermediate stress intensity factor range, crack initiation, crack sharpening and crack propagation were conducted at loads corresponding to 14 MPa√m, 12 MPa√m, and 10 MPa√m respectively. However testing at the higher stress intensity factor region all the three stages were performed at 16 MPa√m.

In order to study and compare the crack growth behavior in each case, a computer program was used for data analysis. This program is based on the assumption that the crack propagates along a curved path given by a polynomial function of (a/W) . The degree of the polynomial was adjusted to provide a least squares fit between the theoretical and experimental curve and was of the order 10^{-5} or less. Once the required level of polynomial fit was achieved by adjusting the degree of the polynomial, then the output of the same program was extended for the relationship between $\log \Delta K$ and $\log (a/W)$.

It is worth mentioning that for the graphical analysis the experimental data was limited to the range for a steady and stable crack growth ($0.23 < (a/W) < 0.7$).

CHAPTER 4

RESULTS AND ANALYSIS

4.1 INTRODUCTION

In this chapter, statistical results from various experimental tests of both 7075-T6 and 2024-T3 aircraft alloys are presented separately. In order to discuss and correlate the reaging conditions to the fatigue life behavior of the alloys, experimental tests have been conducted in the following areas:

1. Mechanical properties tests: tensile test.
2. Material hardness tests: micro-hardness, macro-hardness.
3. Electrical conductivity tests.
4. The fatigue crack growth behavior: da/dN fatigue tests.

Analysis of each of the tests is presented. A general discussion of the possible correlation between the reaging conditions and the fatigue life of each of the two alloys is made in Chapter 5.

4.2 ALUMINUM ALLOY BEHAVIOR: 7075-T6

4.2.1 GENERAL

The original heat treatment for the -T6 condition involves solution treating the material followed by quenching and then artificial aging at 120°C for a time period of 24 hours. To conform to good practice, the aged condition should be slightly under aged as compared to an optimum aged condition. Among the reaging temperatures, 175°C is considerably above the original aging temperature of 120°C , therefore would likely lead to extensive amounts of over aging in the alloy. Thus it would be expected to have considerable effect on the material strength and property behavior even with a small amount of reaging above 120°C and especially at a high temperature of 175°C .

4.3 MECHANICAL PROPERTY ANALYSIS OF 7075-T6 ALLOY

4.3.1 TENSILE TEST

The tensile properties of the alloys in air at room temperature were established by using ASTM standard E8 [37]. The dimensions of the test specimens, and the physical measurements for the mechanical properties such as yield stress, tensile (ultimate) stress, and ductility were experimentally determined by the tensile test as described in Section 3.5. The results are recorded in Table 4.1 and the results of each mechanical property has been discussed separately in the following section. The graphical analysis of the behavior of these mechanical properties has been presented in the Figures 4.1 through 4.9.

4.3.2 YIELD STRESS BEHAVIOR OF 7075-T6 ALLOY

When, the original 7075-T6 alloy is heat treated at 107°C for 300 hours, it showed a slight improvement of approximately 4% in its yield stress. Beyond this condition, reaging at higher temperatures provides a continuous decrease in the yield stress (Fig. 4.1 and 4.3). The alloy, when reaged at 135°C for 300 hours, lost approximately 16% of its yield stress as compared to the original -T6 alloy. At higher temperatures the reaging effect on the yield stress is much more pronounced. There is a substantial loss of yield stress for the reaging condition at 175°C for 38 hours. The drop off in yield stress for this reaging condition is almost 42% over the original -T6 material (Fig. 4.2). Beyond the 38 hours reaging condition, reaging at 175°C for longer periods resulted in relatively smaller losses. Reaging for 150 and 300 hours provided successive losses of 25% and 28% respectively. As compared to the original alloy, reaging at 175°C for 150, and 300 hours provided losses of 56% and 69% respectively (Fig. 4.2).

Table 4.1: Tensile mechanical properties of 7075-T6 aluminum alloy.

Reaging condition	Tensile mechanical properties							
	Yield		Ultimate		Ultimate		Fracture	
	stress		stress		strain		strain	
	(MPa)		(MPa)		(%)		(%)	
Mean	Std.	Mean	Std.	Mean	Std.	Mean	Std.	
value	Dev.	value	Dev.	value	Dev.	value	Dev.	
As received.	508.23±27.92		588.54±8.62		7.05±0.69		9.75±0.20	
Reaged at 107°C								
for 300 hours .	528.01±3.38		572.82±4.41		6.14±0.21		8.72±0.22	
Reaged at 135°C								
for 300 hours .	426.95±7.03		501.61±6.14		6.65±0.50		8.96±0.24	
Reaged at 175°C								
for 38 hours .	294.79±1.72		392.34±2.34		6.55±0.33		9.00±0.09	
Reaged at 175°C								
for 150 hours .	222.06±3.58		336.43±1.86		6.78±0.30		7.72±0.59	
Reaged at 175°C								
for 300 hours .	159.80±20.41		276.93±20.54		6.56±0.42		8.73±0.14	

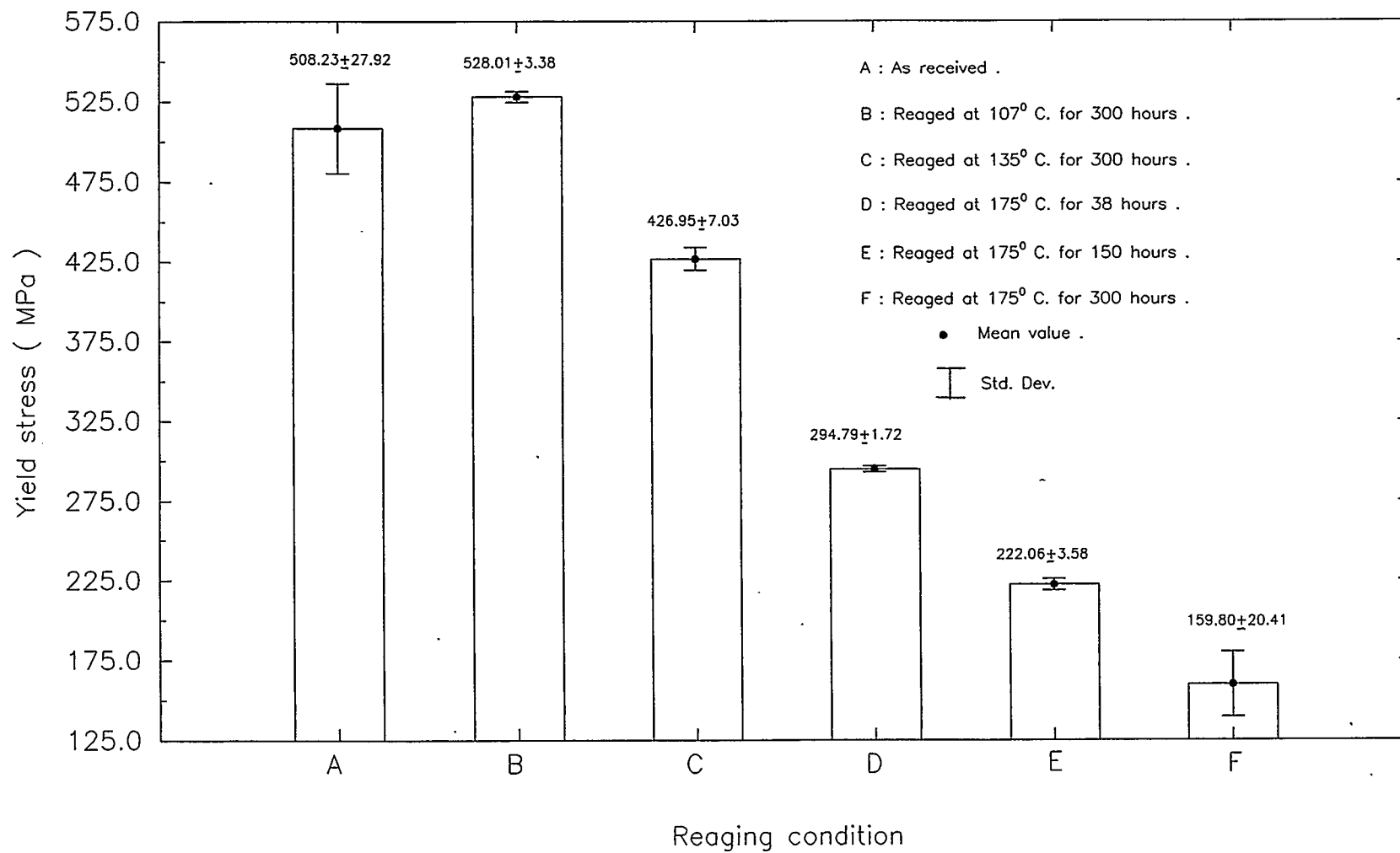


Figure 4.1: Variation of yield stress of 7075-T6 alloy under various reaging conditions .

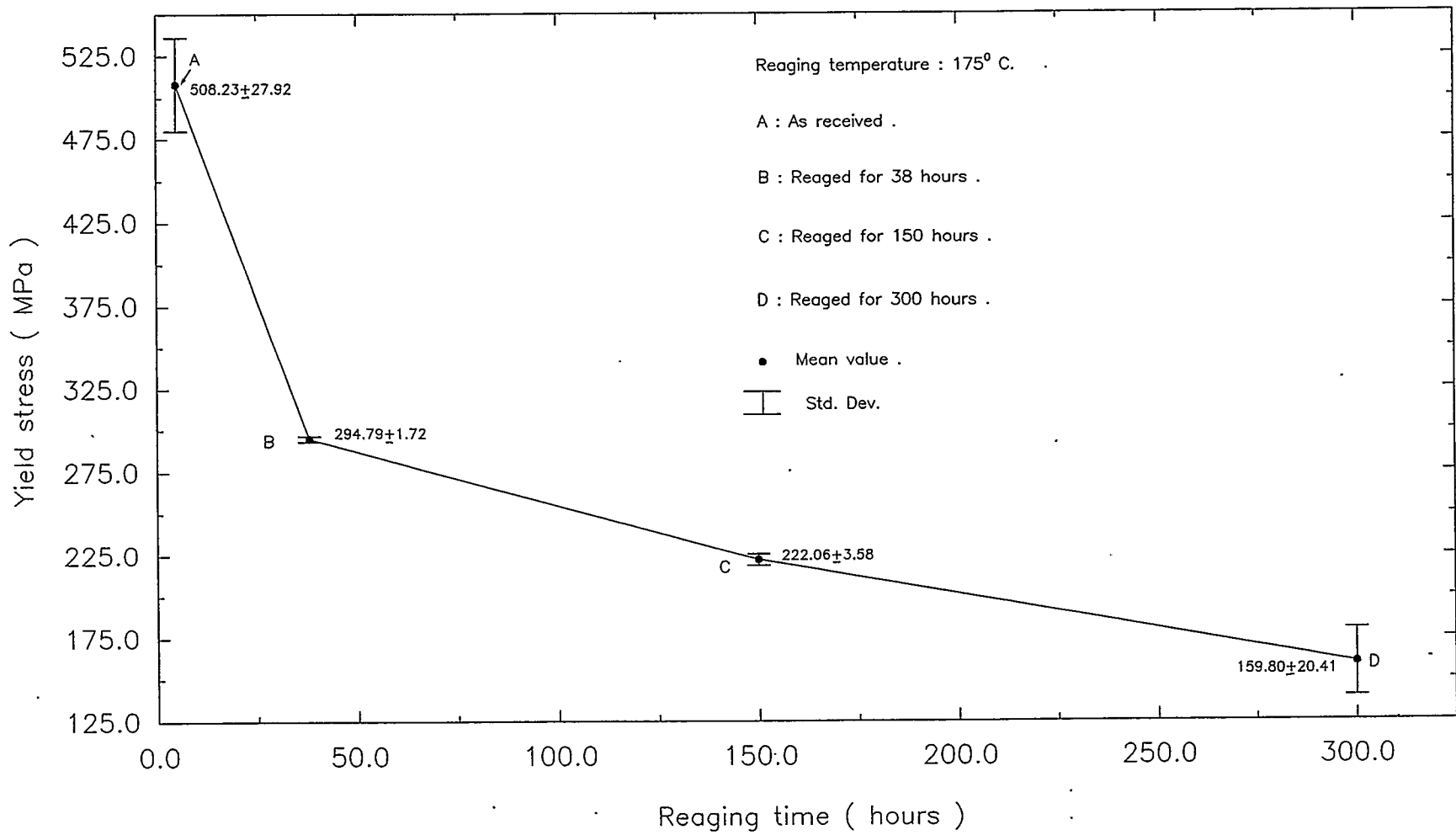


Figure 4.2: Relationship between yield stress and reaging time of 7075-T6 alloy at 175° C.

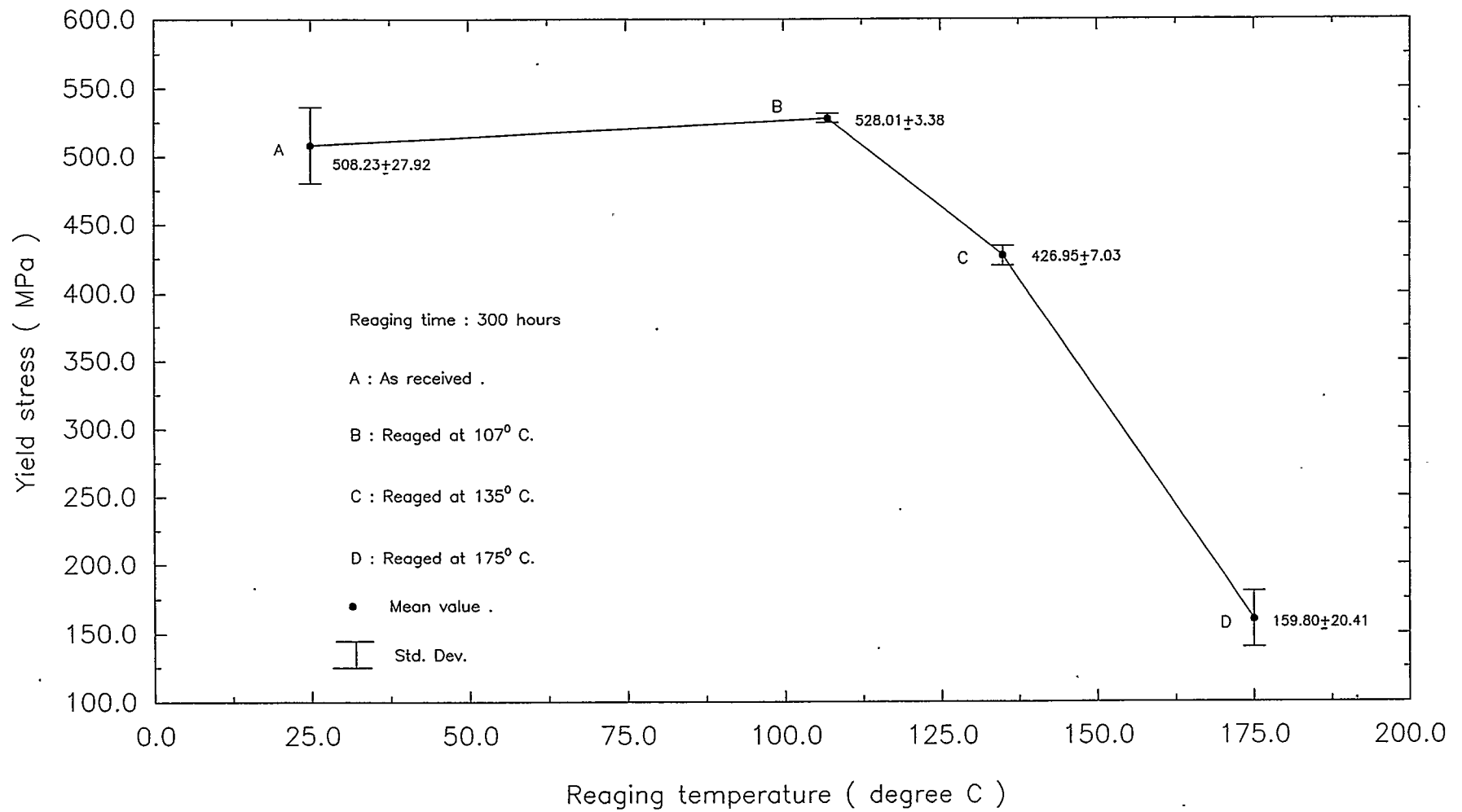


Figure 4.3: Relationship between yield stress and reaging temperature of 7075-T6 alloy at 300 hours.

4.3.3 ULTIMATE TENSILE STRESS BEHAVIOR OF 7075-T6 ALLOY

Examination of tensile test results show that on reaging, the ultimate stress of 7075-T6 continuously decreases (Table 4.1 and Fig. 4.4). The reaging effect above 120°C is much more pronounced. In general for reaging at higher temperatures and longer time periods, loss in ultimate stress of 7075-T6 alloy occurs continuously. This is quite evident from the fact that when 7075-T6 alloy is reaged at 175°C for 38, 150, and 300 hours, the losses in ultimate stress of the original alloy were found as 33%, 43%, and 53% respectively (Fig. 4.5). Beyond the reaging condition of 38 hours, reaging for 150 and 300 hours, provided relatively smaller losses. The successive losses under these two conditions when compared to 38 hours reaging condition were 14% and 18% respectively. In contrast to the wide spread change in the ultimate stress behavior above the original temperature of 120°C , the change in ultimate stress behavior below 120°C was quite minimal. Reaging at 107°C for 300 hours, shows a very slight decrease in ultimate stress being approximately 3% as compared to the original -T6 material. As expected, there is a considerable reaging effect above 120°C . A substantial drop off of approximately 15% occurs for the reaging condition at 135°C for 300 hours (Fig. 4.6).

4.3.4 DUCTILITY BEHAVIOR OF 7075-T6 ALLOY

The ductility behavior of 7075-T6 is measured in terms of fracture strain of the alloy. From the tensile test results (Table 4.2 and Fig. 4.7), it appears that material ductility is insensitive to the reaging conditions considered for the project. Both higher temperatures and longer reaging time periods have a insignificant effect (Fig. 4.8 and 4.9). However the graphical analysis as in Figure 4.8 and 4.9 show that although very small, there is a loss of the material ductility for all reaging conditions.

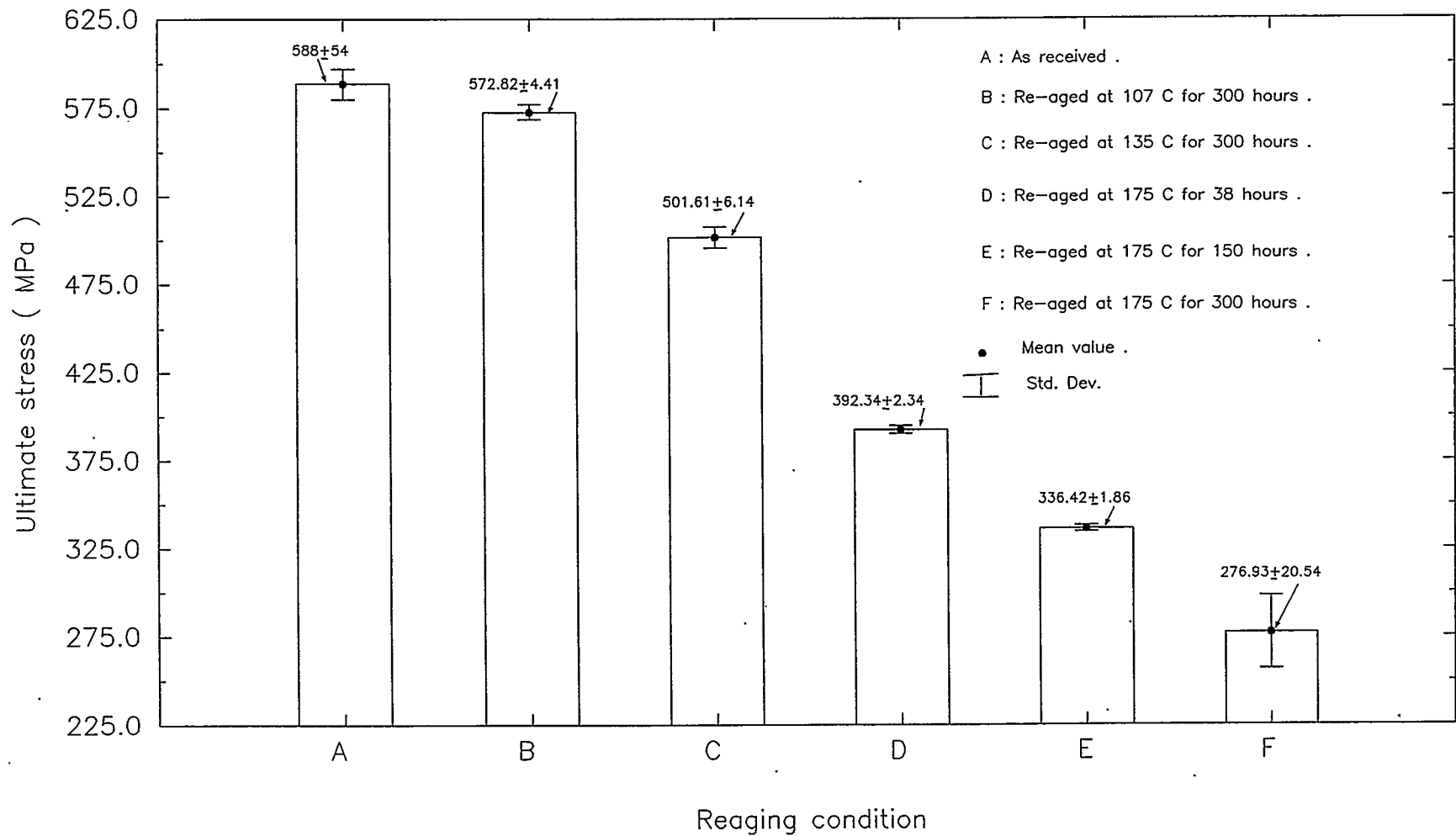


Figure 4.4: Variation of ultimate stress of 7075-T6 alloy under various reaging conditions.

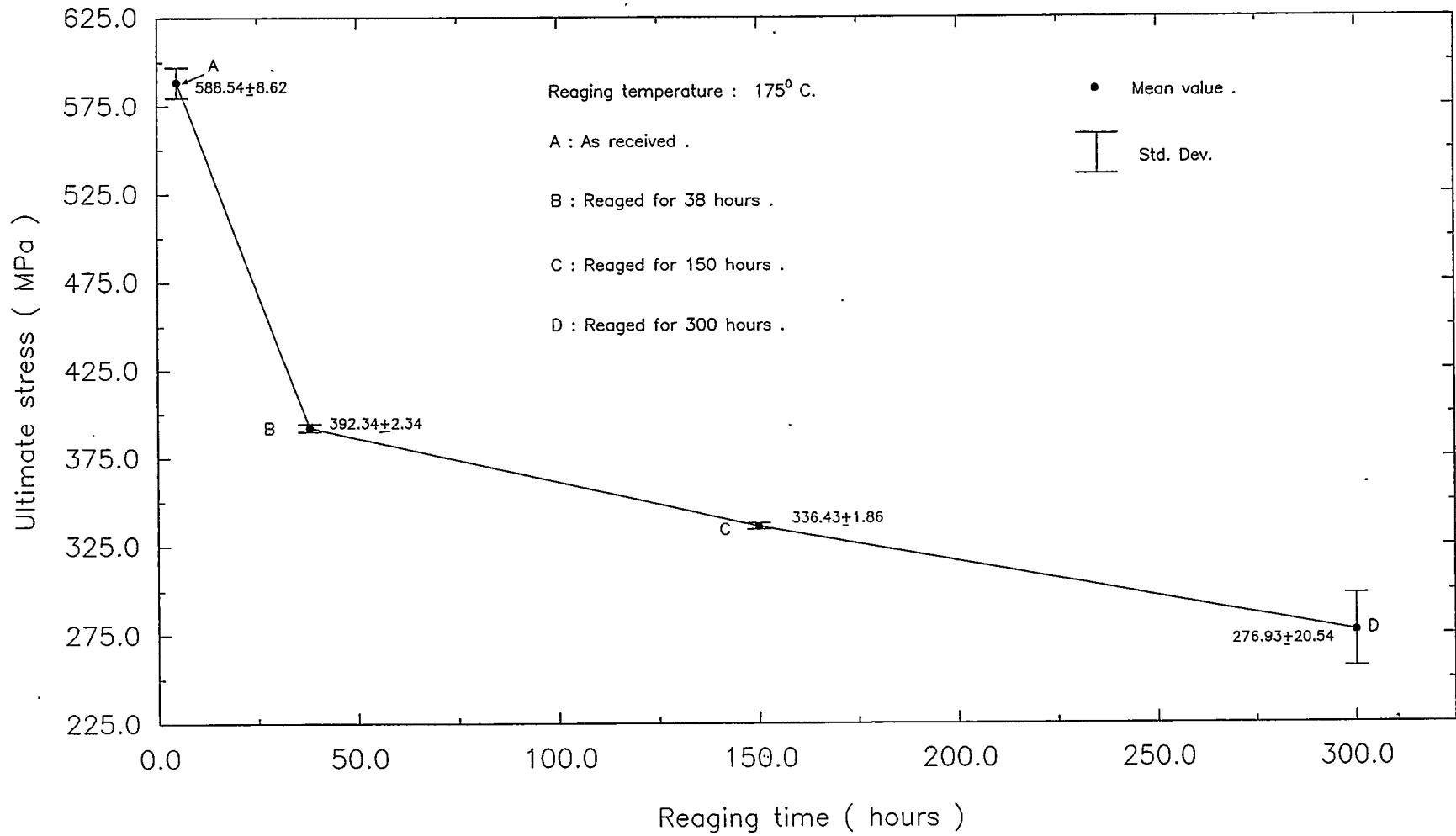


Figure 4.5: Relationship between ultimate stress and reaging time of 7075-T6 alloy at 175^o C.

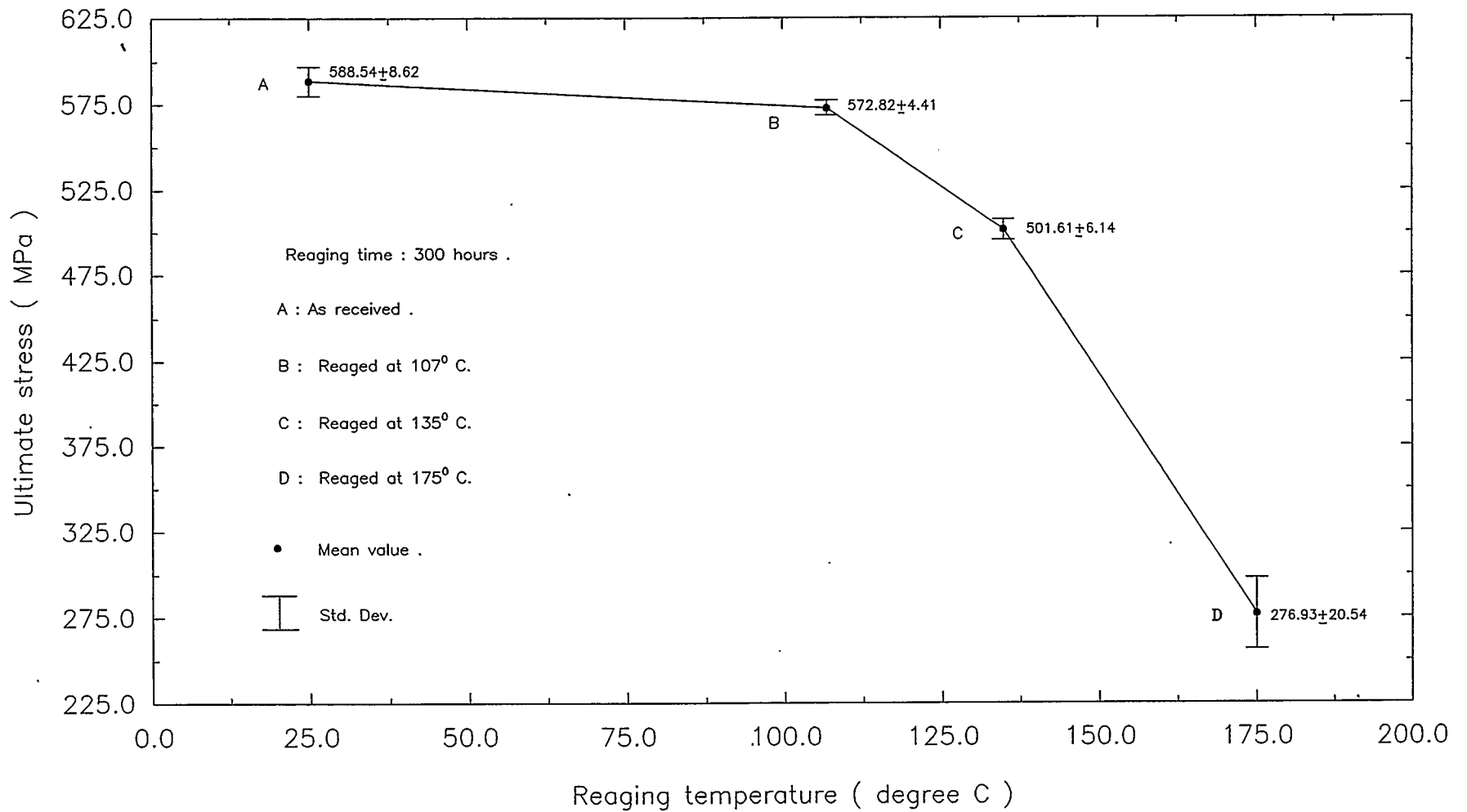


Figure 4.6: Relationship between ultimate stress and reaging temperature of 7075-T6 alloy at 300 hours .

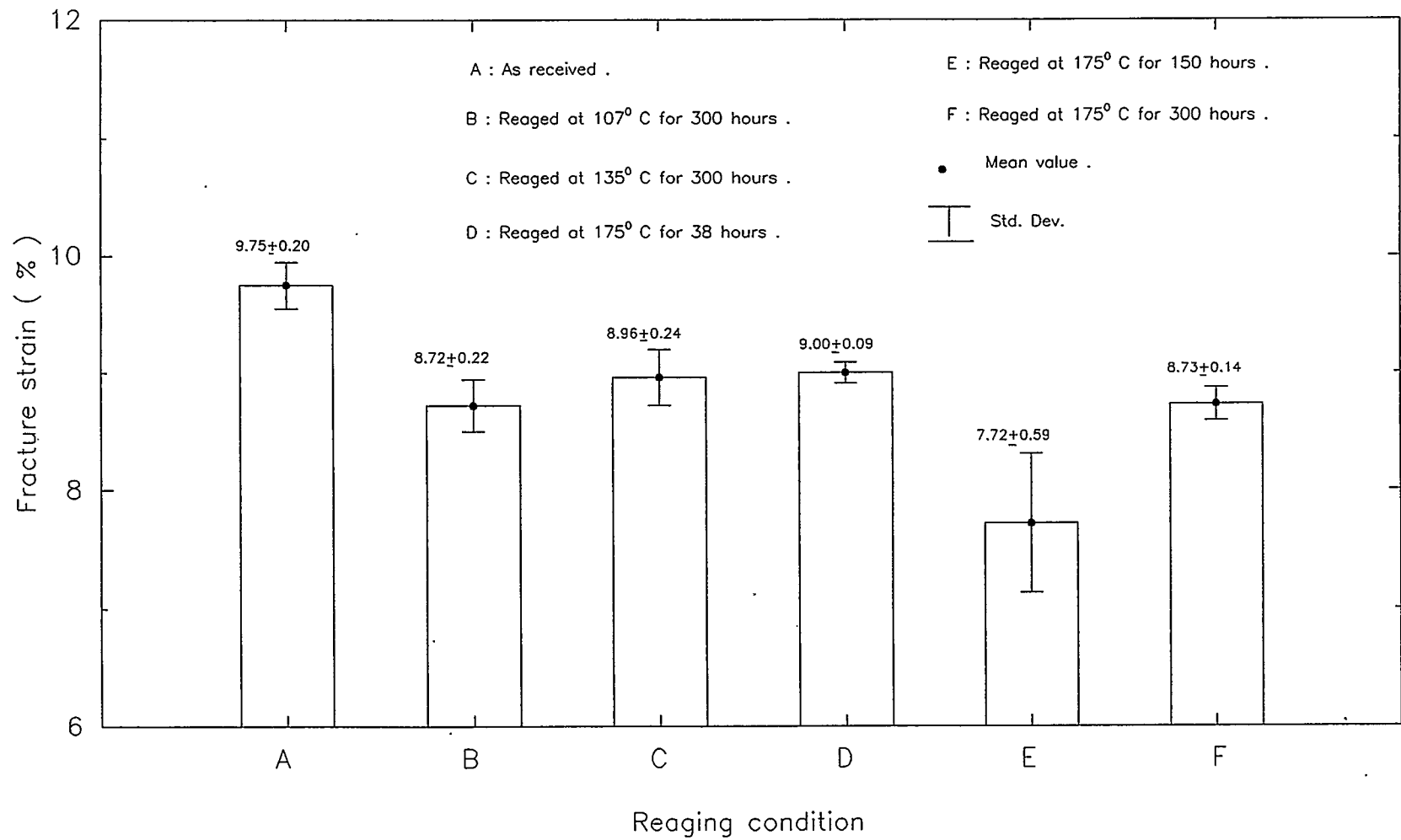


Figure 4.7: Variation of fracture strain of 7075-T6 alloy under various Reaging conditions .

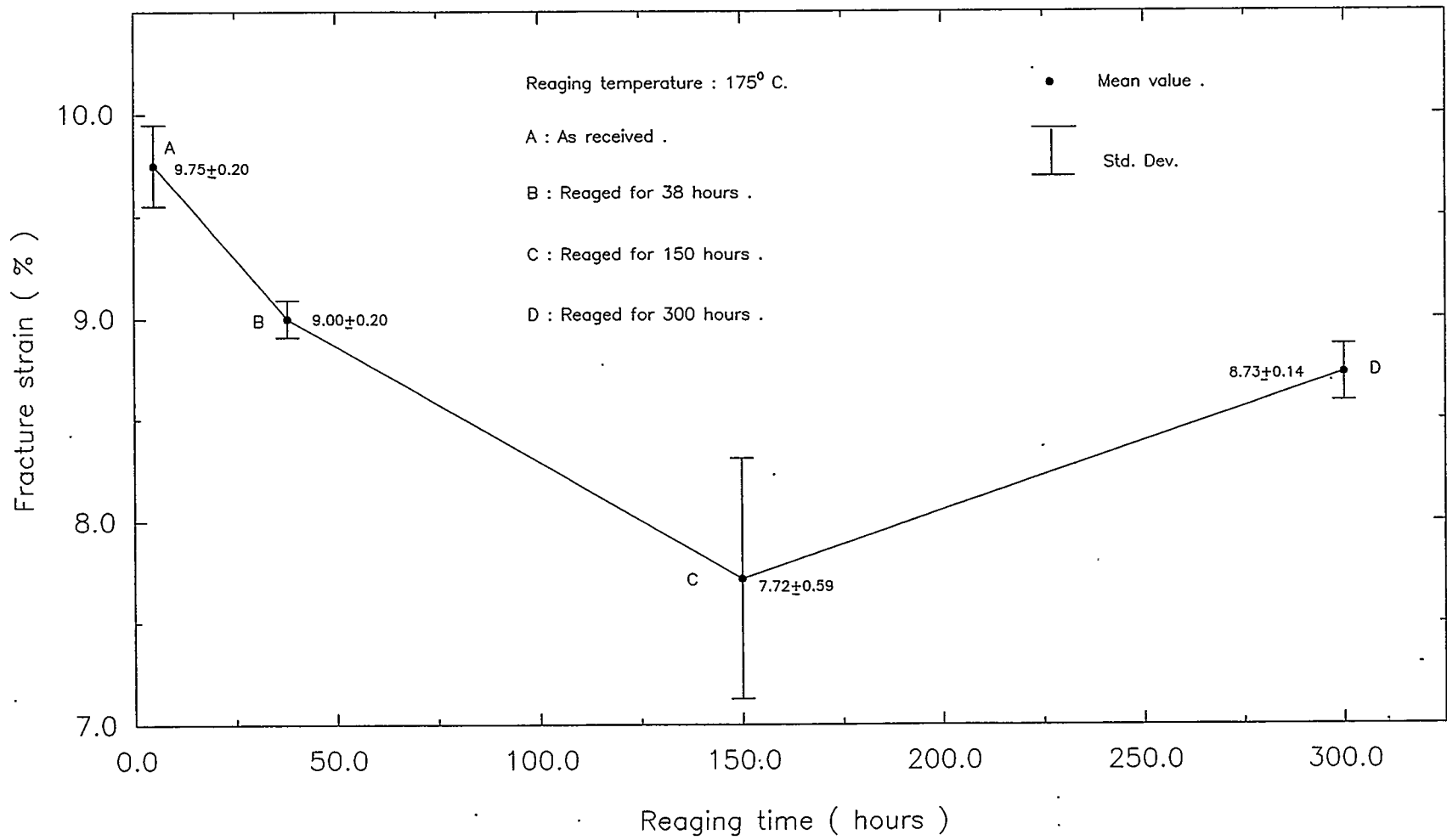


Figure 4.8: Relationship between fracture strain and reaging time of 7075-T6 alloy at 175° C.

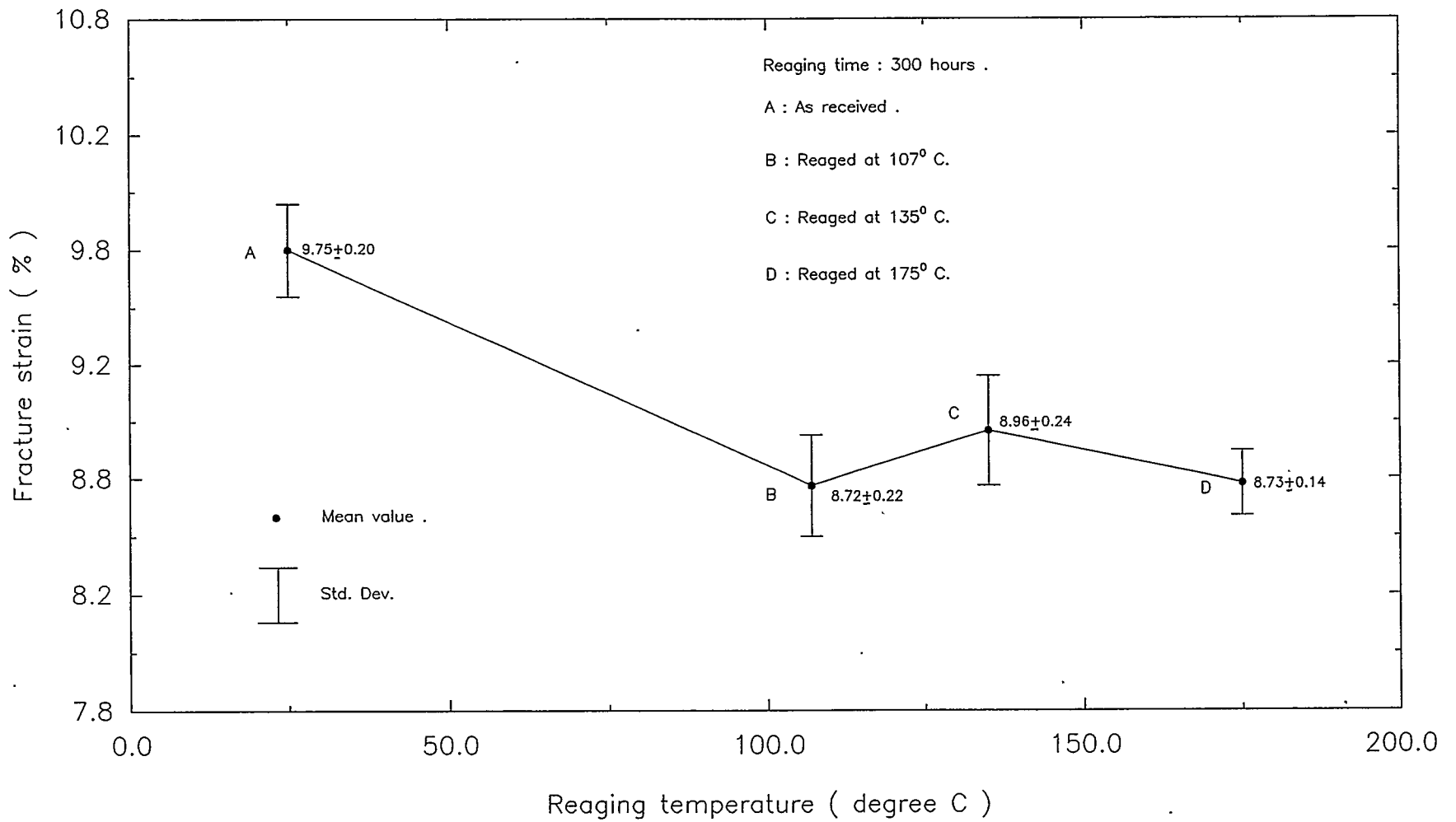


Figure 4.9: Relationship between fracture strain and reaging temperature of 7075-T6 alloy at 300 hours .

4.4 REAGING AND HARDNESS BEHAVIOR: 7075-T6

4.4.1 GENERAL

The material hardness behavior of an aluminum alloy as measured through macro-hardness and micro-hardness are indicative of microstructural changes occurring in the reaged alloy. The material hardness tests of the aluminum alloy were conducted by using ASTM E92 and E18 standards. The experimental results of both the regular hardness (macro-hardness) and the micro-hardness have been recorded in Tables 4.2 and 4.3 respectively. The statistical behavior of the macro-hardness and micro-hardness test results are given separately in the following sections.

4.4.2 MACRO-HARDNESS BEHAVIOR OF 7075-T6 ALLOY

Macro-hardness values of the original as well the reaged material at different reaging conditions were tested according to ASTM standard E18 [39]. The statistical behavior of the test results is presented in Table 4.2.

Reaging at 107°C for 300 hours results in a slight increase of approximately 2% in the macro-hardness (Fig. 4.10). Beyond this condition, there is a continuous decrease in the macro-hardness both for higher reaging temperatures and longer reaging times. When, reaged at 135°C for 300 hours, the alloy lost approximately 7% of its hardness. A loss in macro-hardness of approximately 29% is shown for the reaging condition at 175°C for 38 hours (Fig. 4.11). Further reaging at this temperature for 150, and 300 hours reaging times have successive losses of 14% and 10% respectively (Fig. 4.12). The higher the reaging temperature above 120°C , the larger the loss in macro-hardness. For reaging conditions of 135°C and 175°C and for the same reaging period of 300 hours, the respective losses are 7.3% and 52.5% (Fig. 4.12).

Table 4.2: Macro-hardness of 7075-T6 alloy measured at room temperature.

Reaging condition	Macro-hardness (Rockwell B) Mean \pm Std.Dev.
As received.	86.62 \pm 0.37
Reaged at 107 $^{\circ}$ C for 300 hours.	88.02 \pm 0.20
Reaged at 135 $^{\circ}$ C for 300 hours.	80.30 \pm 0.23
Reaged at 175 $^{\circ}$ C for 38 hours.	61.61 \pm 0.21
Reaged at 175 $^{\circ}$ C for 150 hours.	49.67 \pm 0.46
Reaged at 175 $^{\circ}$ C for 300 hours.	41.13 \pm 0.60

Table 4.3: Micro-hardness of 7075-T6 alloy measured at room temperature.

Reaging condition	Micro-hardness (VHN) Mean \pm Std.Dev.
As received.	175.25 \pm 6.34
Reaged at 107 $^{\circ}$ C for 300 hours.	176.45 \pm 3.72
Reaged at 135 $^{\circ}$ C for 300 hours.	145.22 \pm 1.86
Reaged at 175 $^{\circ}$ C for 38 hours.	111.86 \pm 0.65
Reaged at 175 $^{\circ}$ C for 150 hours.	95.46 \pm 1.54
Reaged at 175 $^{\circ}$ C for 300 hours.	91.15 \pm 1.98

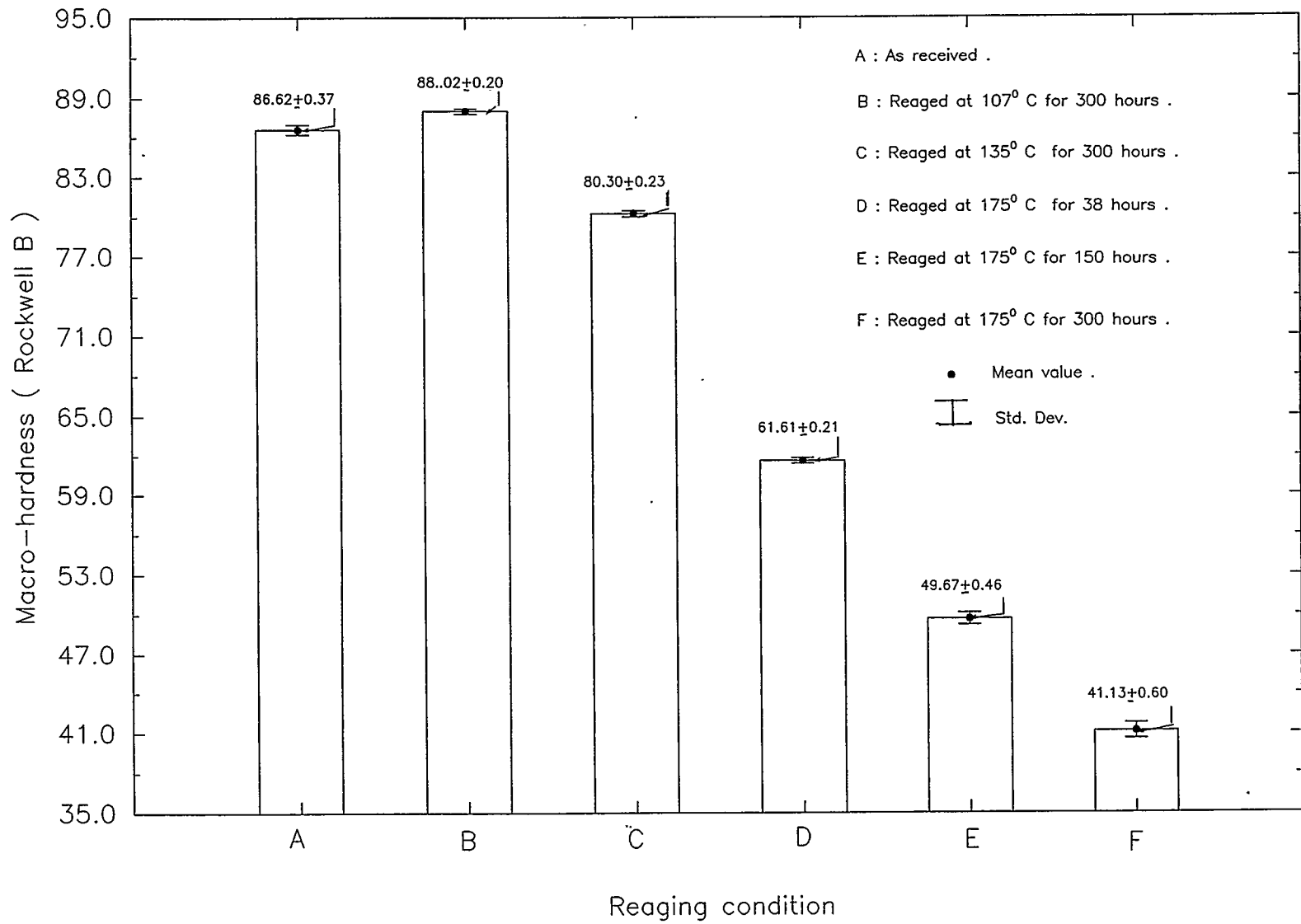


Figure 4.10: Variation in macro-hardness of 7075-T6 alloy under various reaging conditions.

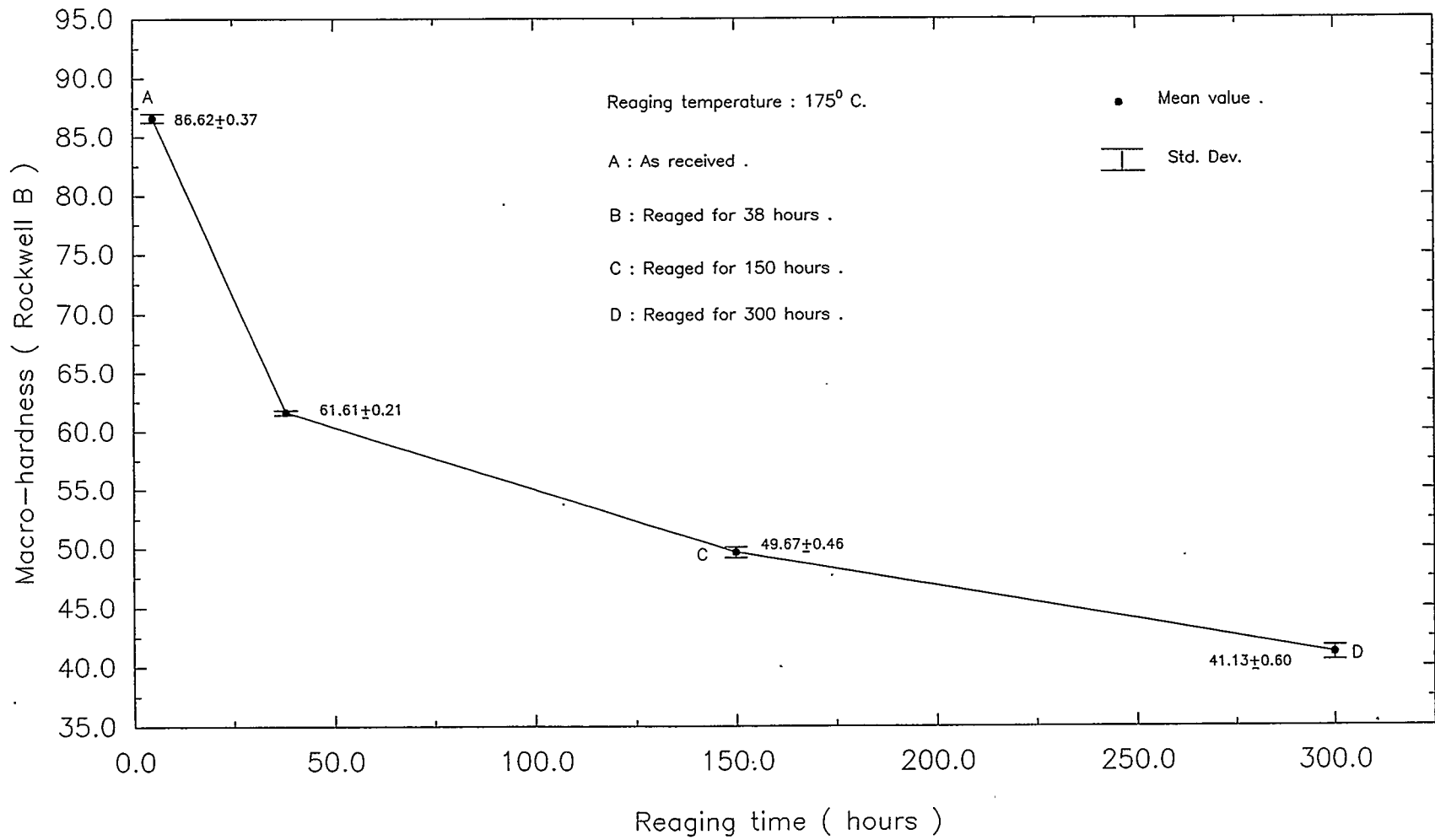


Figure 4.11: Relationship between macro-hardness and reaging time of 7075-T6 alloy at 175° C.

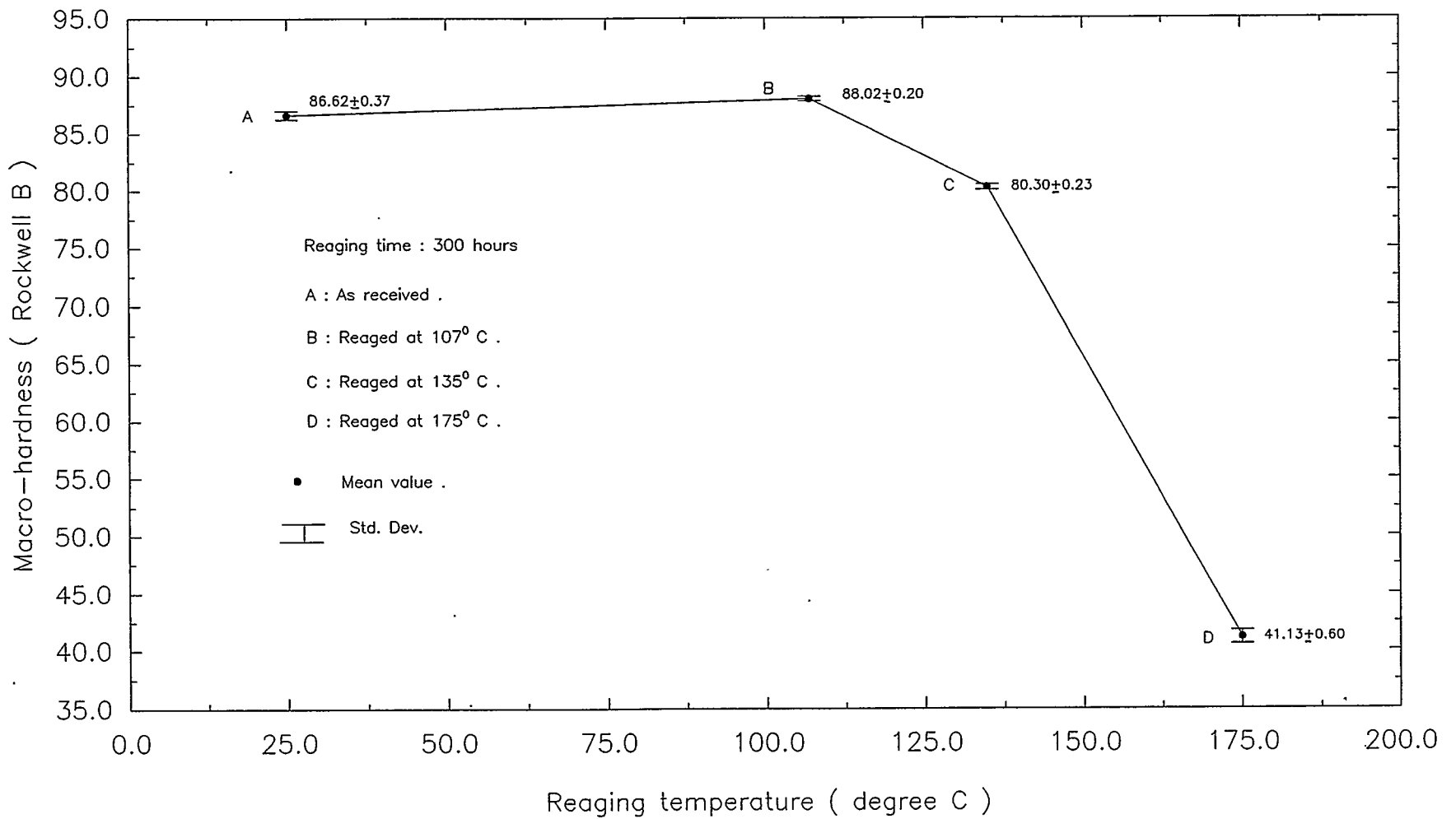


Figure 4.12: Relationship between macro-hardness and reaging temperature of 7075-T6 alloy at 300 hours .

4.4.3 MICRO-HARDNESS BEHAVIOR OF 7075-T6 ALLOY

The micro-hardness behavior of the original -T6 and reaged material at various conditions is presented in Table 4.3. Testing was conducted according to ASTM standard E92 [38]. The statistical variation has also been recorded in Table 4.3 and is graphically presented in Figures 4.13 to 4.15.

Reaging at 107°C for 300 hours results in a slight increase in the micro-hardness of approximately 1 % over that of the original alloy (Table 4.3 and Fig. 4.13). Beyond this condition, there is a continuous drop in micro-hardness. Reaging at 135°C for 300 hours results in a loss of micro-hardness of 17 % over the original alloy. At a higher temperature of 175°C, even for a smaller reaging time of 38 hours, there is substantial drop in micro-hardness of approximately 36 % over that of the original alloy (Fig. 4.14 and 4.15). Beyond this condition further reaging time periods show much smaller decrease in the micro-hardness although it keeps on decreasing continuously. The reaging conditions at 175°C for 38, 150, and 300 hours time periods result in successive losses of 36 %, 11 %, and 2 % respectively. As compared to the original material these successive changes are approximately 36%, 47% and 49% respectively (Fig. 4.14).

4.5 ELECTRICAL CONDUCTIVITY BEHAVIOR OF 7075-T6 ALLOY

The behavior of electrical conductivity of the aluminum alloy for each heat treated condition was measured using the eddy-current technique and results have been recorded in Table 4.4.

The measured values of electrical conductivity follow a similar pattern as that found for hardness. The conductivity of as received 7075-T6 was measured as being 33.11% IACS. On reaging at 107°C for 300 hours, conductivity of the alloy increased very slightly to 34.29% IACS. However, the conductivity value then rises quite rapidly for other more severe reaging conditions (Fig. 4.16). Reaging at 135°C

Table 4.4: Electrical conductivity of 7075-T6 alloy at room temperature

Reaging condition	Electrical conductivity (% IACS) Mean \pm Std.Dev.
As received.	33.11 \pm 0.06
Reaged at 107 ^o C for 300 hours.	34.29 \pm 0.12
Reaged at 135 ^o C for 300 hours.	39.64 \pm 0.15
Reaged at 175 ^o C for 38 hours.	43.57 \pm 0.22
Reaged at 175 ^o C for 150 hours.	45.04 \pm 0.11
Reaged at 175 ^o C for 300 hours.	45.64 \pm 0.25

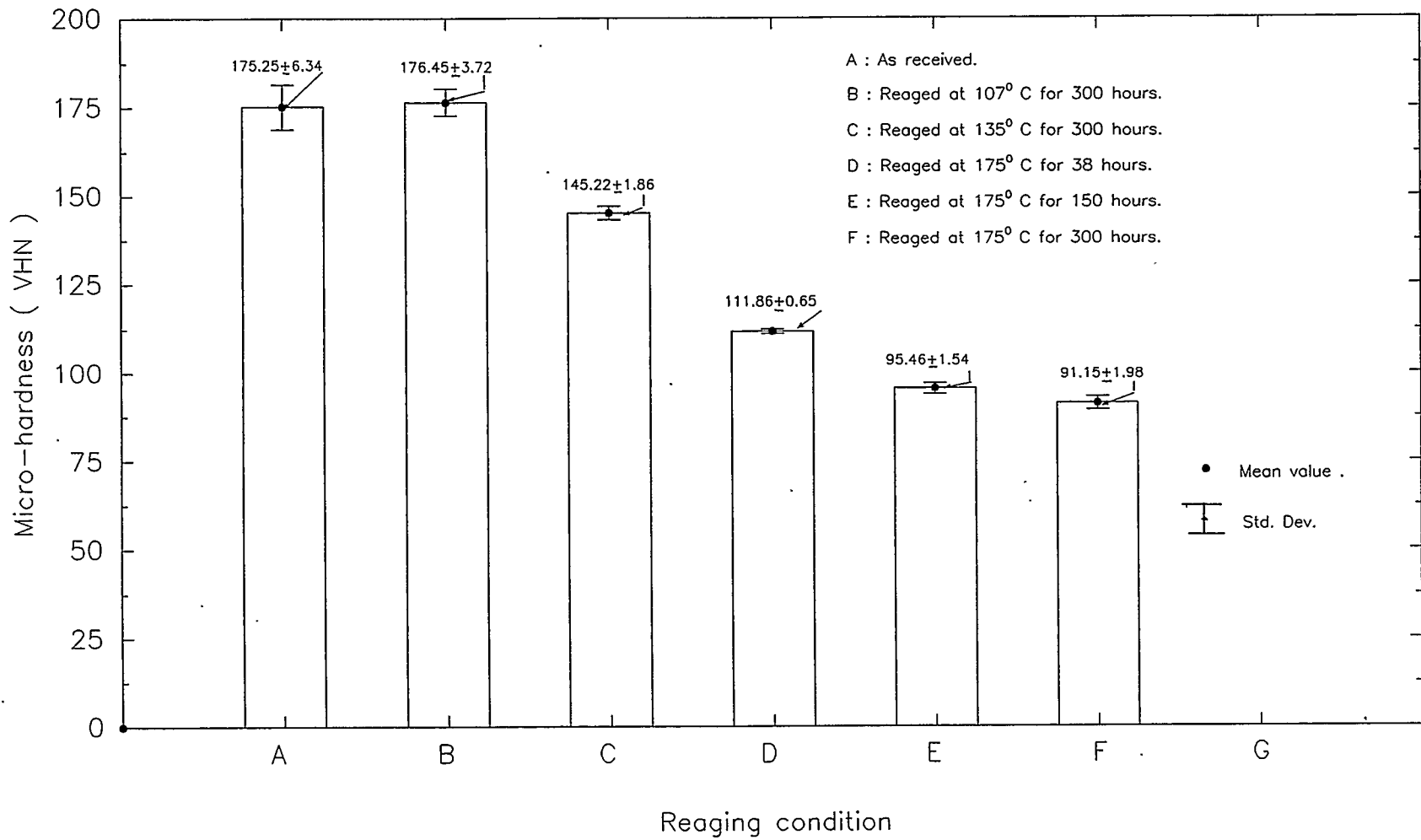


Figure 4.13: Variation of micro-hardness of 7075-T6 alloy under various reaging conditions .

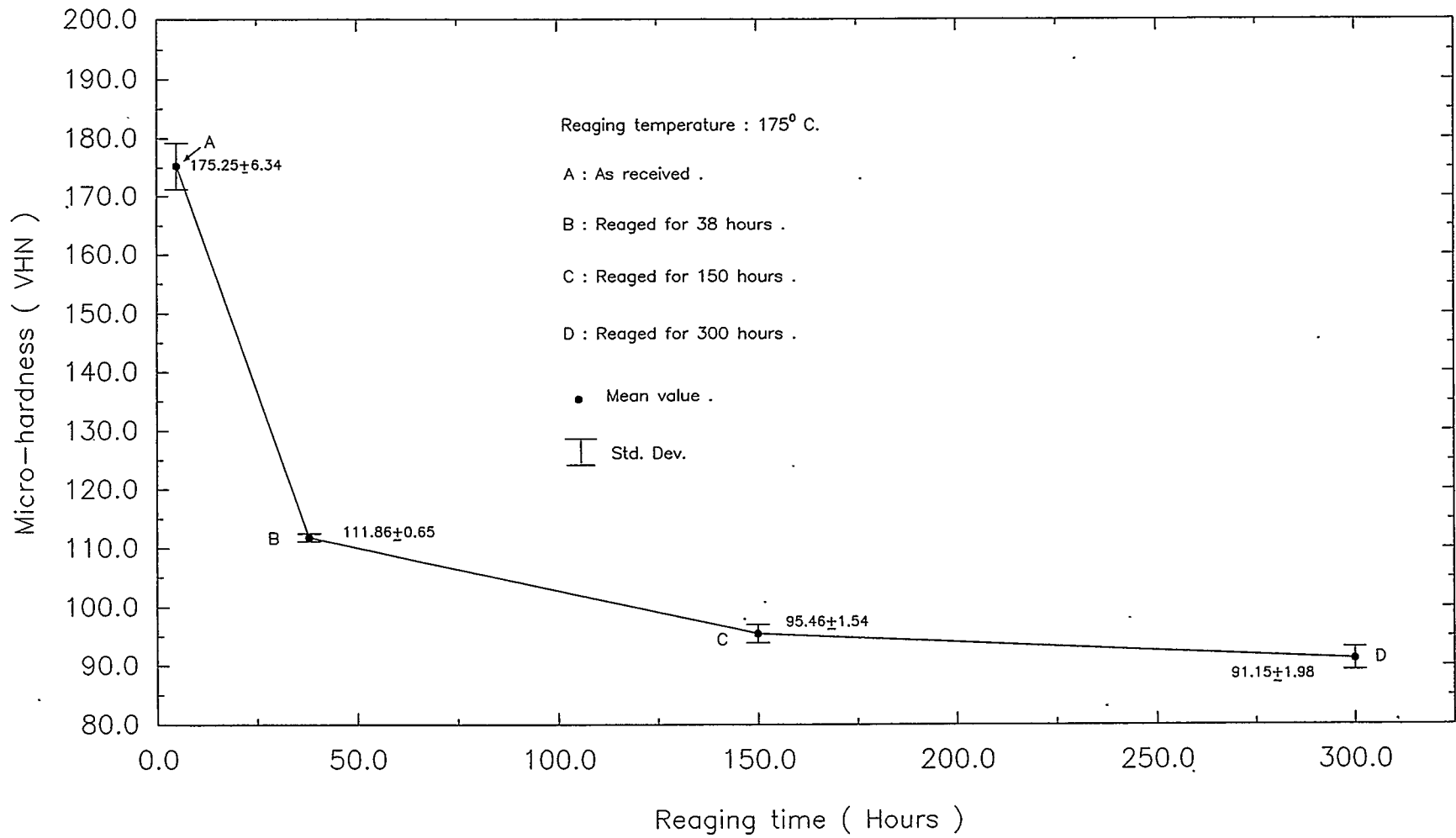


Figure 4.14: Relationship between micro-hardness and reaging time of 7075-T6 alloy at 175^o.

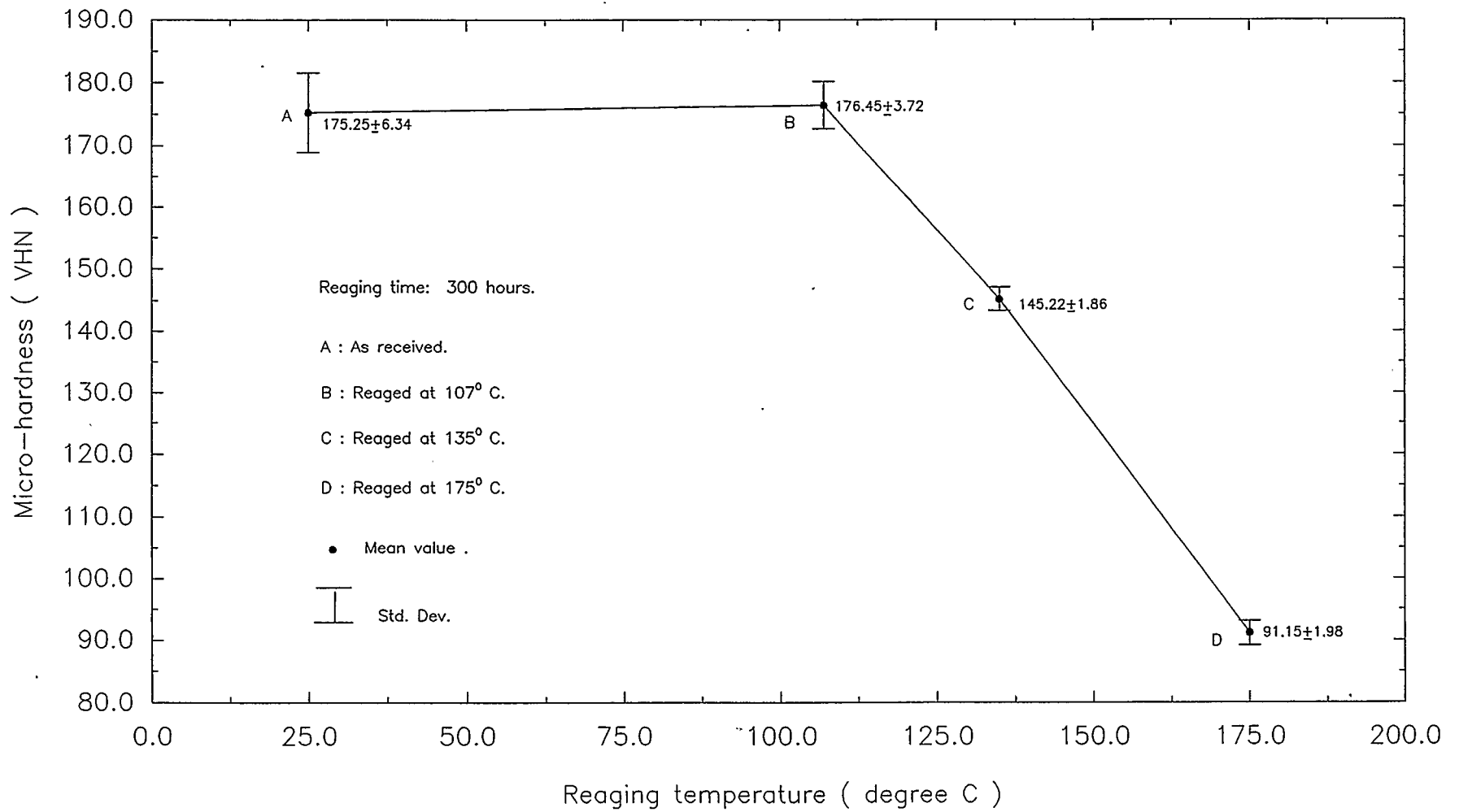


Figure 4.15: Relationship between micro-hardness and reaging temperature of 7075-T6 alloy at 300 hours.

for 300 hours provided an increase of about 19.7% and the reaging condition at 175°C for 38 hours provided an increase of about 32% over the original material. Further reaging beyond 175°C for 38 hours, did not result in anywhere near as large an effect on the conductivity values although they did continue to increase. Reaging at 175°C for 150, and 300 hours bring very slight additional changes of 4%, and 1.8% respectively (Fig. 4.17). Higher reaging temperatures for the same reaging time period, results in larger increase in the electrical conductivity. This is very much evident from the reaging temperatures of 135°C and 175°C, where the corresponding increases in the electrical conductivities are 19.7 % and 37.8 % respectively (Fig. 4.17).

4.6 FATIGUE CRACK GROWTH BEHAVIOR OF 7075-T6 ALLOY

The fatigue crack growth behavior of 7075-T6 alloy as related to its reaging conditions, was examined through crack growth fatigue tests conducted at a frequency of 5 Hz using a "Haversine" function as has been outlined previously in Section 3.6. This experimental data was then analyzed by using computer programs to generate crack growth rate information. The graphical analysis of the results are presented in Figure 4.19 through Figure 4.24. The fatigue crack behavior as it relates to the fatigue life under different reaging conditions is presented in this section.

It has been observed from the graphical analysis of crack growth life (crack length versus fatigue cycles), crack propagation relations (crack growth rate versus change in stress intensity factor), and fatigue failure life (reaging conditions versus fatigue cycles to failure) that a considerable effect is occurring in this alloy for a reaging condition as low as 107°C for 300 hours. There is no detrimental effect on the fatigue life of the alloy up to and including a reaging condition of 175°C for 300 hours. An examination of both the crack growth life (Fig. 4.19-4.21) and crack propagation relations (Fig. 4.23 and 4.24) show that under all the reaging

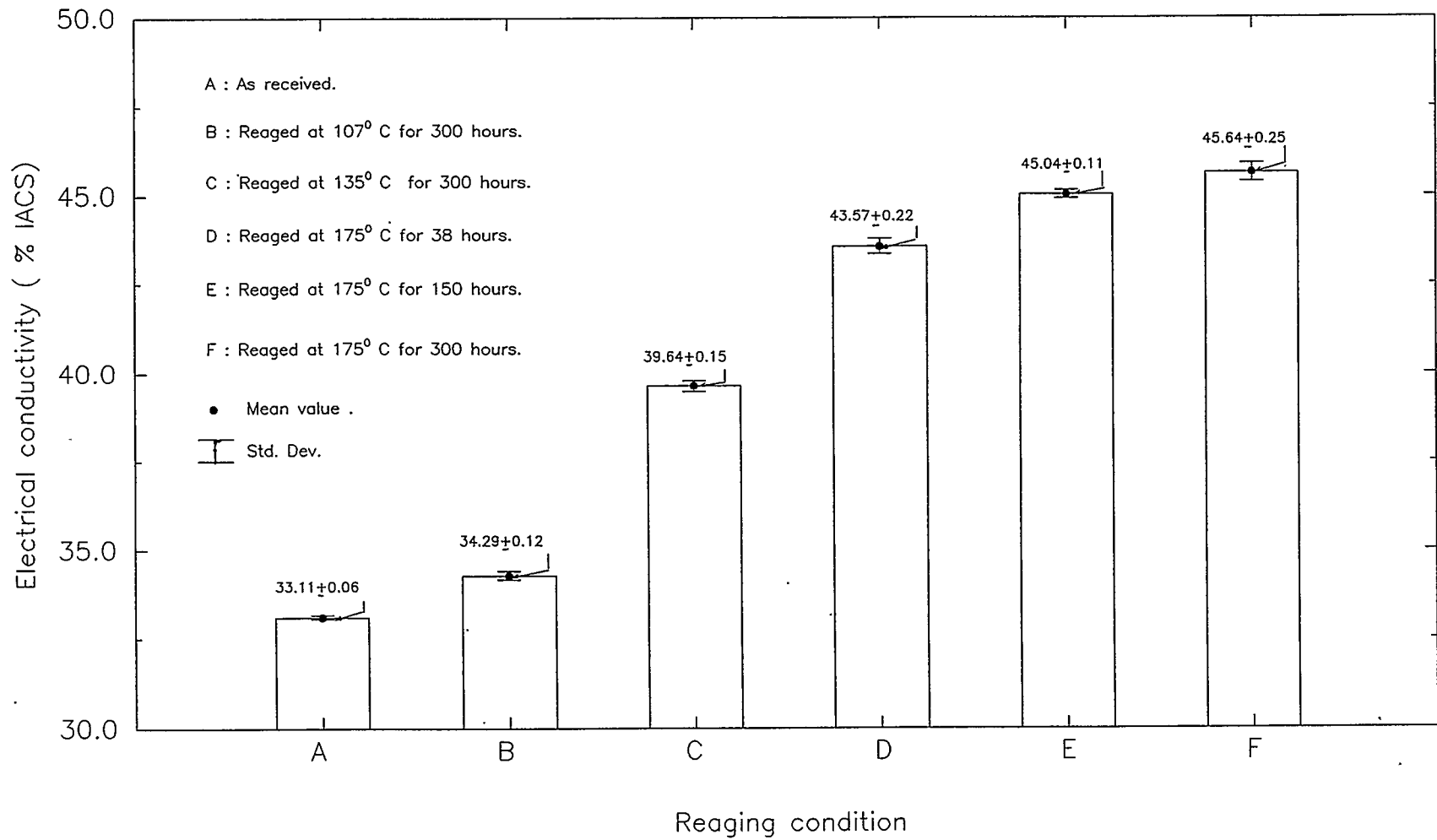


Figure 4.16: Variation of electrical conductivity of 7075-T6 alloy under various reaging conditions .

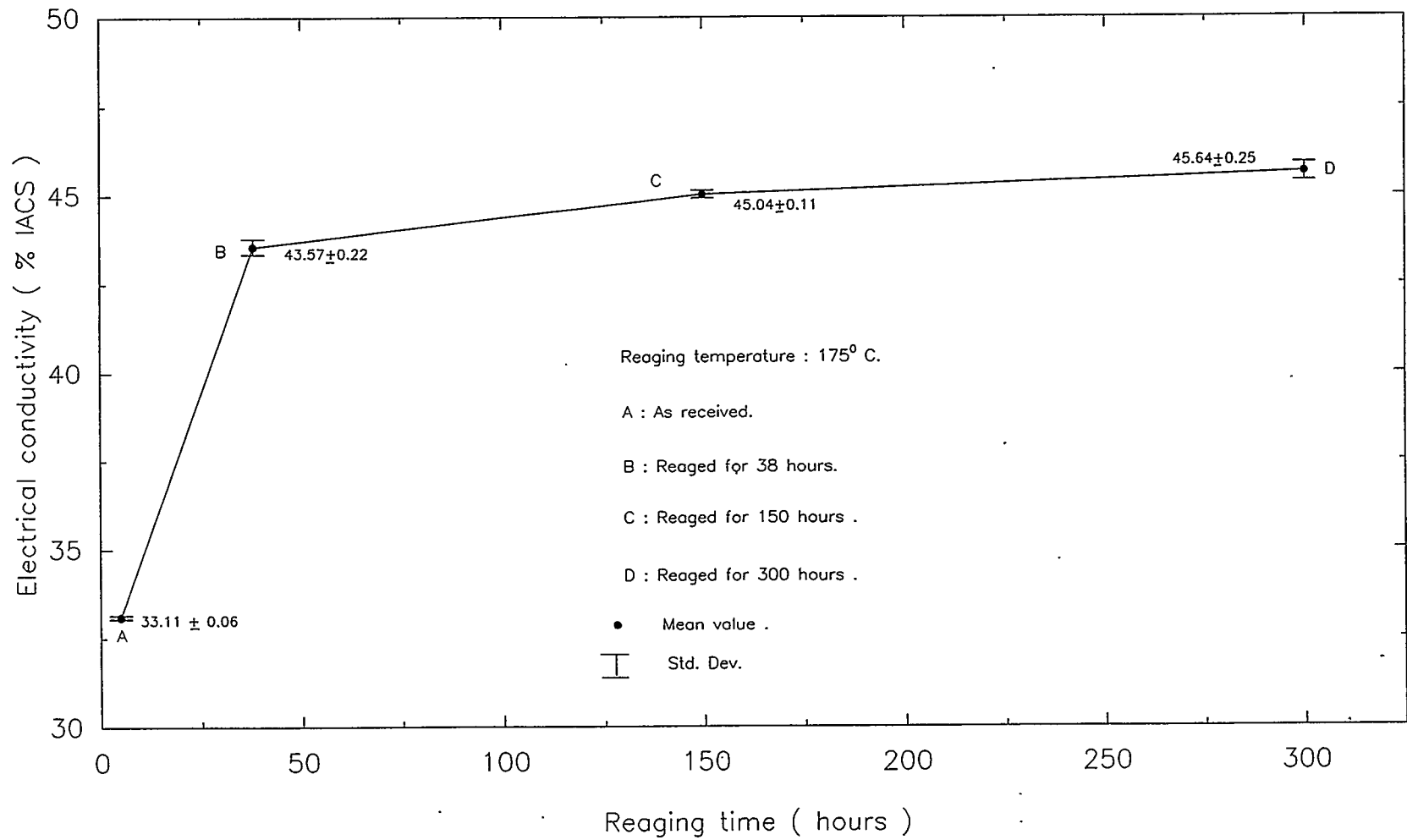


Figure 4.17: Relationship between electrical conductivity and reaging time of 7075-T6 alloy at 175° C.

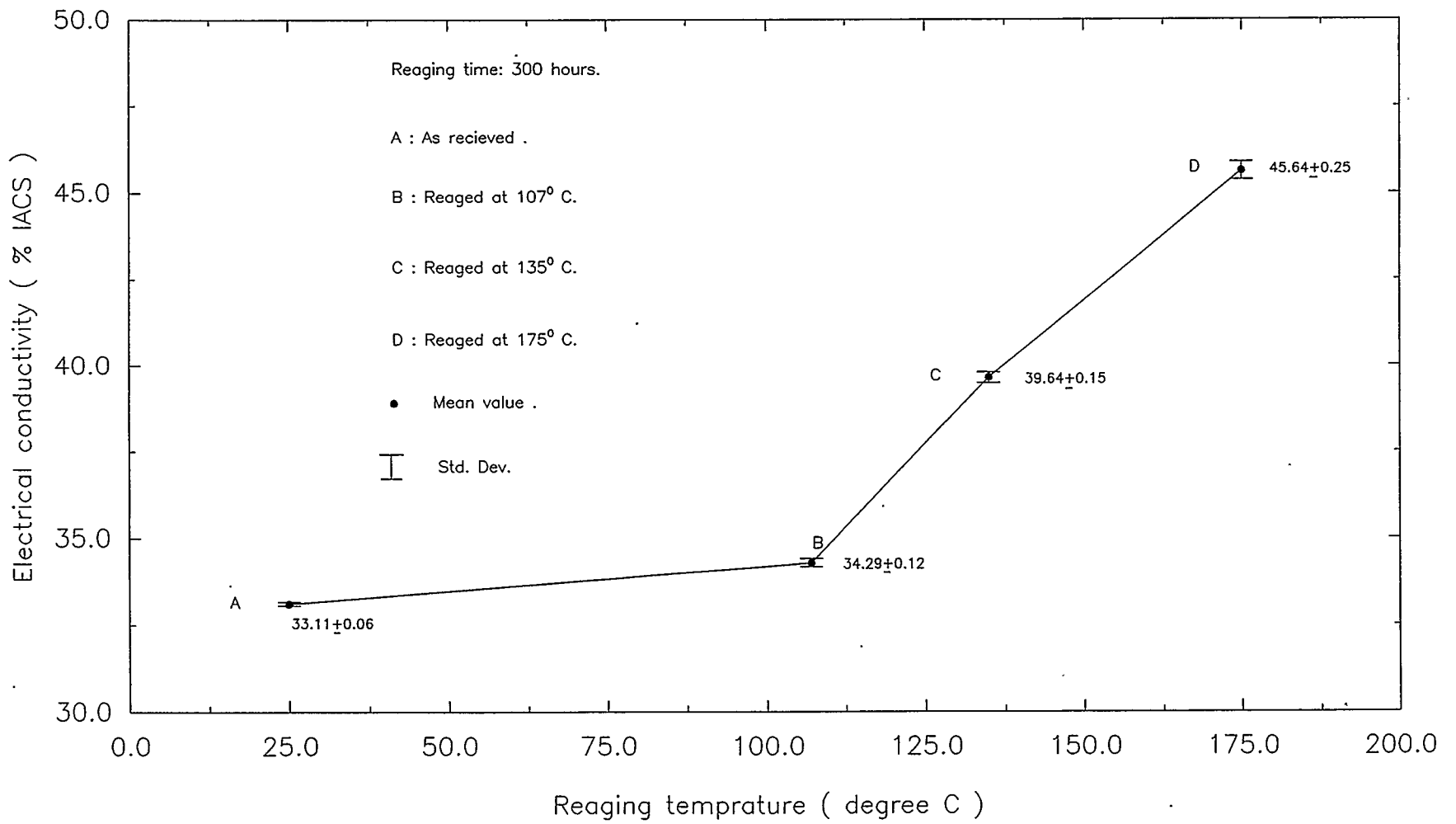


Figure 4.18: Relationship between electrical conductivity and reaging temperature of 7075-T6 alloy .93

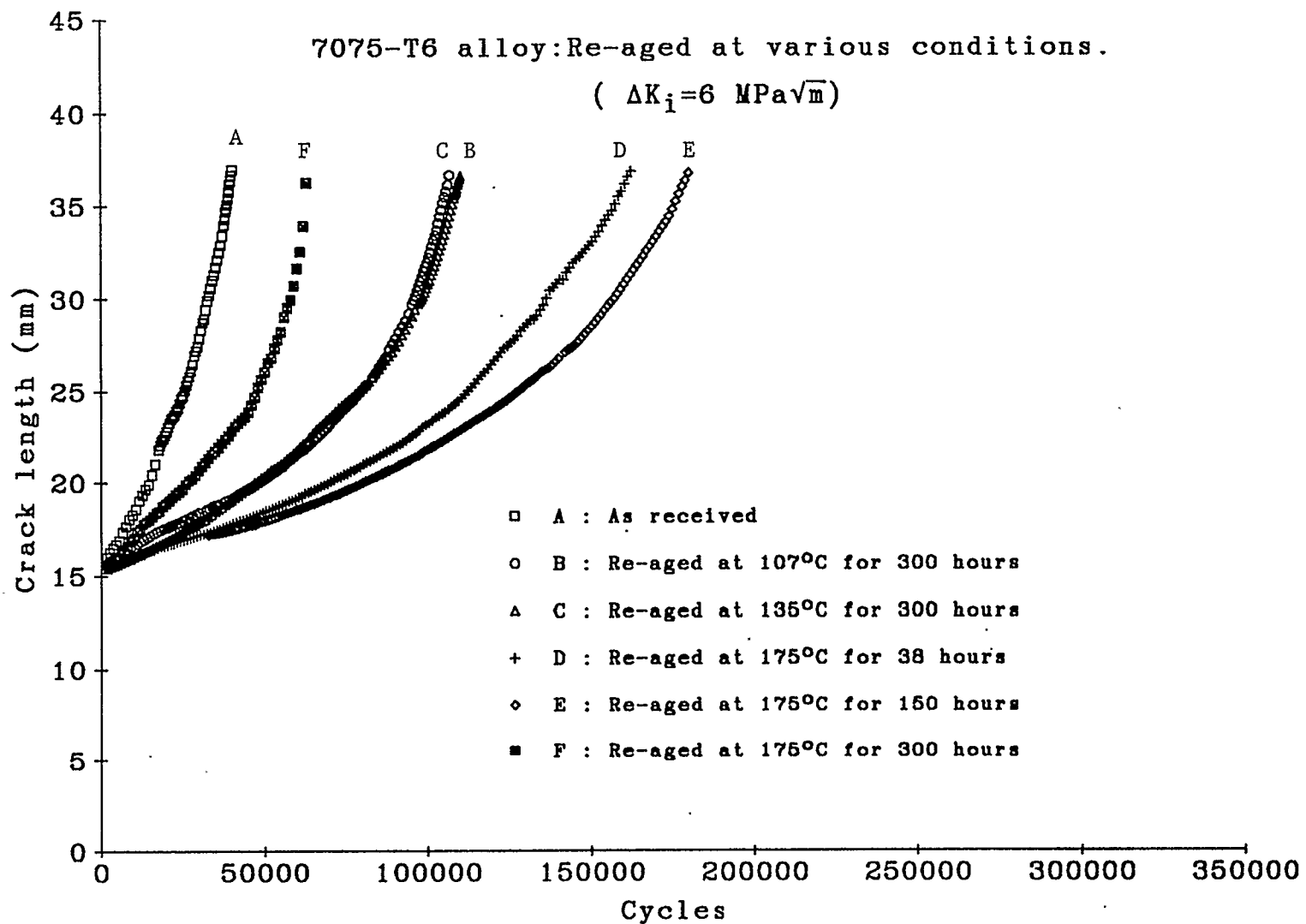


Figure 4.19: Relationship between crack length and fatigue life cycles of 7075-T6 alloy; reaged at various conditions.

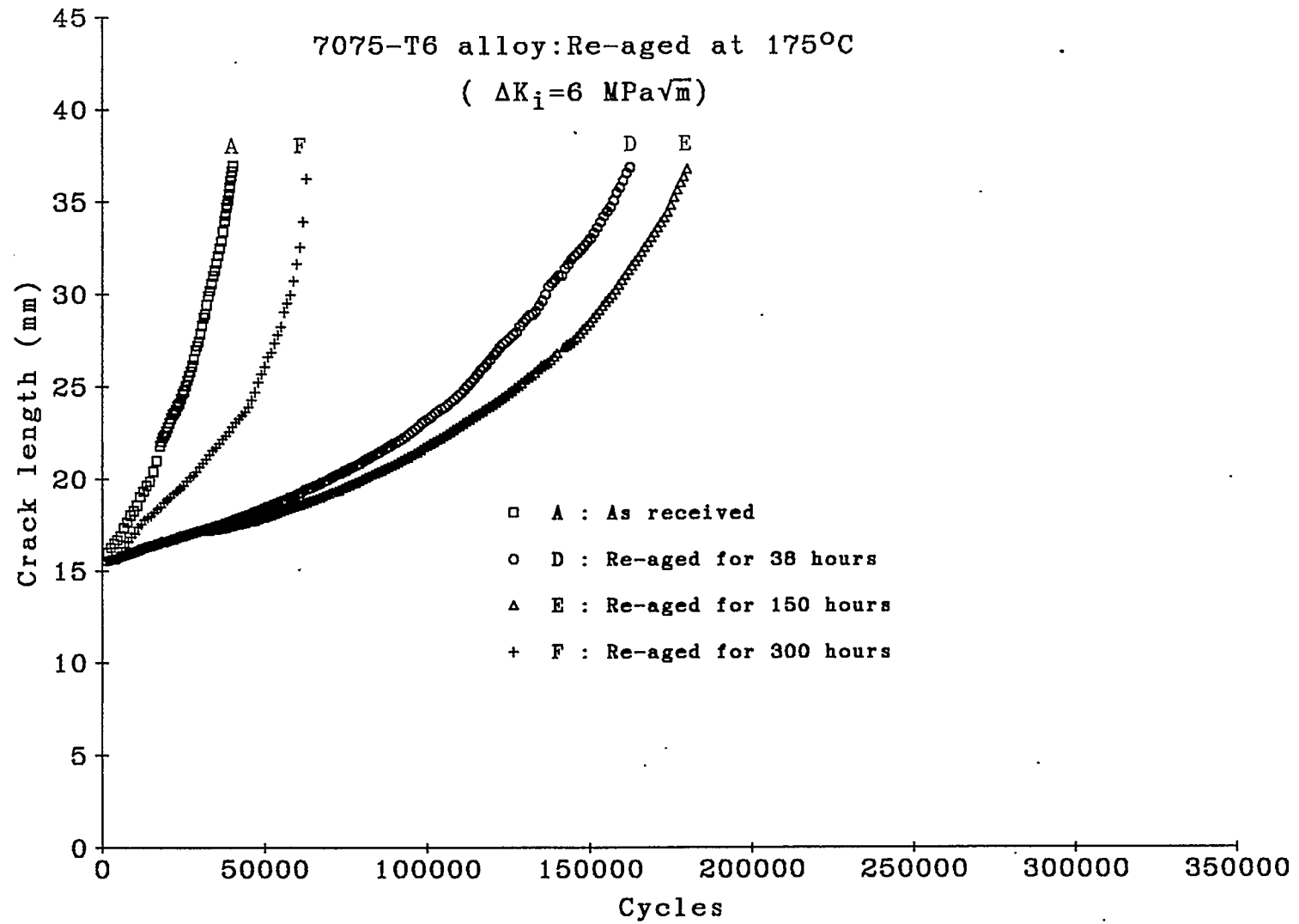


Figure 4.20: Relationship between crack length and fatigue life cycles of 7075-T6 alloy; reaged at 175°C.

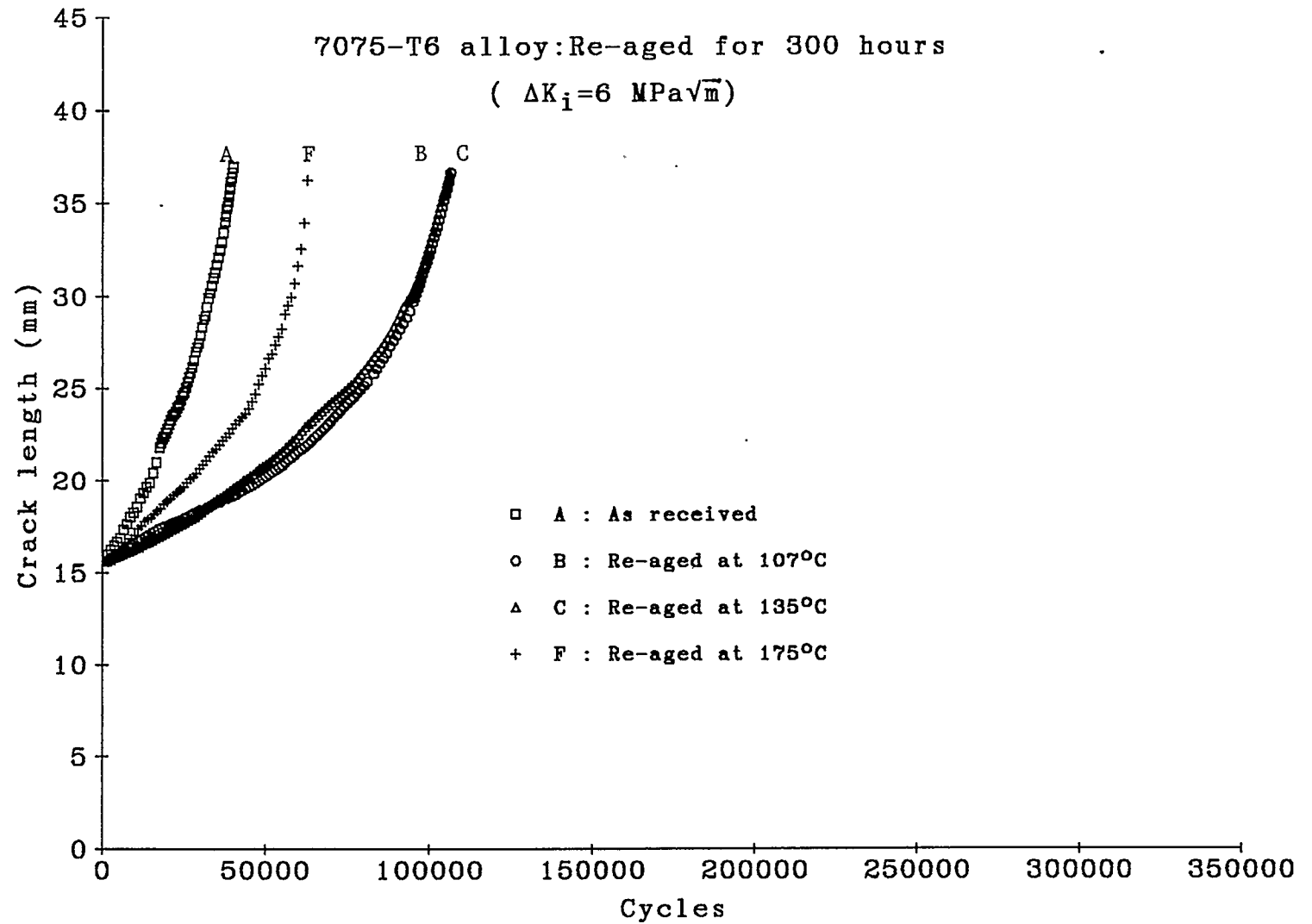


Figure 4.21: Relationship between crack length and fatigue life cycles of 7075-T6 alloy; reaged for 300 hours.

Table 4.5: Reaging conditions and normalized fatigue life of 7075-T6.

Reaging condition.	Total life (cycles)	Normalizing cycles.	Normalized fatigue life. (cycles)
As received.	65,500	10,404	50,358 ± 16,263
Reaged at 107°C for 300 hours.	227,500	113,644	113,856
Reaged at 135°C for 300 hours.	146,000	10,798	135,202
Reaged at 175°C for 38 hours.	204,000	20,498	183,502
Reaged at 175°C for 150 hours.	190,000	44,033	145,967
Reaged at 175°C for 300 hours.	90,000	25,847	64,153

* Normalized at a crack length of 17.23 mm

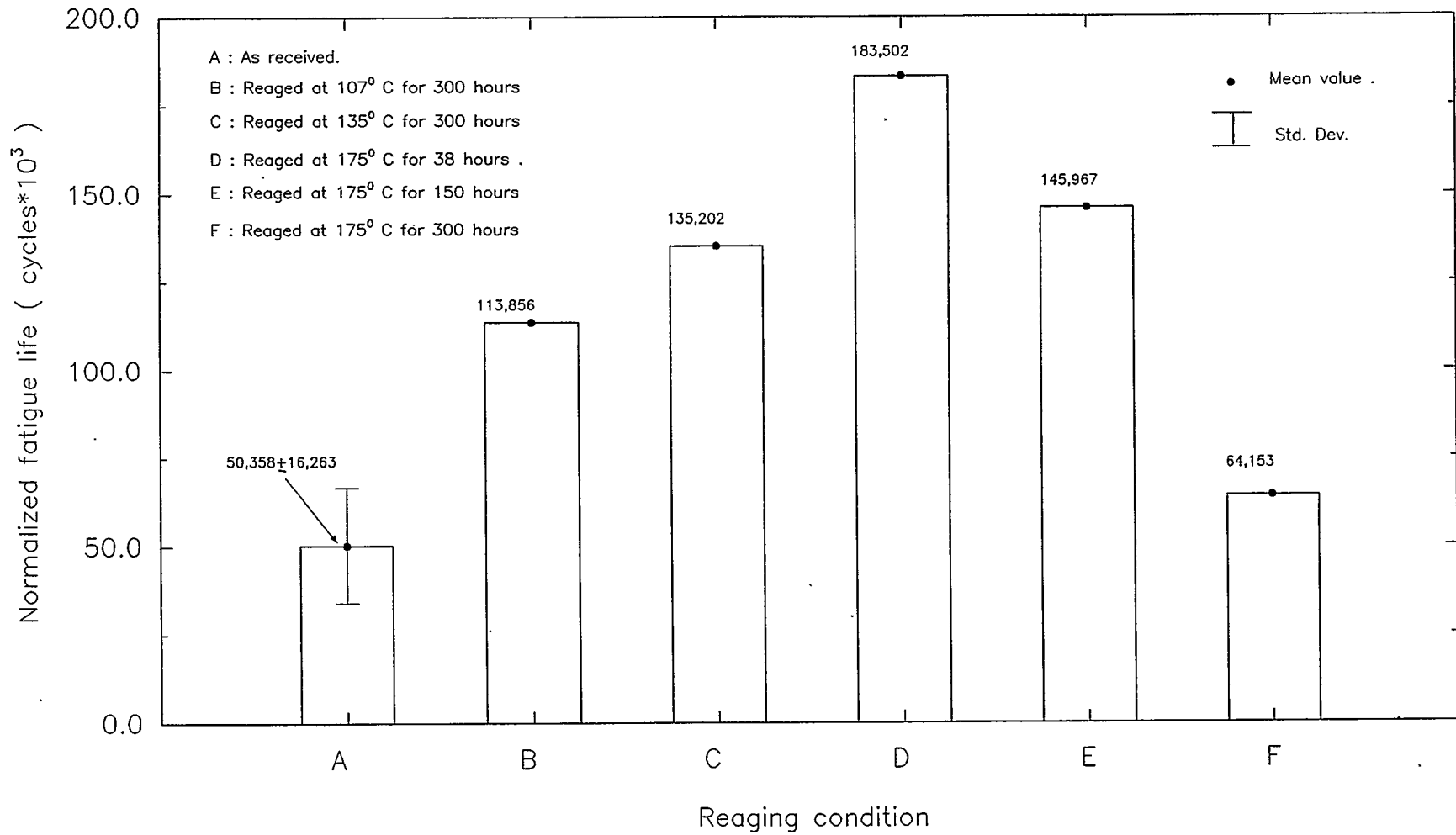


Figure 4.22 : Variation of normalized fatigue life of 7075-T6 alloy under various reaging conditions.

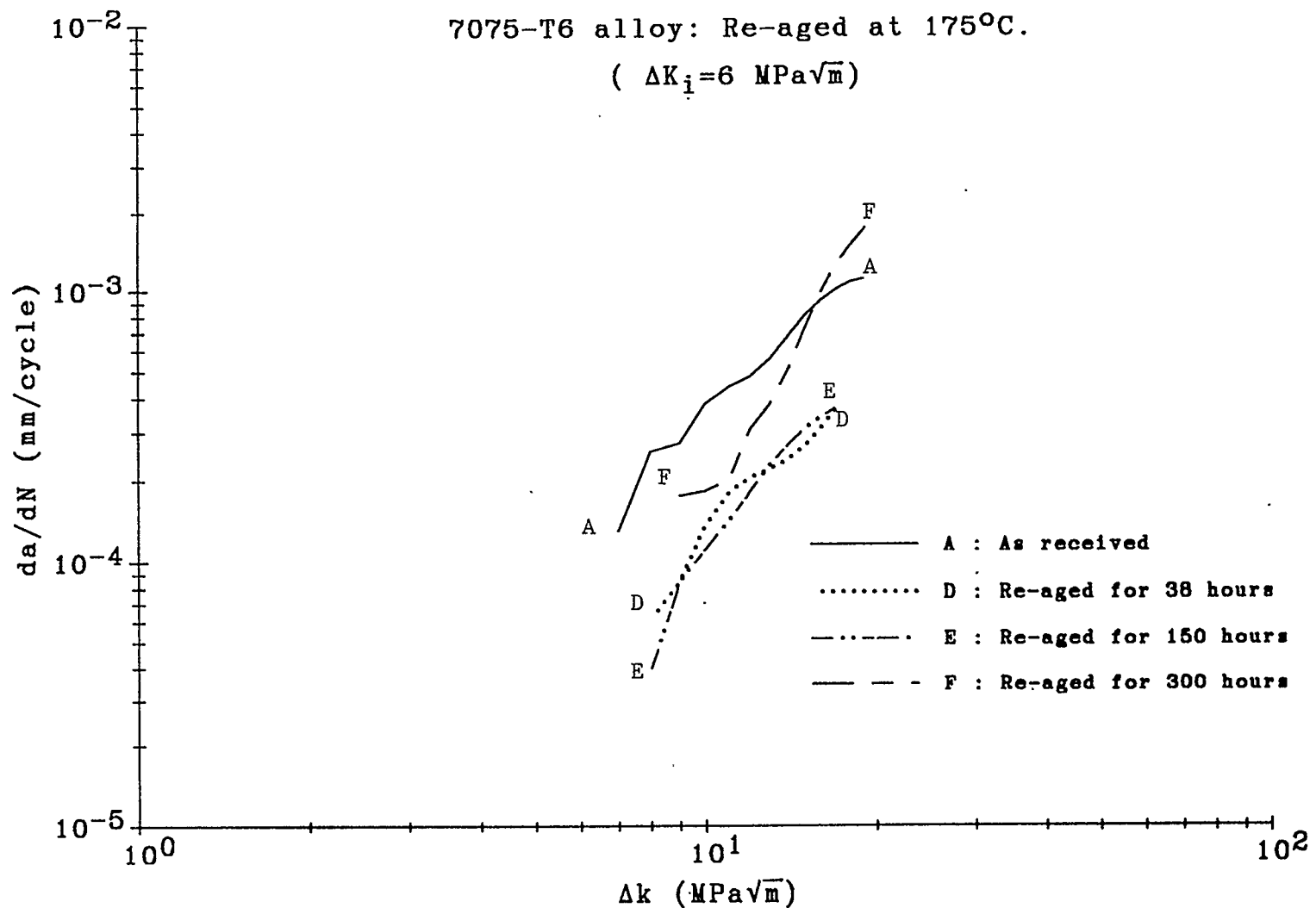


Figure 4.23: Relationship between the crack growth rate and change in stress intensity factor of 7075-T6 alloy; reaged at 175°C.

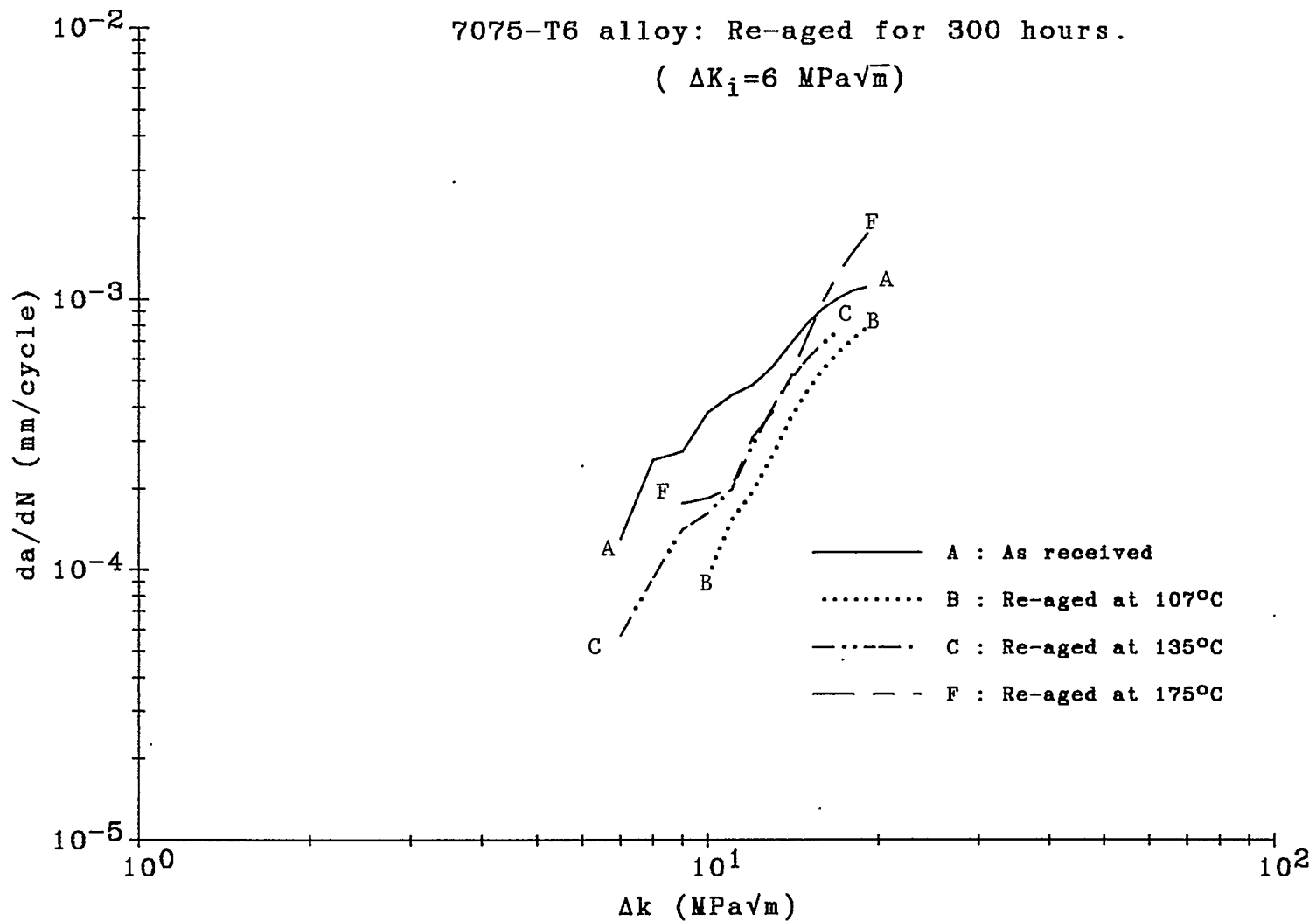


Figure 4.24: Relationship between the crack growth rate and change in stress intensity factor of 7075-T6 alloy; reaged for 300 hours.

conditions considered for this project, the fatigue life of 7075-T6 alloy improves. This very fact can be verified through the fatigue failure life analysis (Table 4.5, Fig. 4.22).

The fatigue crack growth life of 7075-T6 alloy under a reaging condition of 107°C for 300 hours (Fig. 4.19 and 4.20), and the fatigue crack propagation rate analysis under the same condition of 107°C (Fig. 4.24) show that the fatigue crack of the reaged alloy grows much slower compared to the original alloy and consequently has a higher fatigue life. This is well supported by fatigue life analysis (Table 4.5, Fig. 4.22) where the improved life due to reaging at 107°C for 300 hours is approximately 164% over the original alloy. The above results also indicate that a reaging condition of 135°C for 300 hours further improves the fatigue strength. Hence the fatigue life of the alloy improves by approximately 184% above the fatigue life of the original alloy.

It is interesting to note that under reaging conditions of 175°C , the alloy shows a complex fatigue crack growth and hence fatigue life behavior. The fatigue life initially increases for a reaging period of 38 hours and then for longer reaging times of 150 and 300 hours it continuously decreases. Initially an increase in the fatigue life of 316.1% occurs for a reaging time of 38 hours. The fatigue life corresponding to 300 hours is only 49.3% above the fatigue life of the as received alloy. For an intermediate time period of 150 hours the fatigue life is 285.4% above the original alloy. The initial improvement in fatigue life tends to disappear for longer reaging times. However even at the reaging condition of 175°C for 300 hours, the fatigue life is still 49.3% higher than the original alloy.

4.7 ALUMINUM ALLOY BEHAVIOR : 2024-T3

4.7.1 GENERAL

The original heat treatment of 2024-T3 aluminum alloy involves a solution heat treatment followed by quenching, cold working and then

naturally aging at room temperature for a number of days to a substantially stable condition. The material so produced will be slightly underaged as compared to an optimum aging condition. A comparable heat treatment would be a -T8 condition which is solution treated, cold worked and artificially aged at a temperature of 190°C for a period of 12 hours. Both of these alloys, -T3 and -T8 have identical tensile strengths, however different yield and ductility values. An important point emerging is that neither material should be highly susceptible to reaging at a temperature of 175°C . Most of the super saturated phases will have diffused from the original aging condition and therefore fairly stable precipitates will be expected in the material.

4.8 MECHANICAL PROPERTY ANALYSIS OF 2024-T3 ALLOY

4.8.1 TENSILE TEST OF 2024-T3 ALLOY

The tensile properties of the alloy in air at room temperature were established by using ASTM standard E8 [37]. The dimensions of the test specimens, the sizes of the test samples, and the physical measurements for the mechanical properties as given in Figure 3.1, referred in Section 3.3 and 3.5 and have been recorded in Table 4.6.

4.8.2 YIELD STRESS BEHAVIOR OF 2024-T3 ALLOY

The effects of reaging on the yield stress shows a continuous increase up to a maximum value of 400.40 ± 1.65 MPa at a reaging condition of 175°C for 150 hours. This increase in yield stress is 13.82% over that of the original -T3 material (Fig. 4.25). Further reaging beyond this time period results in a continuous decrease in yield strength. However even after reaging for 600 hours, the yield strength is still slightly better than it was in the original -T3 material (Fig. 4.26). It is interesting to note that the reaging time gradient of yield stress is higher at higher temperature. This is quite evident from the fact that there is an increase of 6.55% in

Table 4.6: Tensile mechanical properties of 2024-T3 aluminum alloy.

Reaging condition	Tensile mechanical properties							
	Yield		Ultimate		Ultimate		Fracture	
	stress		stress		strain		strain	
	(MPa)		(MPa)		(%)		(%)	
Mean	Std.	Mean	Std.	Mean	Std.	Mean	Std.	
value	Dev.	value	Dev.	value	Dev.	value	Dev.	
As received .	351.80±1.17	483.06±2.41	10.38±2.09	12.06±1.94				
Reaged at 95°C for 300 hours .	353.66±2.28	483.27±2.62	12.96±1.13	13.45±1.30				
Reaged at 135°C for 300 hours .	374.83±2.07	485.54±2.21	10.85±0.48	11.28±0.85				
Reaged at 175°C for 150 hours .	400.40±1.65	454.94±2.21	3.78±0.32	4.77±0.34				
Reaged at 175°C for 300 hours .	388.27±1.31	447.83±4.27	3.71±0.71	4.45±1.05				
Reaged at 175°C for 600 hours .	368.07±3.58	432.81±4.62	4.24±0.25	4.23±0.25				
Reaged at 207°C for 300 hours .	301.47±0.97	391.30±2.07	4.78±0.26	5.71±1.04				

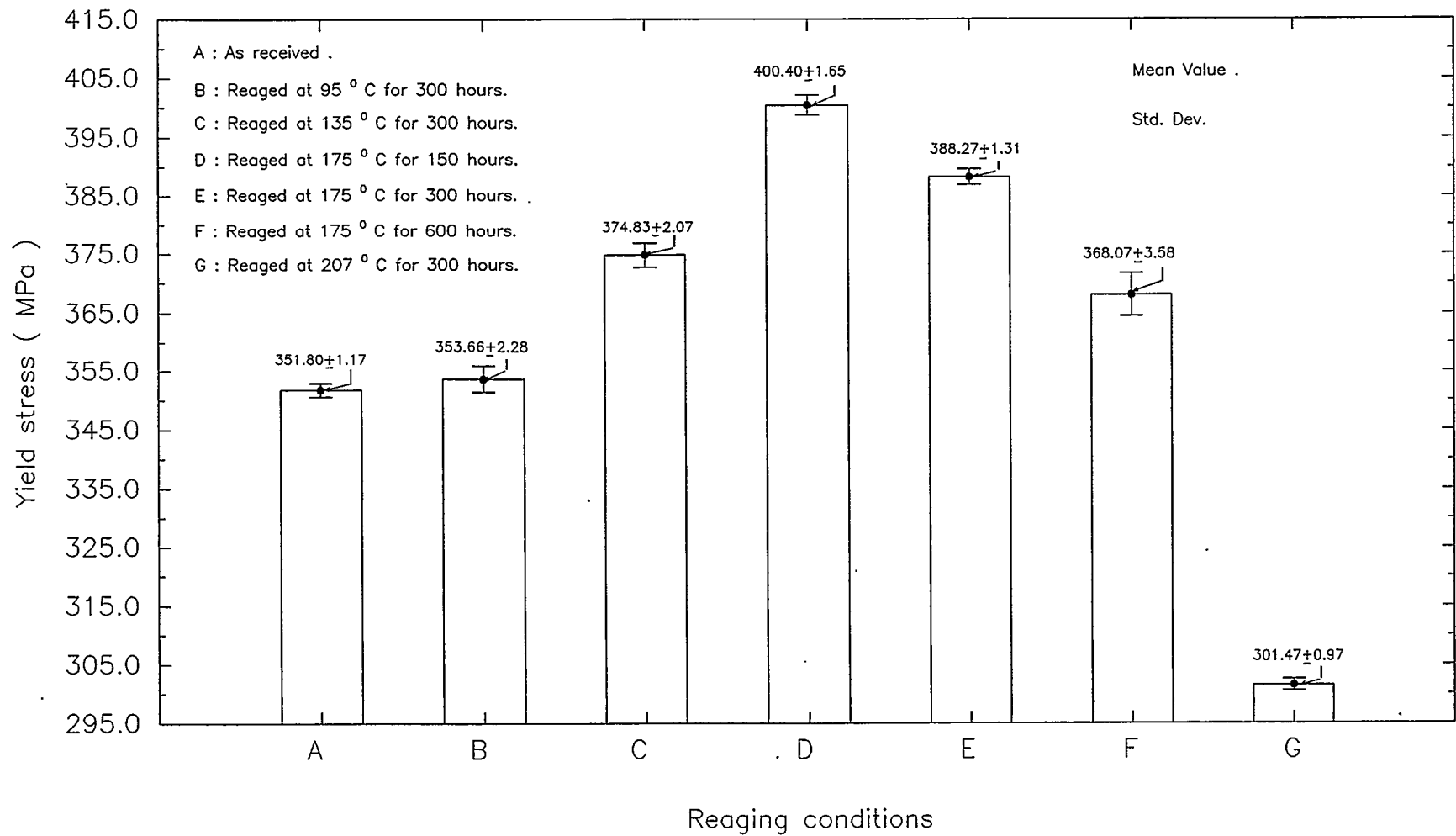


Figure 4.25 : Variation of yield stress of 2024-T3 alloy under different reaging conditions .

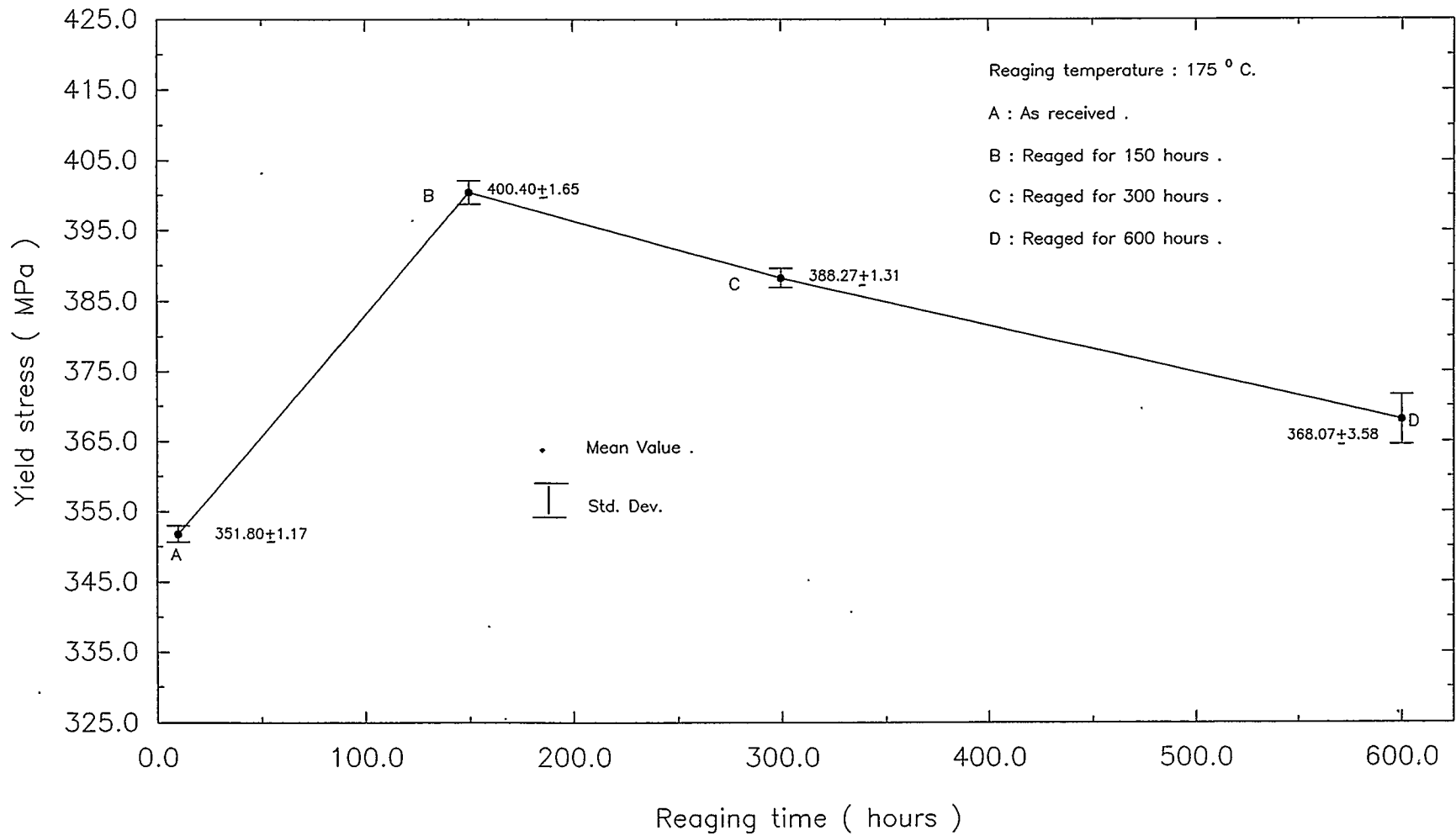


Figure 4.26: Relationship between yield stress and reaging time of 2024-T3 alloy at 175 ° C.

yield stress for reaging condition of 135°C and 300 hours compared to 13.81% increase in yield stress for a reaging at 175°C for 150 hours. A similar trend of faster overaging of the material is evident at higher temperatures that occur when comparing the reaging conditions at 175°C and 207°C for same reaging period of 300 hours. Under these reaging conditions, the loss in yield stress amounts to 10.37% and 14.31% respectively (Fig. 4.25, 4.27).

4.8.3 ULTIMATE TENSILE STRESS BEHAVIOR OF 2024-T3 ALLOY

The ultimate stress level remains fairly constant up to the reaging condition of 135°C for 300 hours (Fig. 4.28). Beyond this reaging condition, the ultimate strength starts to drop off and continues do so both for longer reaging periods and higher reaging temperatures (Fig. 4.29 and 4.30). When the alloy is reaged at 175°C for reaging time periods of 150, 300 & 600 hours, the corresponding loss in the ultimate strength has been found to be 5.82%, 7.29%, and 10.4% respectively over that of the as received -T3 material (Fig. 4.29). Reaging at temperature higher than 175°C , has much more pronounced effect. In contrast to 7.29% loss in ultimate strength at a reaging condition of 175°C for 300 hours, there is a 19% loss in ultimate stress for reaging at 207°C over the same time period of reaging (Fig. 4.30).

4.8.4 DUCTILITY BEHAVIOR OF 2024-T3 ALLOY

The ductility behavior of 2024-T3 is measured in terms of fracture strain as was the 7075-T6 material. A measure of ductility is fracture strain which maintains a fairly constant value up to a reaging condition of 135°C for 300 hours, as seen in Figure 4.31. Longer reaging times or higher reaging temperatures results in a greater drop in the value of fracture strain. There is a slight improvement in the material ductility at a reaging condition of 95°C for 300 hours. The behavior then shows a reversal at a reaging condition of 135°C for 300 hours (Fig. 4.32). However since these

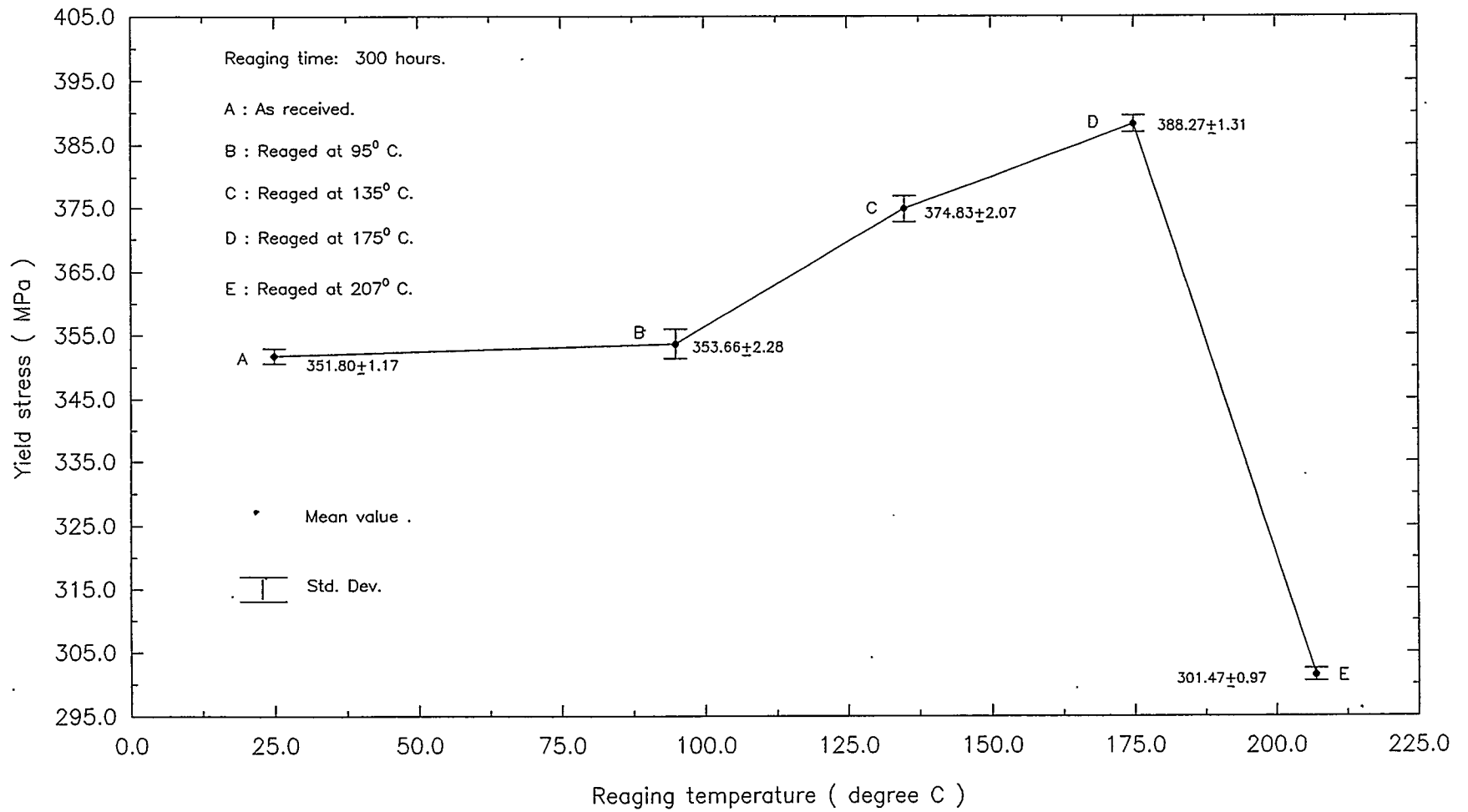


Figure 4.27: Relationship between yield stress and reaging temperature of 2024-T3 alloy at 300 hours.

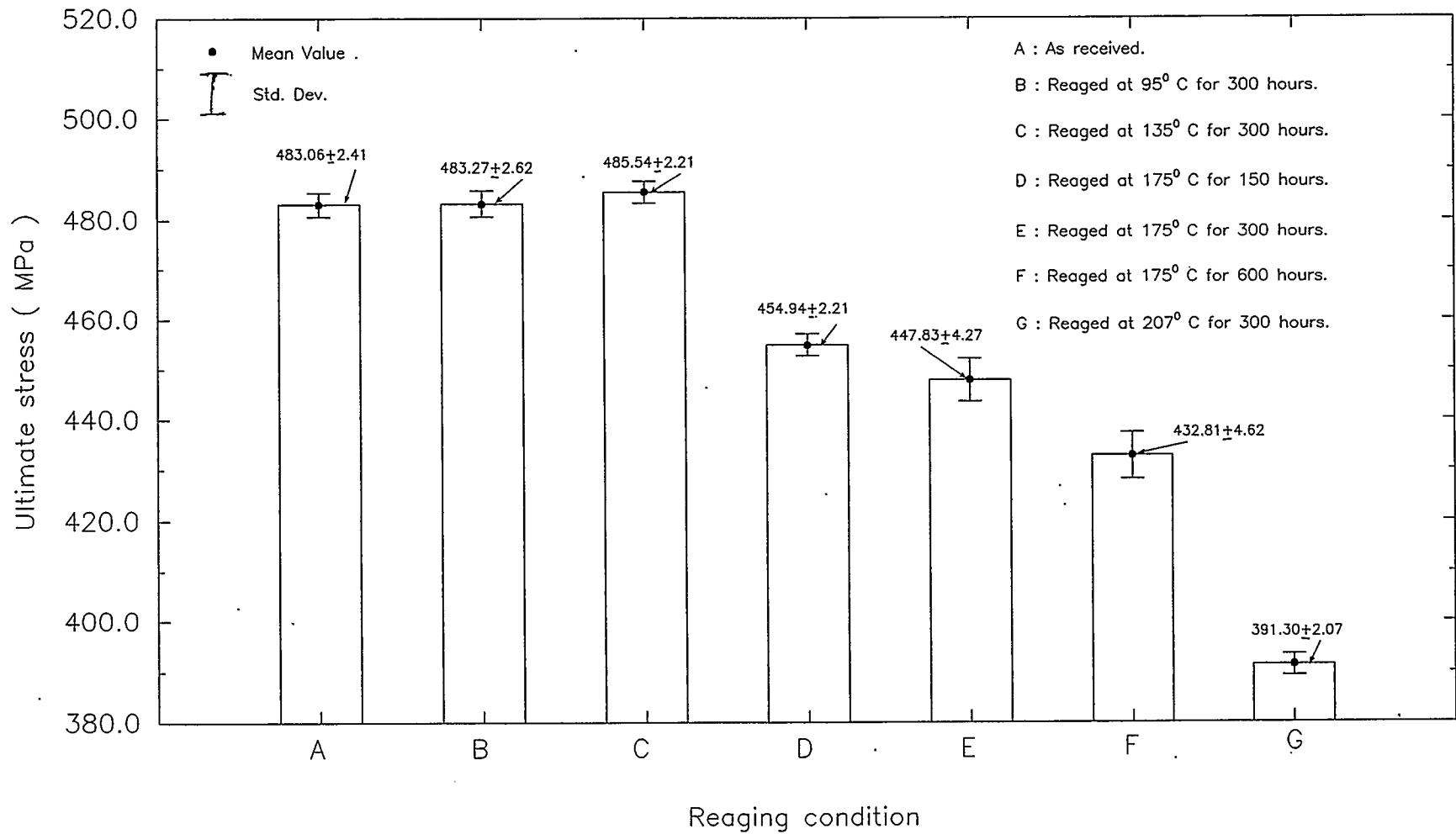


Figure 4.28: Variation of ultimate stress of 2024-T3 alloy under various reaging conditions.

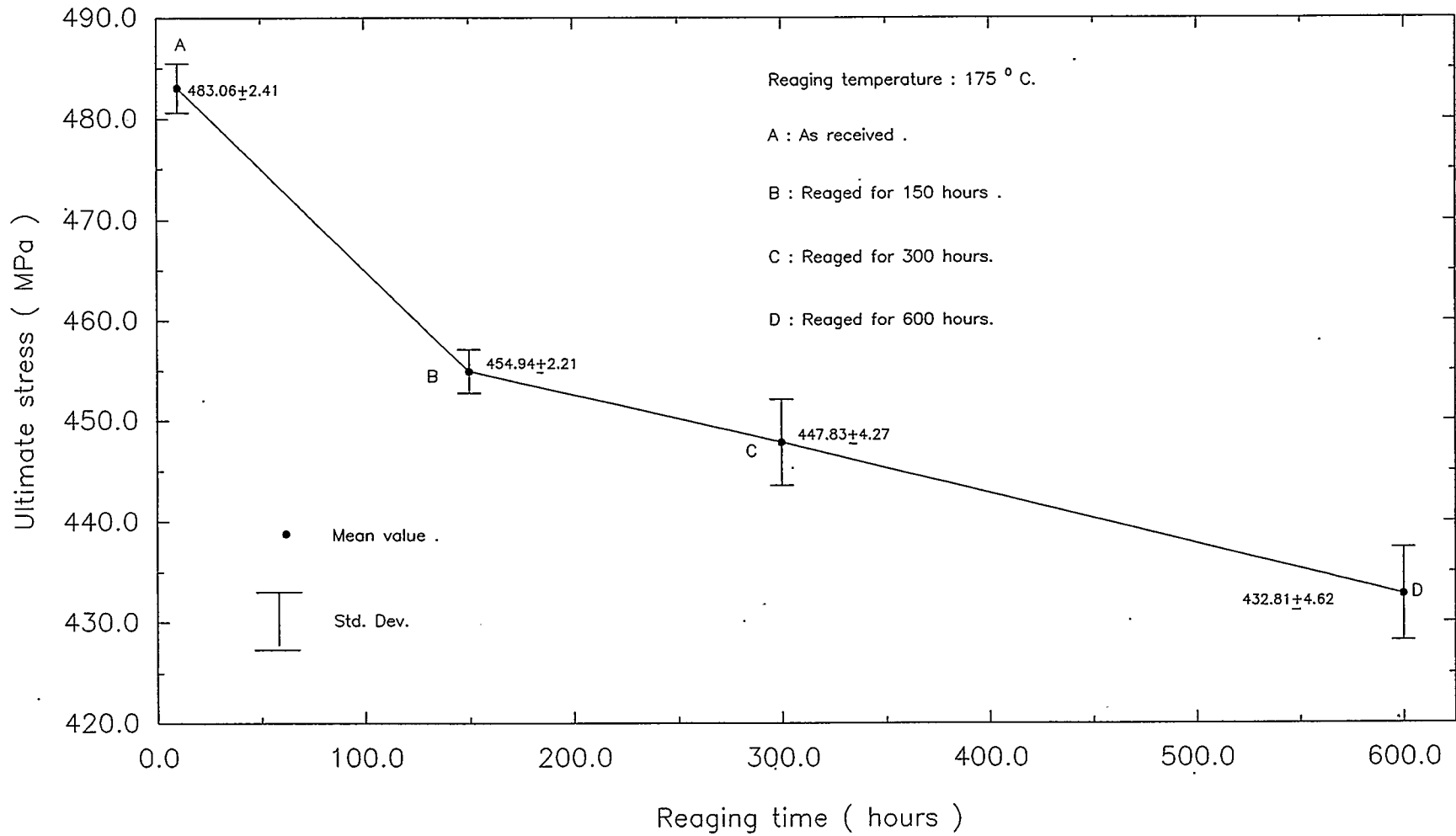


Figure 4.29 : Relationship between ultimate stress and reaging time of 2024-T3 alloy at 175 ° C .

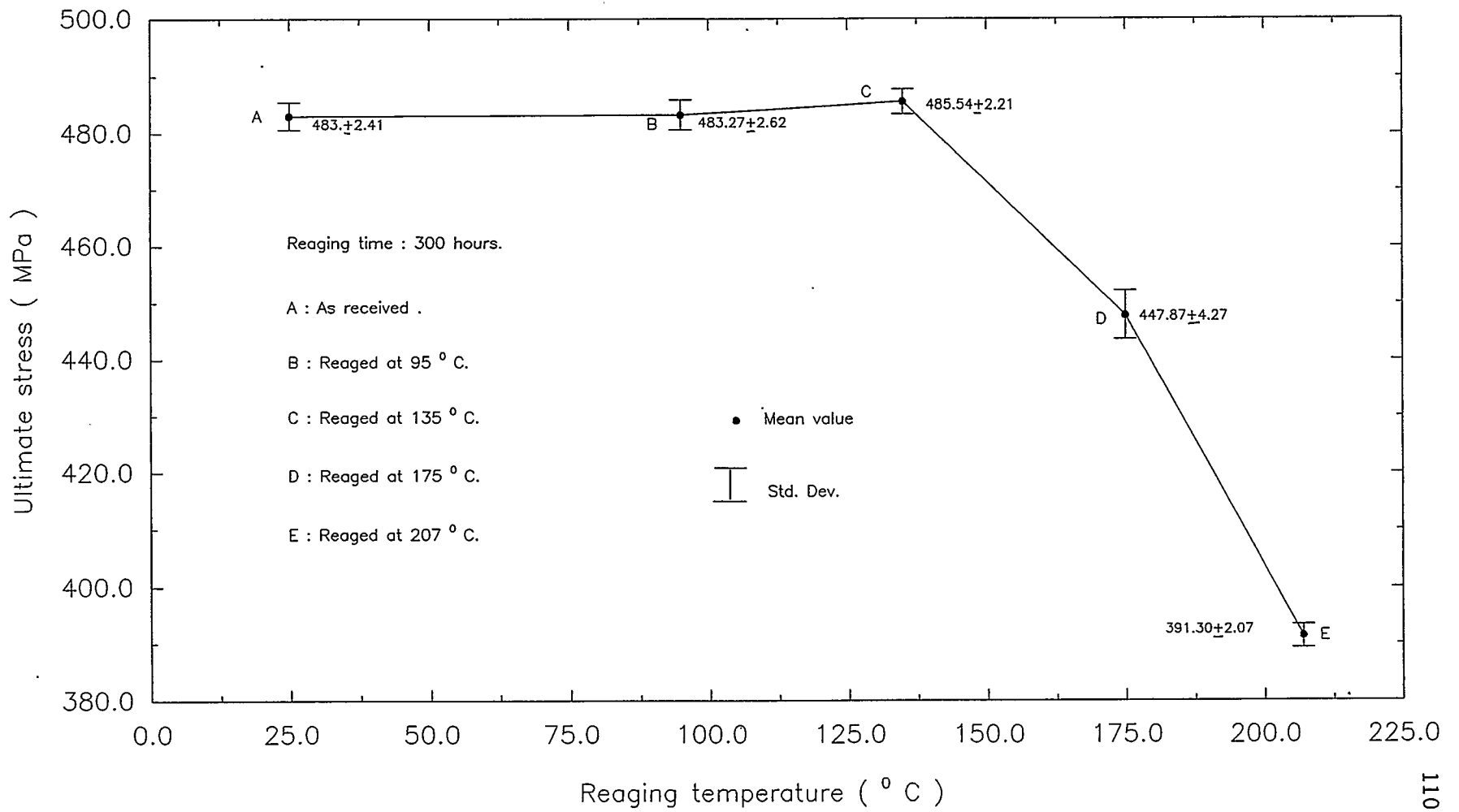


Figure 4.30 : Relationship between ultimate stress and reaging temperature of 2024-T3 alloy at 300 hours .

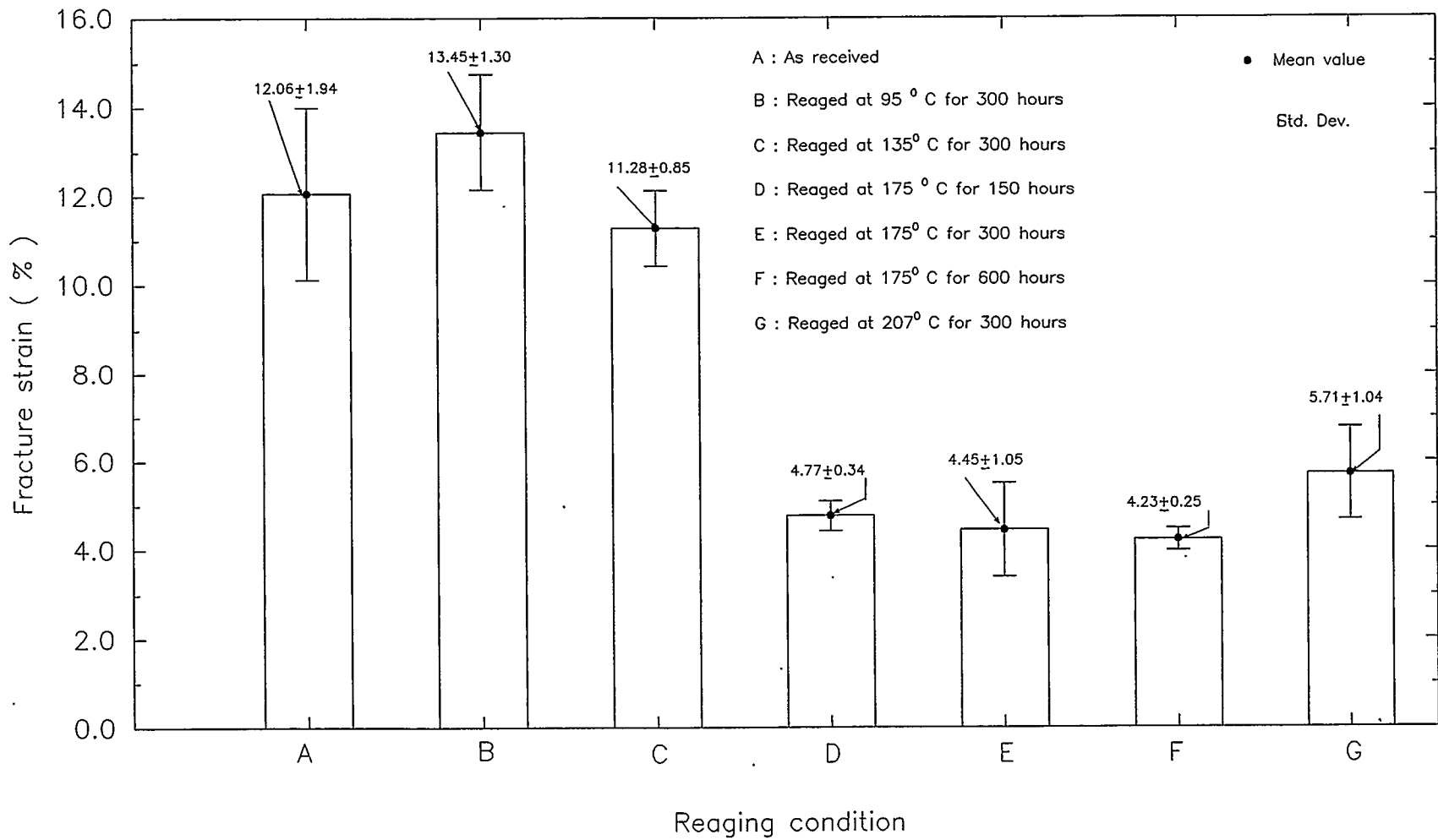


Figure 4.31: Variation of fracture strain of 2024-T3 alloy under various reaging conditions .

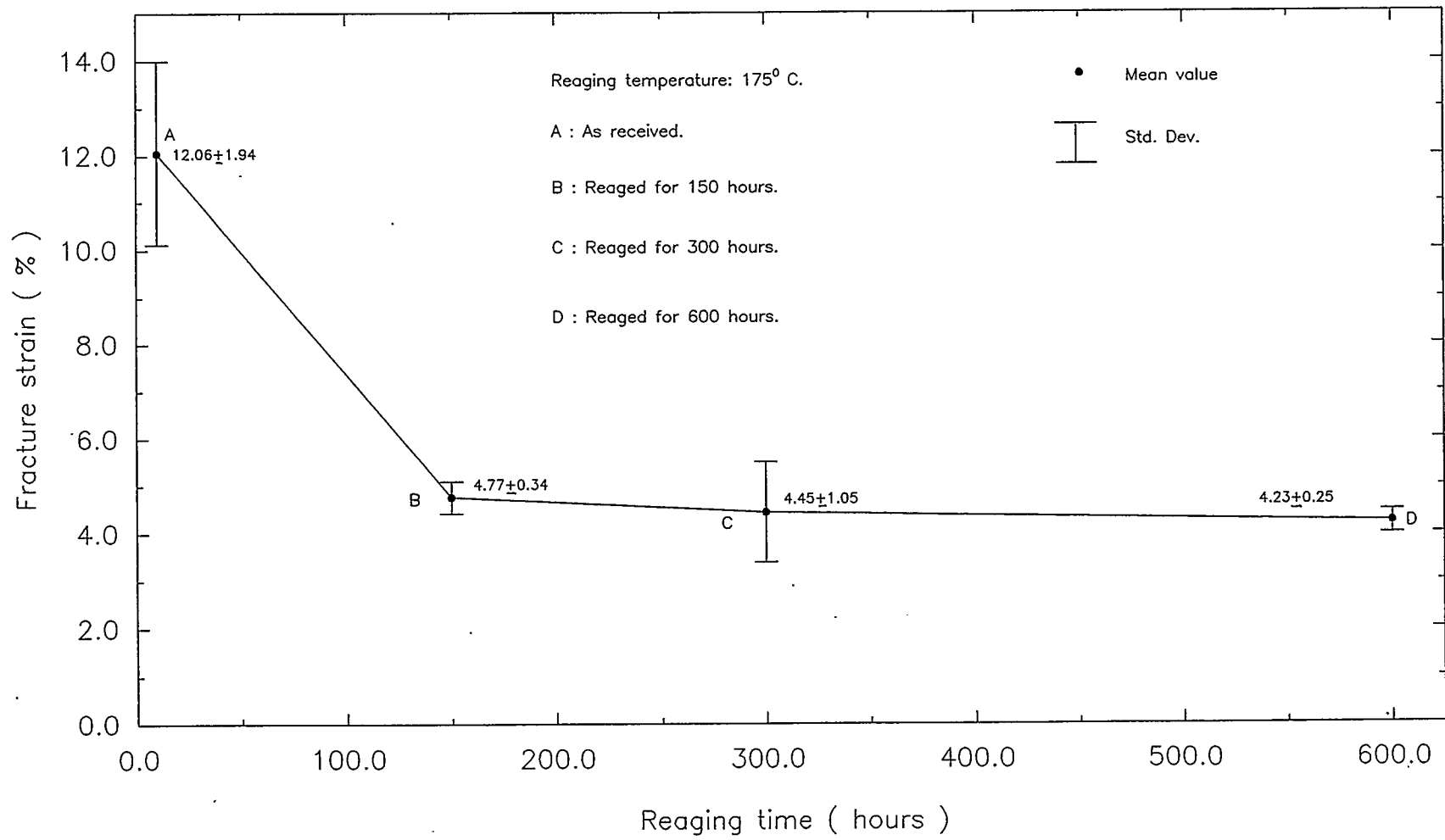


Figure 4.32: Relationship between fracture strain and reaging time of 2024-T3 alloy at 175° C.

changes are within a standard deviation of the base material behavior, it is therefore reasonable to assume that the material ductility remains fairly constant up to and including the reaging condition of 135°C. Beyond this point, ductility drops off quite sharply. There is approximately 60.5% loss in ductility at the reaging condition of 175°C for 150 hours as compared to the original -T3 material. After this initial drop off at 175°C reaging condition, the material ductility then remains fairly constant for longer time periods and even at higher reaging temperature (Fig. 4.31 and 4.32).

4.9 REAGING AND HARDNESS BEHAVIOR: 2024-T3

4.9.1 MACRO-HARDNESS BEHAVIOR OF 2024-T3 ALLOY

Hardness tests were conducted using ASTM standards E92 & E18 as mentioned in Sections 4.4.1 and 4.4.2 respectively. The results have been recorded in Tables 4.7 and 4.8. Micro-hardness behavior and the regular hardness (macro-hardness) behavior are indicative of microstructural changes occurring in the reaged alloy.

Macro-hardness values of the original as well the reaged material at different reaging conditions were tested. The statistical behavior of the test results is presented in Table 4.7. The micro-hardness behavior is very similar to the macro-hardness behavior. The measured values are also quite insensitive to reaging up to 175°C for 300 hours. There is a slight increase in macro-hardness of the alloy at 95°C for 300 hours. For reaging conditions of 135°C, 175°C for 150 hours, and 175°C for 300 hours, the macro-hardness of the alloy is close to the macro-hardness of the original alloy. The macro-hardness is relatively more sensitive to higher reaging conditions (Fig. 4.34-4.36) when reaged at conditions greater than 175°C for 300 hours. It is interesting to note that at the reaging condition of 207°C for 300 hours, the original material loses macro-hardness by about 16% (Fig. 4.34 and 4.35).

Table 4.7: Macro-hardness of 2024-T3 alloy measured at room temperature.

Reaging condition	Macro-hardness (Rockwell B) Mean \pm Std.Dev.
As received.	70.78 \pm 0.21
Reaged at 95 $^{\circ}$ C for 300 hours.	72.09 \pm 1.67
Reaged at 135 $^{\circ}$ C for 300 hours.	71.61 \pm 0.68
Reaged at 175 $^{\circ}$ C for 150 hours.	71.46 \pm 0.50
Reaged at 175 $^{\circ}$ C for 300 hours.	70.68 \pm 0.88
Reaged at 175 $^{\circ}$ C for 600 hours.	68.40 \pm 0.29
Reaged at 207 $^{\circ}$ C for 300 hours.	59.51 \pm 0.54

Table 4.8: Micro-hardness of 2024-T3 alloy measured at room temperature.

Reaging condition	Micro-hardness (VHN) Mean \pm Std.Dev.
As received.	131.77 \pm 3.76
Reaged at 95 $^{\circ}$ C for 300 hours.	137.31 \pm 4.61
Reaged at 135 $^{\circ}$ C for 300 hours.	136.40 \pm 4.05
Reaged at 175 $^{\circ}$ C for 150 hours.	134.68 \pm 2.65
Reaged at 175 $^{\circ}$ C for 300 hours.	132.40 \pm 3.13
Reaged at 175 $^{\circ}$ C for 600 hours.	128.30 \pm 3.20
Reaged at 207 $^{\circ}$ C for 300 hours.	115.55 \pm 3.10

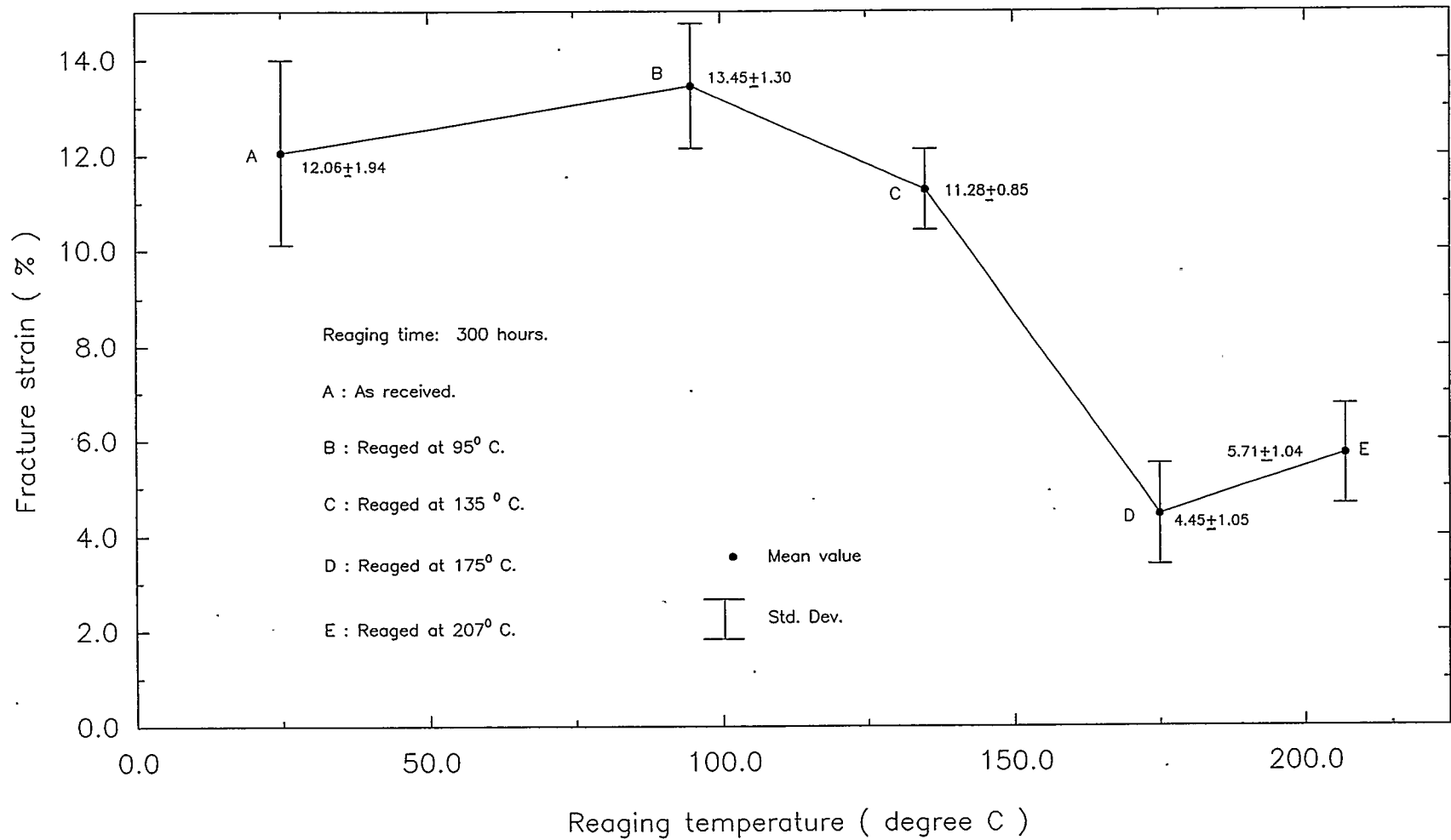


Figure 4.33: Relationship between fracture strain and reaging temperature of 2024-T3 alloy at 300 hours.

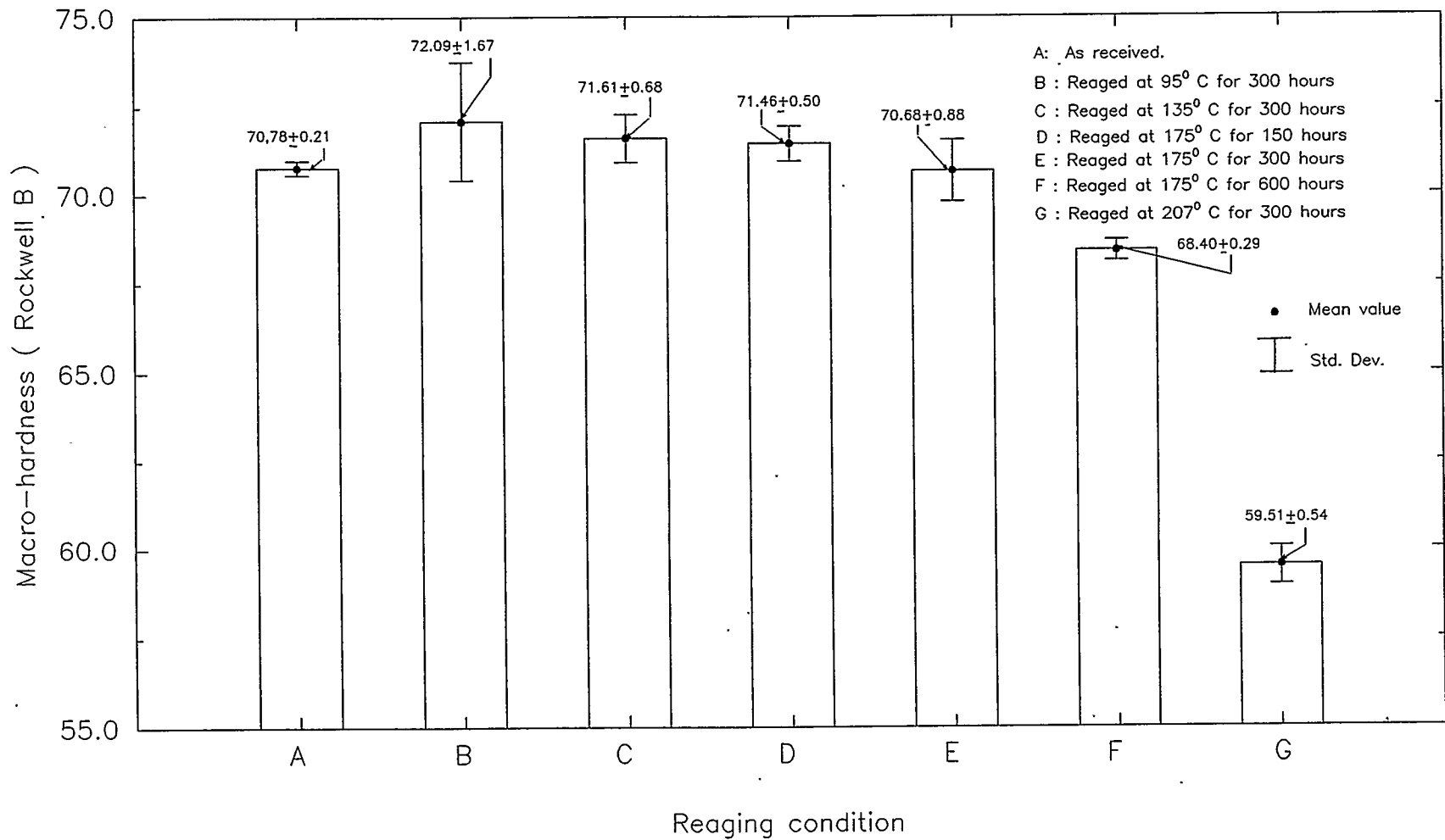


Figure 4.34: Variation of macro-hardness of 2024-T3 alloy under various reaging conditions .

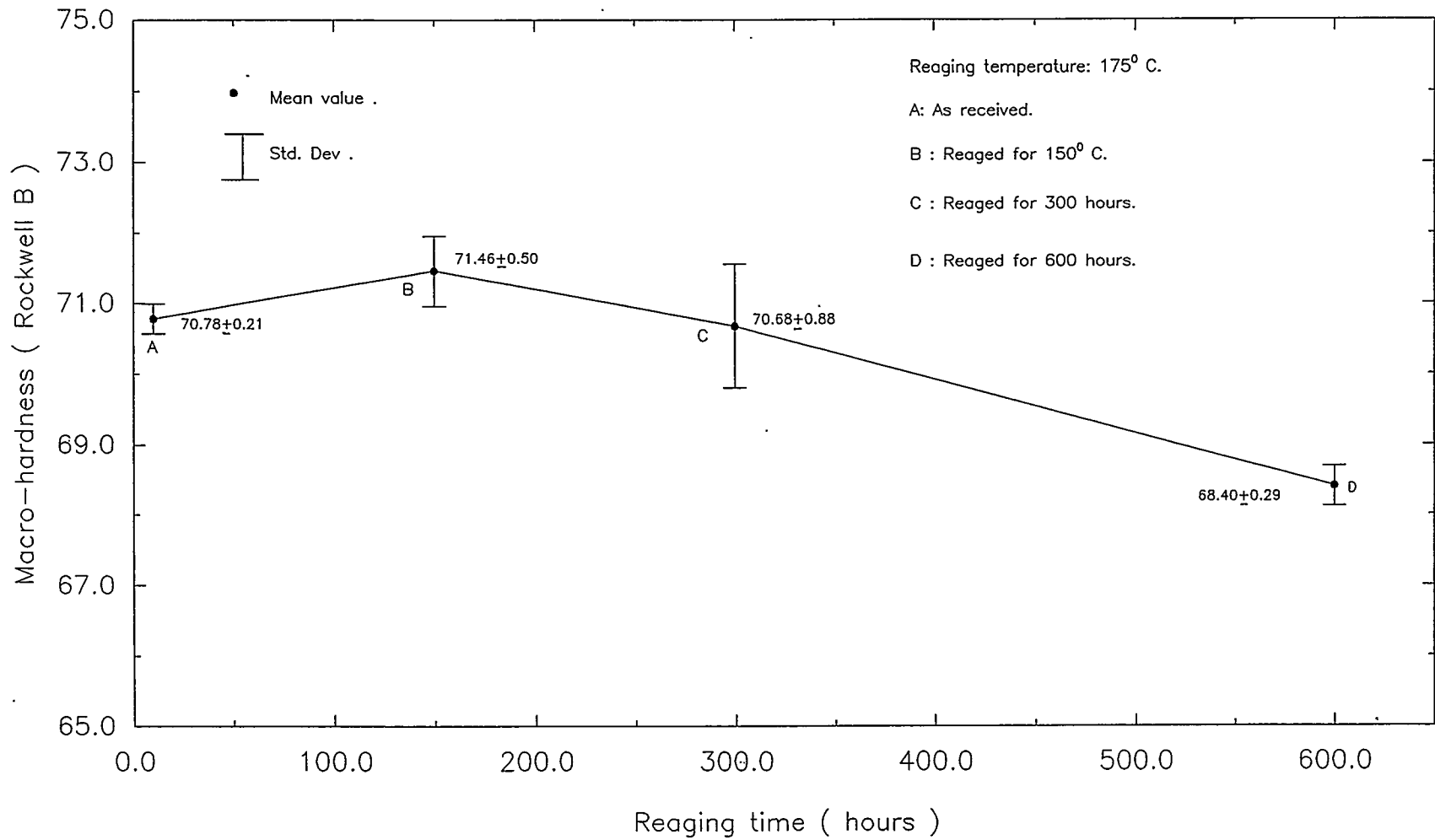


Figure 4.35: Relationship between macro-hardness and reaging time of 2024-T3 alloy at 175^o C.

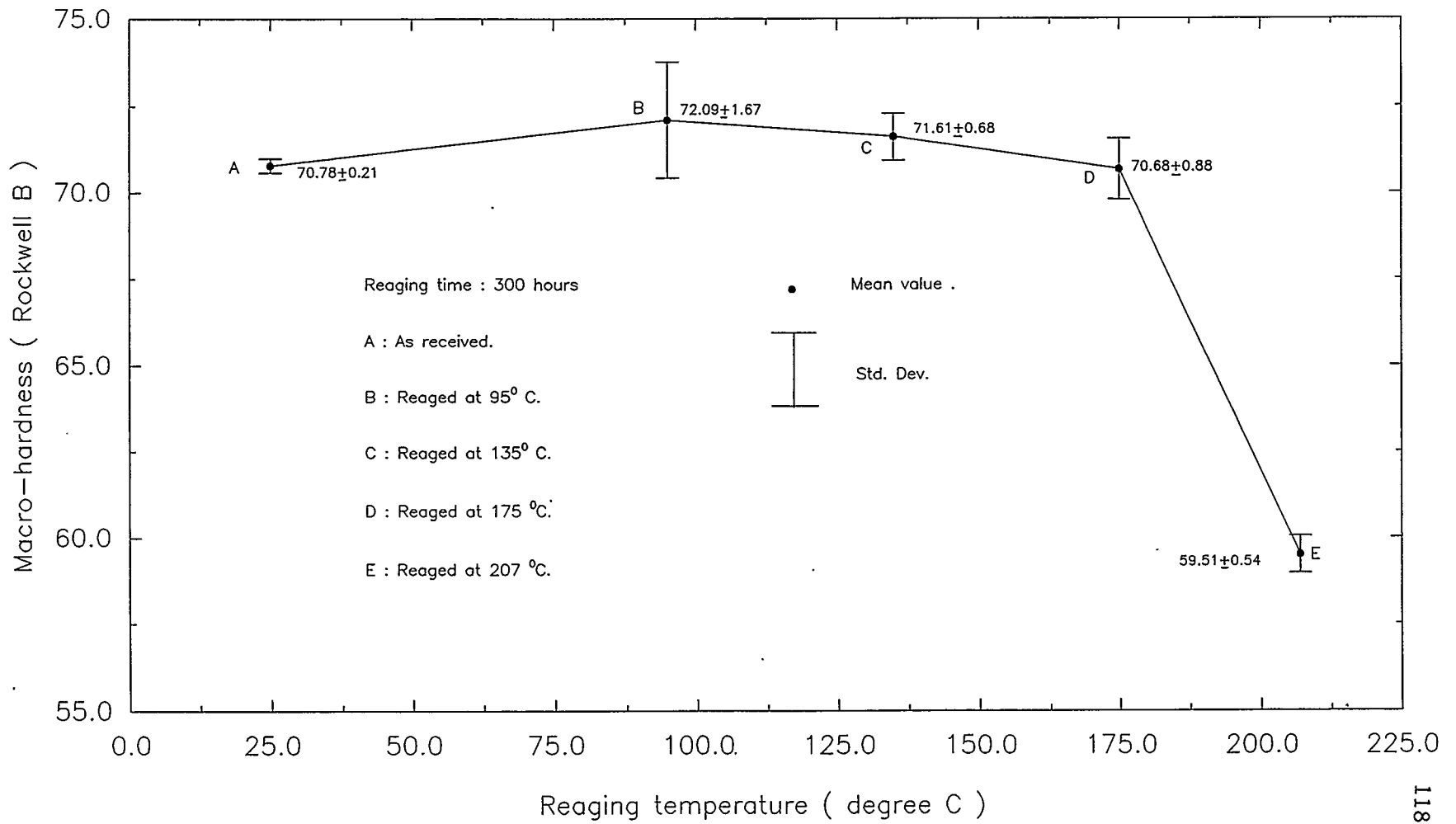


Figure 4.36: Relationship between macro-hardness and reaging temperature of 2024-T3 alloy at 300 hours.

4.9.2 MICRO-HARDNESS BEHAVIOR OF 2024-T3 ALLOY

The micro-hardness behavior of the original -T3 and reaged material at various conditions is presented in Table 4.8. The statistical variation recorded in Table 4.8 and is graphically presented in Figures 4.37, 4.38 and 4.39. There is very marginal increase of approximately 4% in micro-hardness up to the reaging condition of 95°C for 300 hours. After this condition the micro-hardness drops off slowly but continuously to the reaging condition of 175°C for 300 hours. However even at this high degree of reaging the micro-hardness is quite close to its original value. Therefore up to a reaging condition of 175°C for 300 hours, micro-hardness is fairly insensitive to reaging conditions (Figure 4.34). Beyond this, the micro-hardness shows comparatively more sensitivity to change both for longer reaging time periods and higher reaging temperatures (Fig. 4.38 & 4.39). At a reaging condition of 207°C for 300 hours, the alloy loses approximately 12% of its micro-hardness value as compared to that of the original material (Fig. 4.38).

4.10 ELECTRICAL CONDUCTIVITY BEHAVIOR OF 2024-T3 ALLOY

The results of the measured electrical conductivity for the aged and reaged conditions are recorded in Table 4.9. The relationship between the reaging conditions and the corresponding conductivities, have been graphically analyzed as shown in Figures 4.40, 4.41 and 4.42. The electrical conductivity is fairly constant up to a reaging condition of 135°C for 300 hours. Although at a reaging condition of 135°C for 300 hours, there is slight increase in the electrical conductivity, this change is so small that it can be considered unaffected up to this reaging condition. However there is a considerable increase in the electrical conductivity value that takes place at the reaging condition of 175°C for 150 hours. The electrical conductivity value rises from 30.61% IACS to 40.57% IACS. Further reaging up to 600 hours at 175°C does not appreciably change the electrical conductivity (Fig. 4.40 and 4.42). It is interesting to

Table 4.9 Electrical conductivity of 2024-T3 alloy at room temperature.

Reaging condition	Electrical conductivity (% IACS) Mean±Std.Dev.
As received.	30.61±0.06
Reaged at 95°C for 300 hours.	30.66±0.07
Reaged at 135°C for 300 hours.	31.79±0.11
Reaged at 175°C for 150 hours.	40.57±0.09
Reaged at 175°C for 300 hours.	40.79±0.23
Reaged at 175°C for 600 hours.	41.30±0.11
Reaged at 207°C for 300 hours.	42.30±0.10

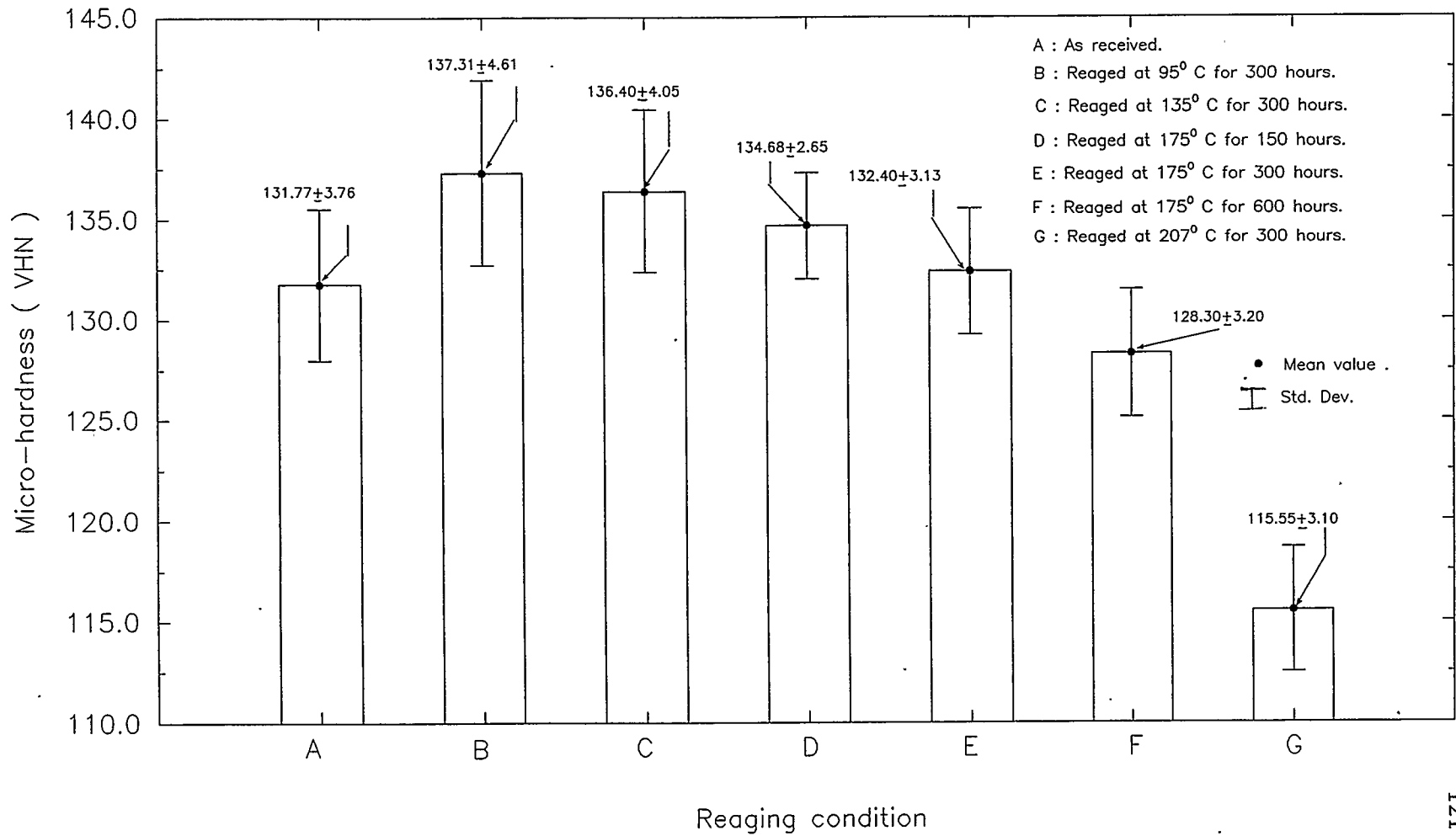


Figure 4.37: Variation of micro-hardness of 2024-T3 alloy under various reaging conditions.

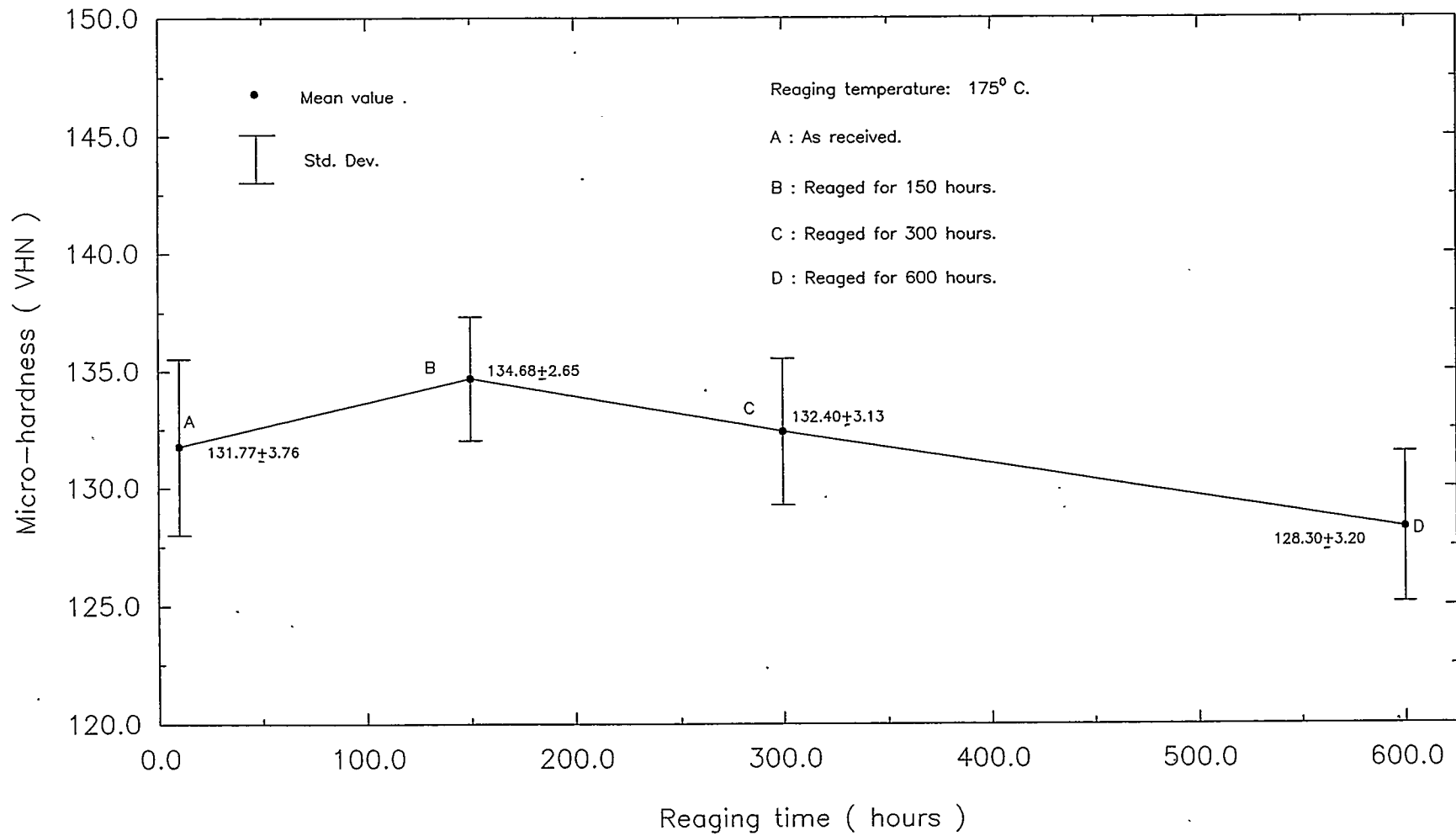


Figure 4.38: Relationship between micro-hardness and reaging time of 2024-T3 alloy at 175° C.

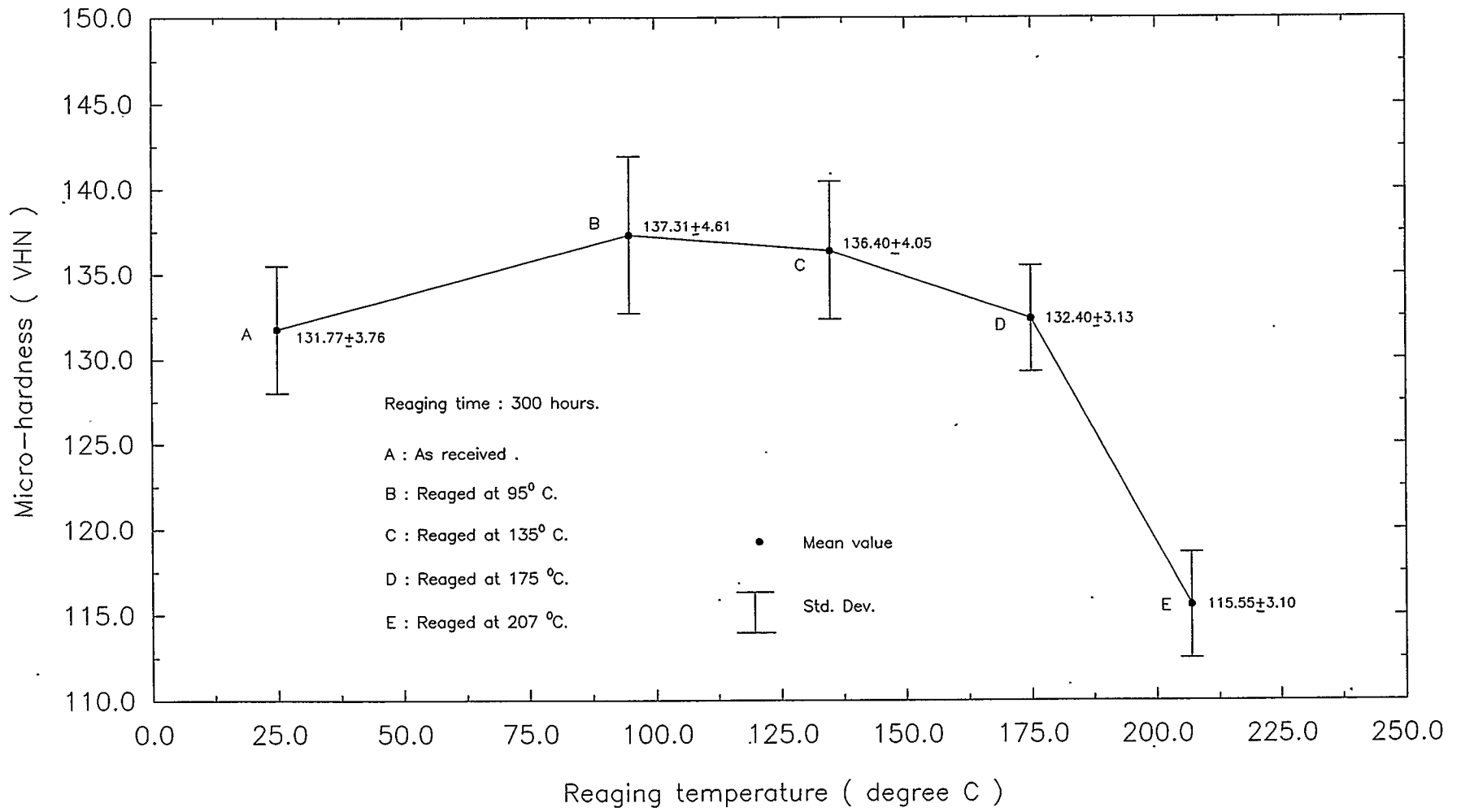


Figure 4.39: Relationship between micro-hardness and reaging temperature of 2024-T3 alloy at 300 hours.

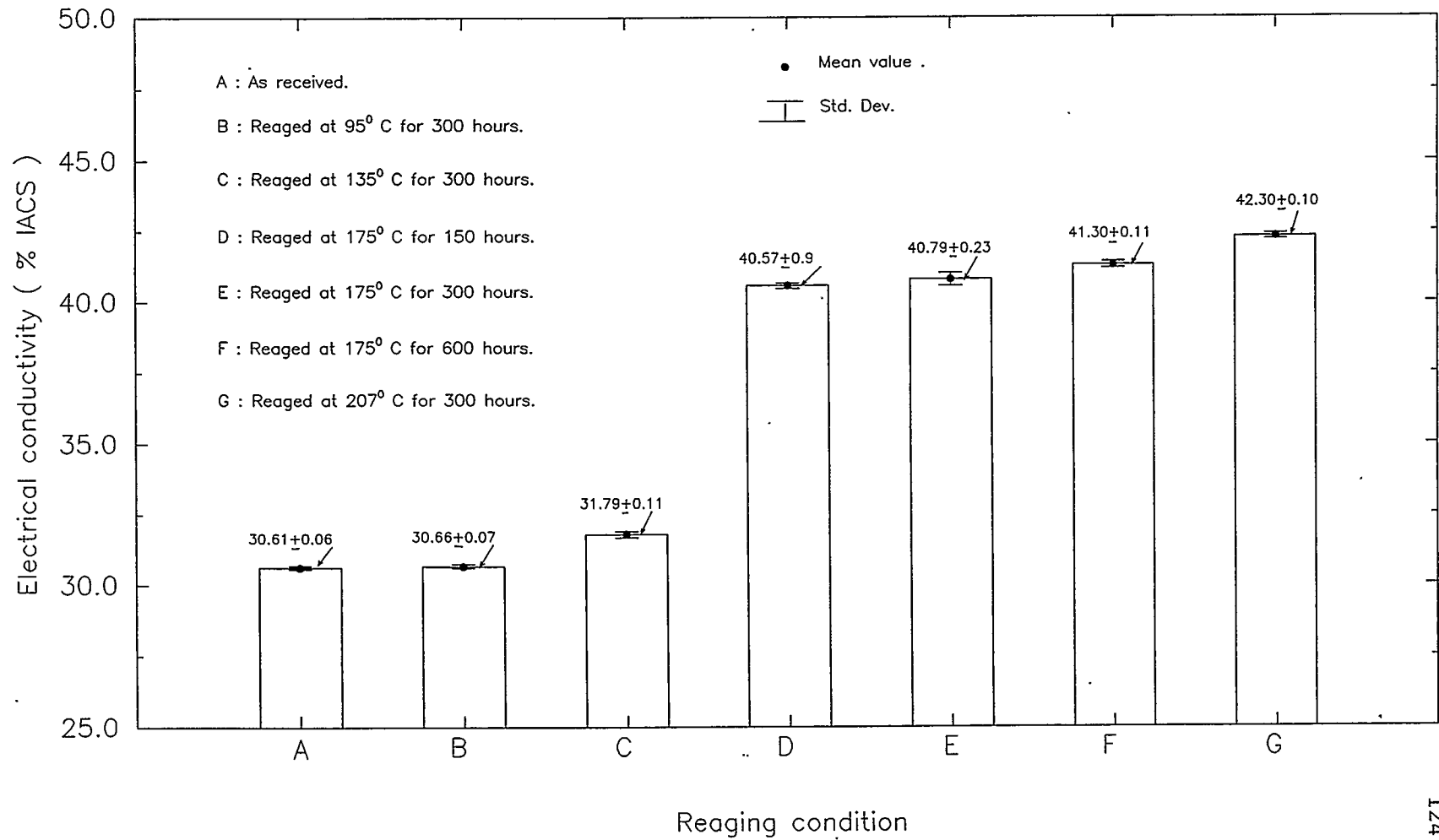


Figure 4.40: Variation of electrical conductivity of 2024-T3 alloy under various reaging conditions.

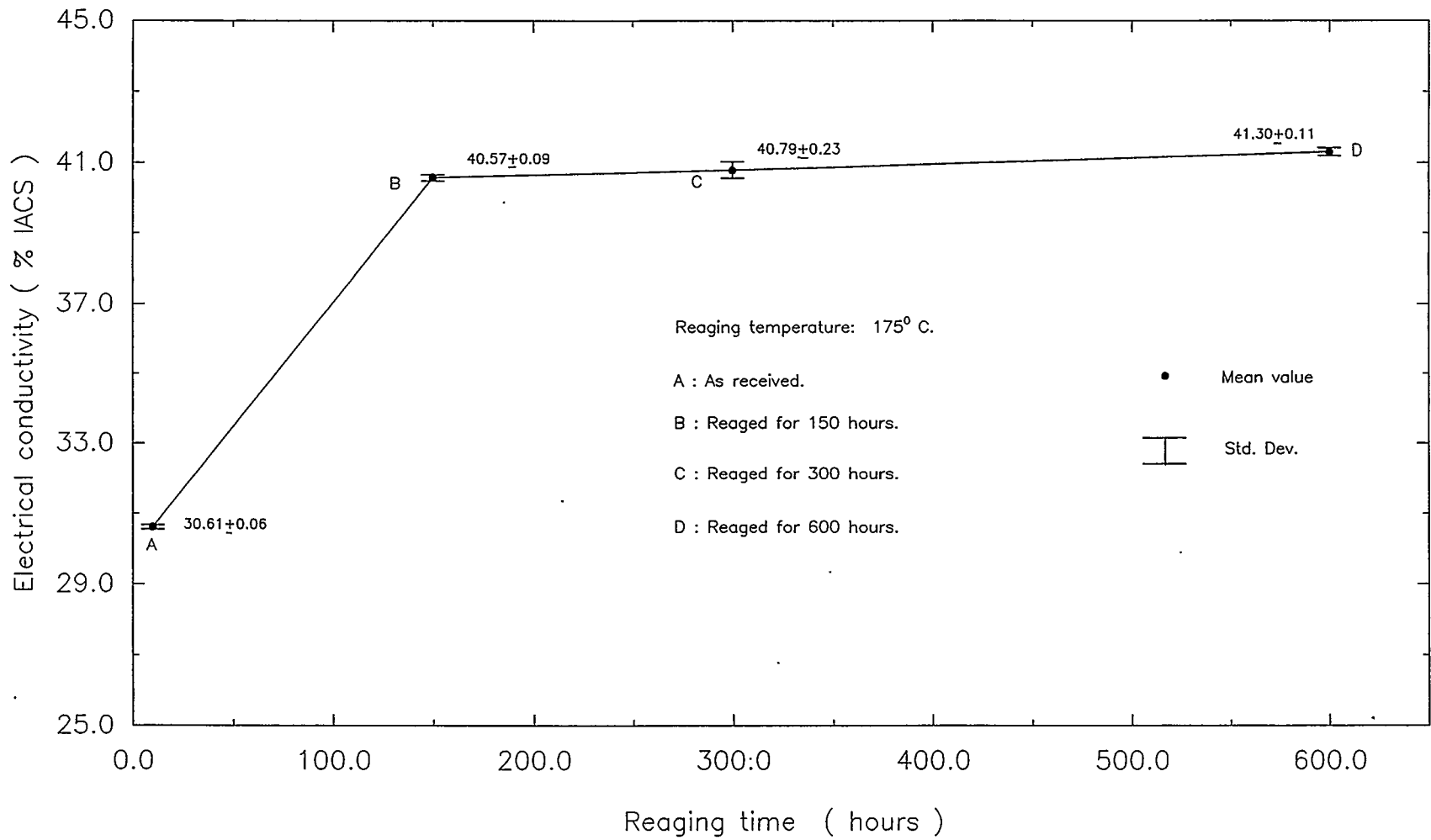


Figure 4.41: Relationship between electrical conductivity and reaging time of 2024-T3 alloy at 175° C.

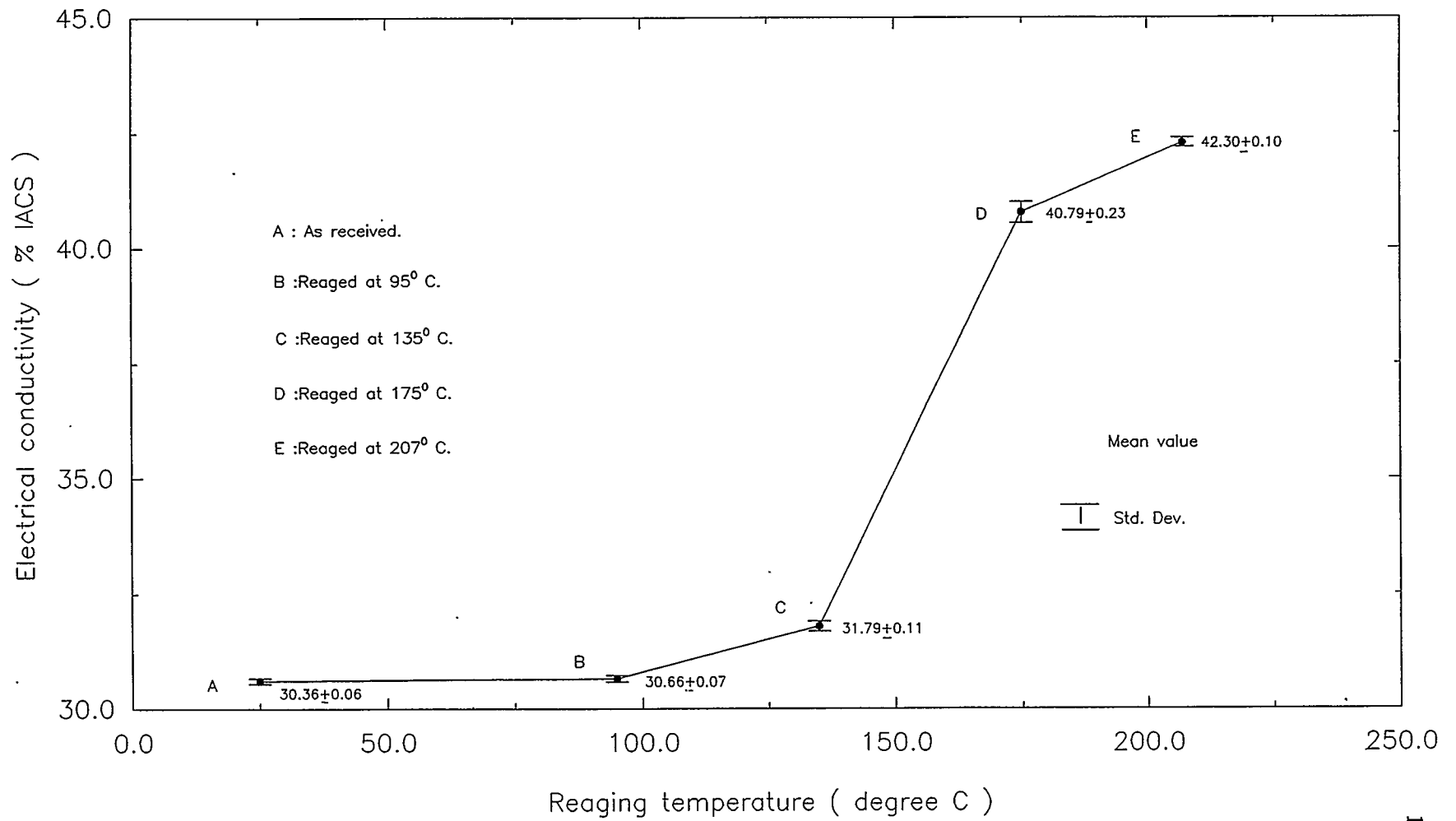


Figure 4.42: Relationship between electrical conductivity and reaging temperature of 2024-T3 alloy at 300 hours.

note that the initial changes in the material are quite sensitive to conductivity measurements. These changes can be accurately monitored using conductivity up to a reaging condition of 175°C for 150 hours. Reaging conditions beyond this result in virtually no further change in electrical conductivity as the technique becomes insensitive in reflecting further corresponding material changes.

4.11 FATIGUE CRACK GROWTH BEHAVIOR OF 2024-T3 ALLOY

The fatigue crack growth behavior of 2024-T3 alloy as related to its reaging conditions, was examined through fatigue crack growth tests as mentioned in Section 4.6. The experimental data of the fatigue test conducted for each reaging condition was then analyzed by using computer programs to generate crack growth rate information. The graphical analysis of the results are presented in Figure 4.43 through Figure 4.48. The normalized fatigue life behavior of 2024-T3 aluminum alloy under different reaging conditions was also analyzed through bar graph (Table 4.10 and Fig. 4.46).

It is observed from the graphical analysis of the crack growth life (crack length versus fatigue cycles), crack propagation relations (crack growth rate versus change in stress intensity factor) and fatigue failure (reaging conditions versus fatigue cycles to failure), that there is no detrimental effect on the fatigue life of the alloy up to and including a reaging condition of 175°C for 150 hours (Fig. 4.45, 4.46 and 4.47). All the above mentioned relations show that reaging at 95°C for 300 hours provides a lower crack propagation rate as compared to the original -T3 alloy and consequently a higher fatigue life (Fig. 4.44, 4.46 and 4.48). This improved fatigue condition is approximately 70% above the original -T3 material. Reaging at higher temperatures such as at 135°C for 300 hours, at 175°C for 150 hours does not show any appreciable effect on the fatigue life of the alloy (Fig. 4.46).

Beyond the reaging condition of 175°C for 150 hours, the alloy

Table 4.10: Reaging conditions and normalized fatigue life of 2024-T3.

Reaging condition.	Total life (cycles)	Normalizing cycles.	Normalized fatigue life. (cycles)
As received.	229,942	94,328	135,614 ±25,370
Reaged at 95°C for 300 hours.	328,758	132,367	196,391
Reaged at 135°C for 300 hours.	172,060	36,344	135,716
Reaged at 175°C for 150 hours.	176,062	35,065	140,997
Reaged at 175°C for 300 hours.	99,888	44,994	54,894
Reaged at 175°C for 600 hours.	217,459	24,148	193,311
Reaged at 207°C for 300 hours.	373,483	170,970	202,513

* normalized at a crack length of 15.70 mm.

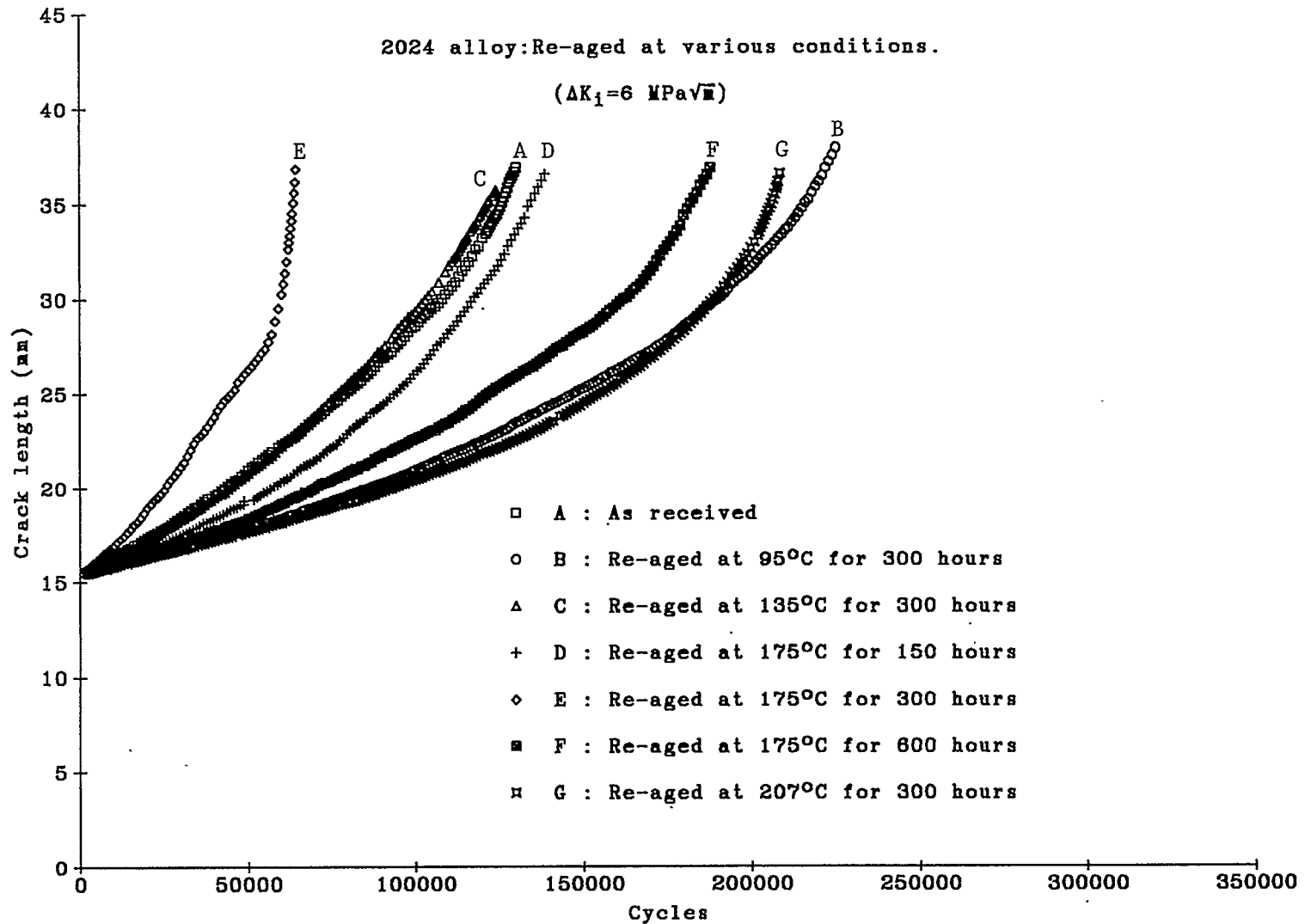


Figure 4.43: Relationship between crack length and fatigue life cycles of 2024-T3 alloy; reaged at various conditions.

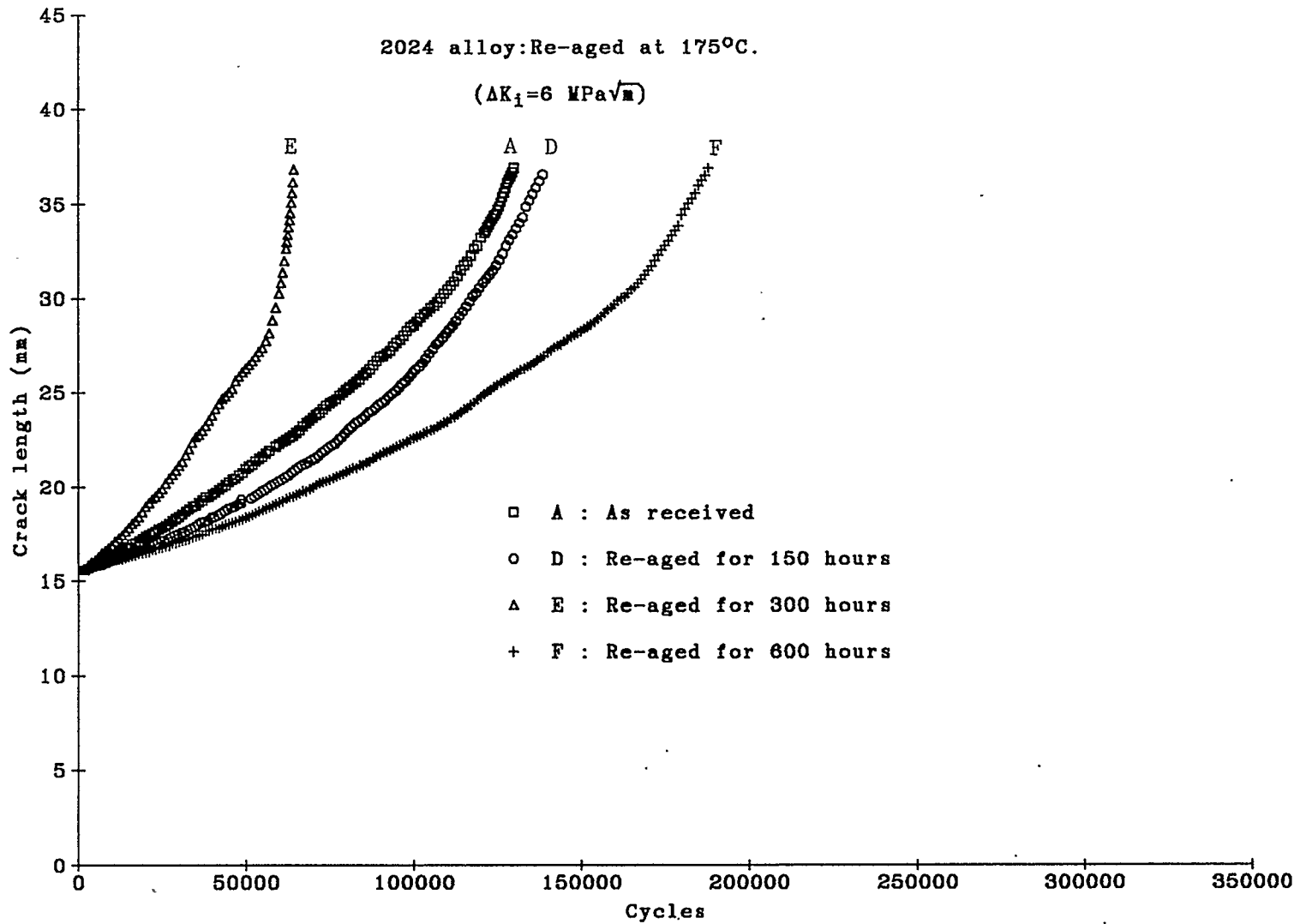


Figure 4.44: Relationship between crack length and fatigue life cycles of 2024-T3 alloy; reaged at 175°C.

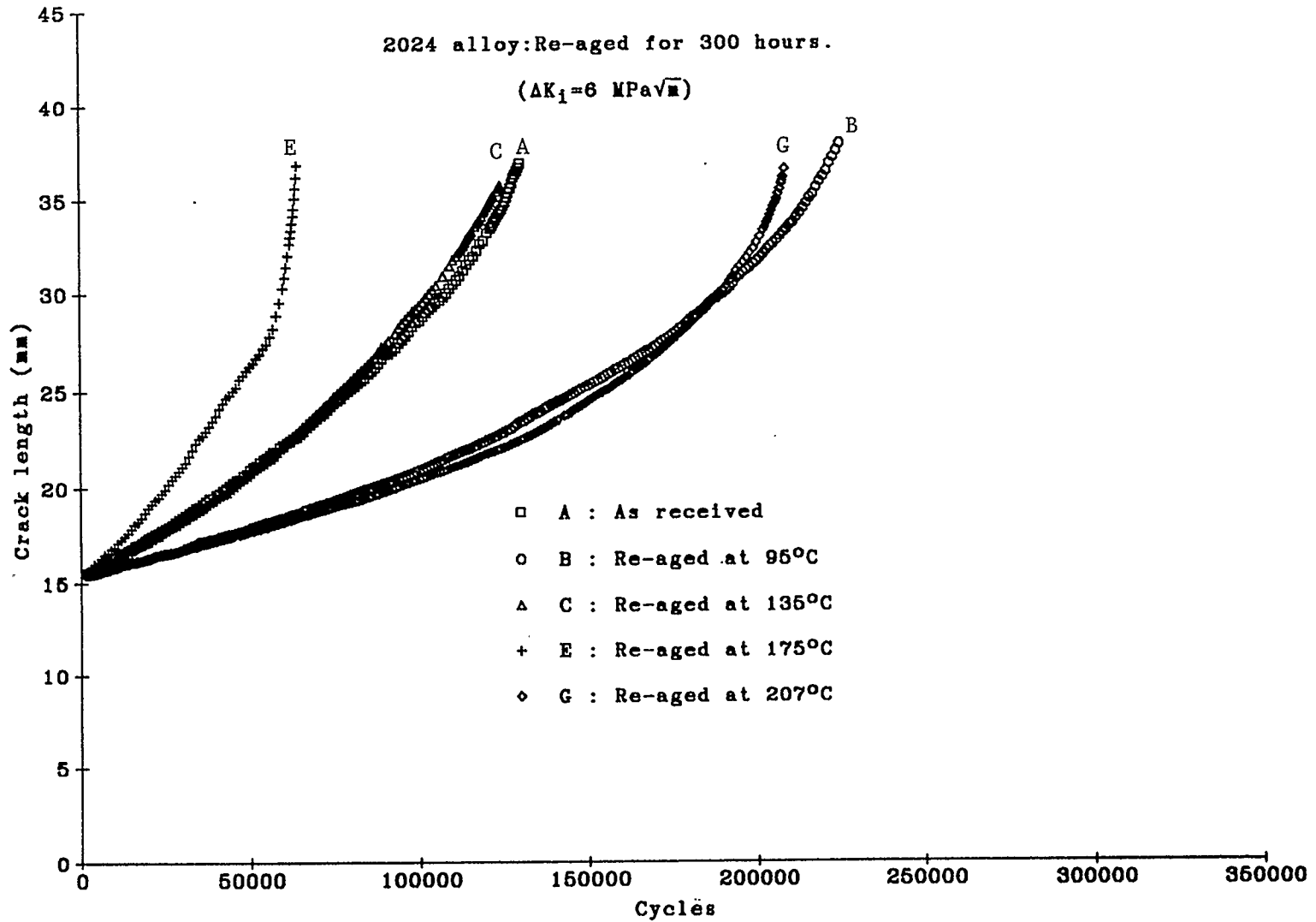


Figure 4.45: Relationship between crack length and fatigue life cycles of 2024-T3 alloy; reaged for 300 hours.

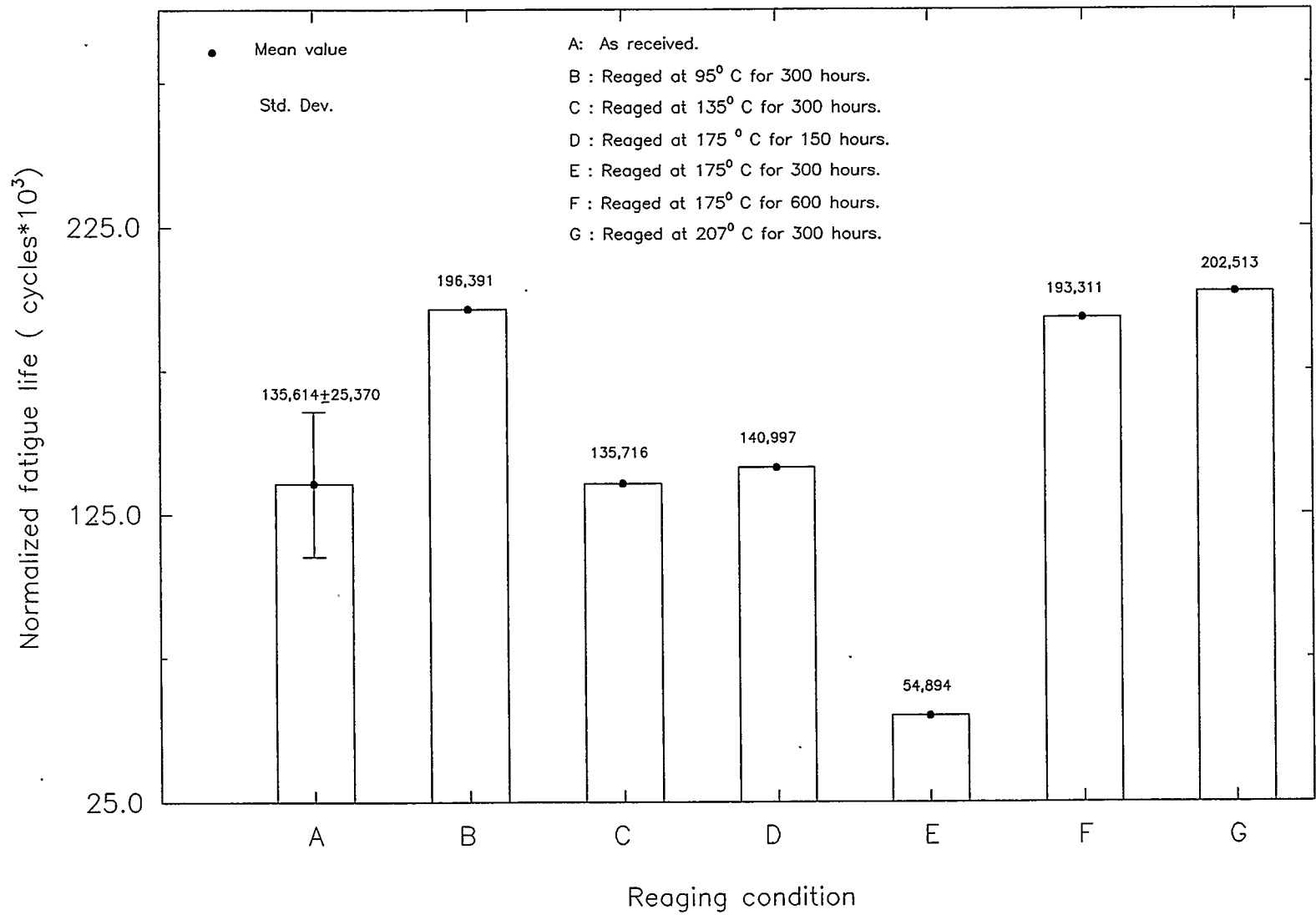


Figure 4.46: Variation of normalized fatigue life of 2024-T3 alloy under various reaging conditions.

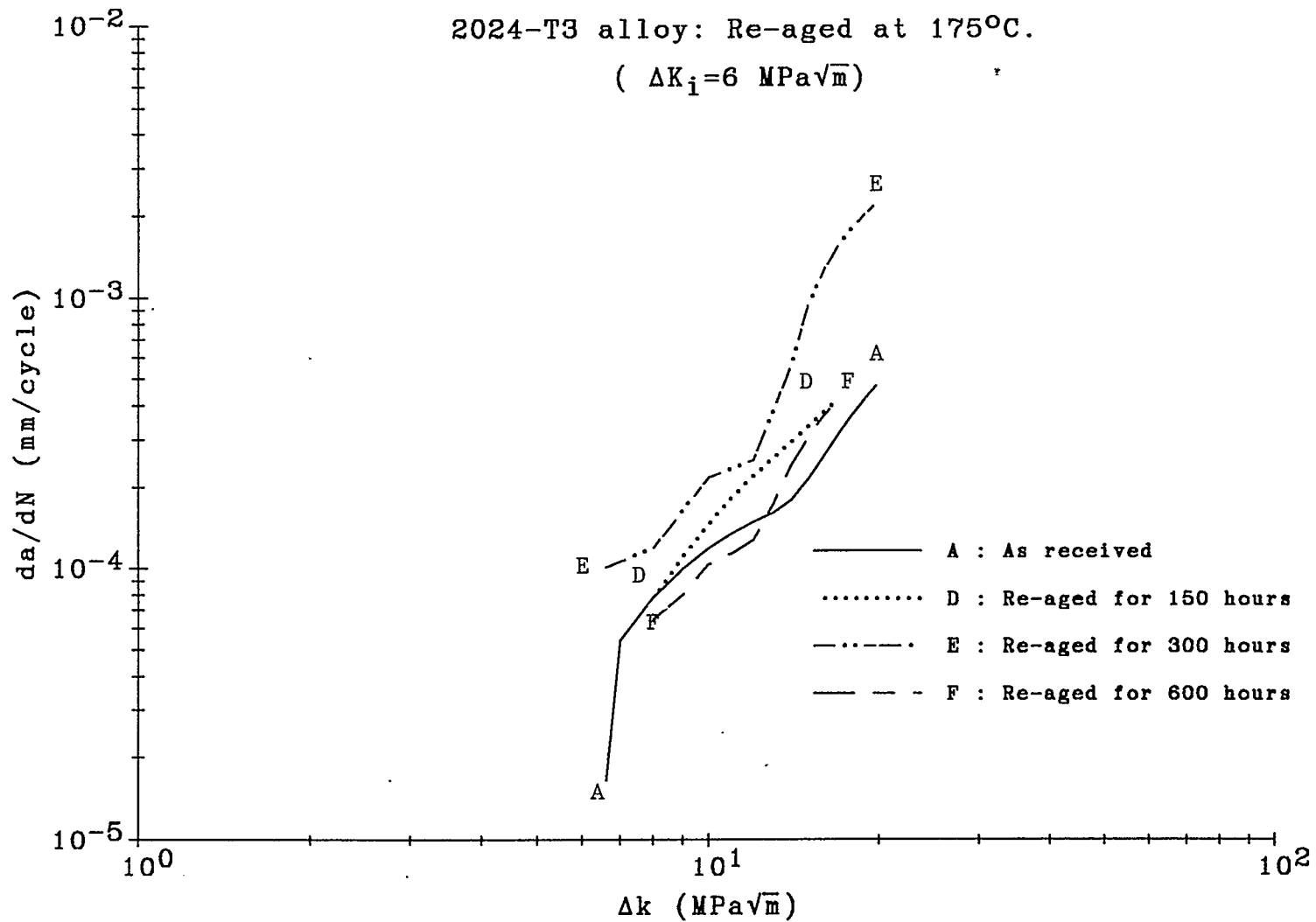


Figure 4.47: Relationship between the crack growth rate and change in stress intensity factor of 2024-T3 alloy; reaged at 175°C.

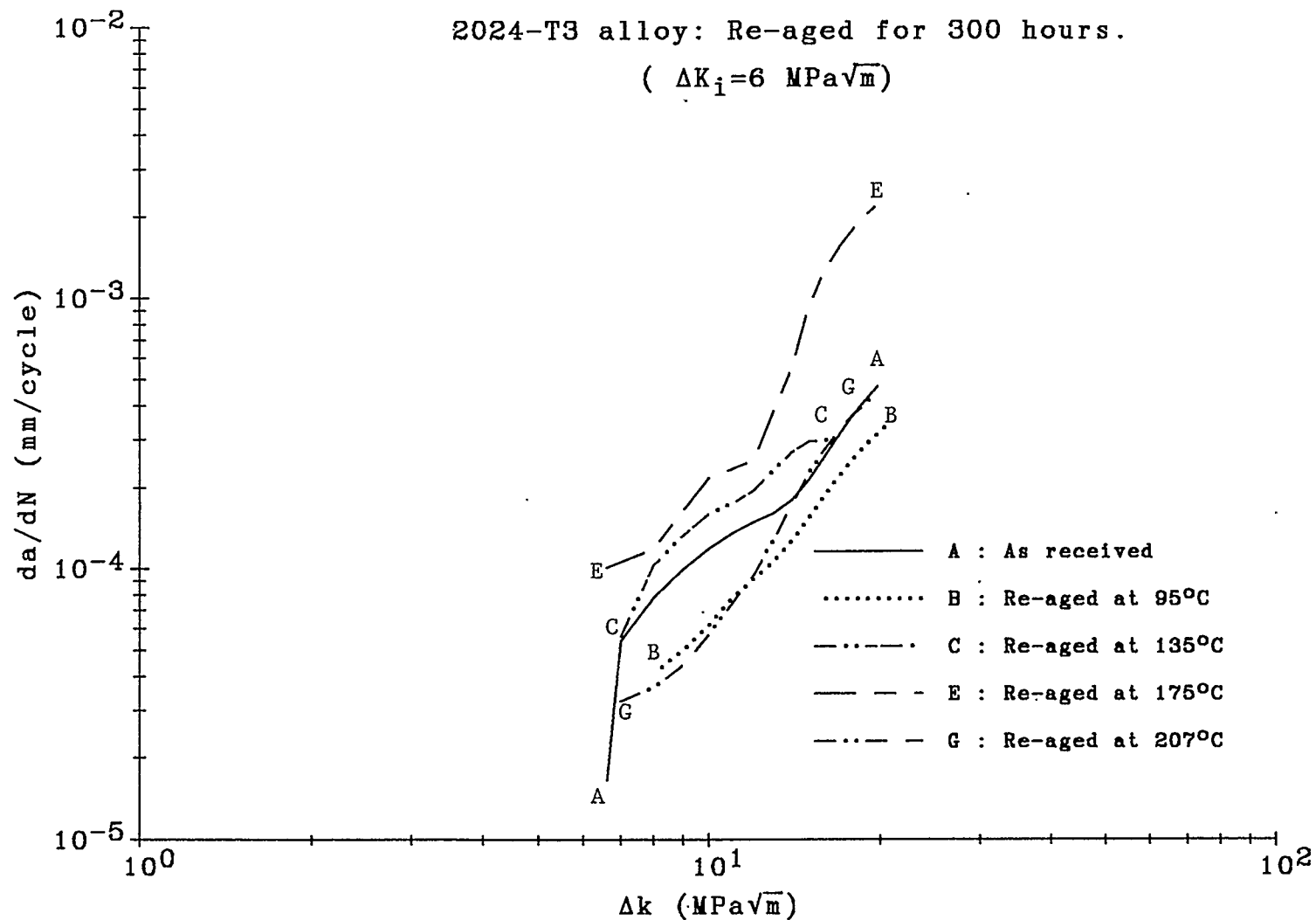


Figure 4.48: Relationship between the crack growth rate and change in stress intensity factor of 2024-T3 alloy; reaged for 300 hours.

shows a complex fatigue life behavior (Fig. 4.45, 4.46 and 4.47). Reaging for 300 hours, results in a faster crack propagation rate as compared to a reaging condition of 175°C for 150 hours, hence a lower fatigue life. The fatigue life corresponding to 175°C for 300 hours is approximately 60% below the fatigue life of the original -T3 material. When the alloy is further reaged at 175°C to 600 hours, it provided comparatively much slower crack propagation growth rate and consequently a much higher fatigue life. This improved fatigue life is approximately 43% above the fatigue life of the original -T3 material (Fig. 4.45).

Reaging the alloy at temperatures higher than 175°C results in lower fatigue crack growth rates and hence much higher fatigue lives. As, reaging of the alloy at 207°C for 300 hours provides a fatigue life that is almost 50% above the fatigue life of the original -T3 material (Fig. 4.46).

CHAPTER 5**DISCUSSION OF EXPERIMENTAL RESULTS****5.1 INTRODUCTION**

This chapter covers general discussion regarding the analysis of the experimental results as given in the previous Chapter 4. The main purpose of the analytical discussion is to identify the state of reaging or precipitate hardening/alteration of 7075-T6 and 2024-T3 aluminum alloys and the microstructural changes associated with each of the reaging conditions. Once the state of underaged, peakaged, and overaged conditions are established, then an examination of the effect of precipitate hardening on the fatigue life of each alloy was made. This is achieved through a number of experimental steps. The material hardness (H) and the electrical conductivity (C) relationship has been analyzed and discussed to establish the underaged, peakaged, and overaged conditions of each alloy. The effect of precipitate hardening on the fatigue life of the aircraft alloys was observed through the effect of aging and overaging on the fatigue related mechanical properties of the alloys followed by an actual fatigue test. The fatigue test data were analyzed through crack propagation tests at both low stress intensity factor range and high stress intensity factor range. The microstructural changes in each alloy due to reaging for underaged, peakaged and overaged were discussed. The precipitates in the two alloys under equivalent reaged conditions have been discussed. This is followed by analysis and discussion of identification of the reaging condition, the effect of reaging on the fatigue related mechanical properties, and finally the effect of the precipitate hardening on the fatigue life of 7075-T6 and 2024-T3 have been discussed as follows.

Table 5.1: Comparison of original 7075-T6 and reaged at 107°C for 300 hours.

Property	As received 7075-T6 alloy.	Heat treated at 107°C.	% Change
σ_y , MPa	508.23	528.01	3.89
σ_u , MPa	588.54	572.82	-2.67
ϵ_f , %	9.75	8.72	-10.56
VHN	175.25	176.45	0.68
C, %IACS	33.11	34.29	3.56
N_f , cycles	50,358	113,856	126.10

Table 5.2: Comparison of original 2024-T3 and reaged at 135°C for 300 hours.

Property	As received 2024-T3 alloy.	Heat treated at 135°C	% Change
σ_y , MPa	351.80	374.83	6.55
σ_u , MPa	483.06	485.54	0.51
ϵ_f , %	12.06	11.28	-6.47
VHN	131.77	136.40	3.51
C, %IACS	30.61	31.79	3.85
N_f , cycles	135,614	135,716	0.08

Table 5.3: Comparison of original 7075-T6 and reaged at 135°C for 300 hours.

Property	As received 7075-T6 alloy	Heat treated at 135°C	% Change
σ_y , MPa	508.23	426.95	-16.00
σ_u , MPa	588.54	501.61	-14.80
ϵ_f , %	9.75	8.96	-8.10
VHN	175.25	145.22	-17.14
C, %IACS	33.11	39.64	19.72
N_f , cycles	50,358	135,202	168.48

Table 5.4: Comparison of original 2024-T3 and reaged at 207°C for 300 hours.

Property	As received 2024-T3 alloy.	Heat treated at 207°C.	% Change
σ_y , MPa	351.80	301.47	-14.31
σ_u , MPa	483.06	391.30	-19.00
ϵ_f , %	12.06	5.71	-52.65
VHN	131.77	115.55	-12.31
C, %IACS	30.61	42.30	38.19
N_f , cycles	135,614	202,513	49.33

5.2 COMPARISON OF GROWTH OF PRECIPITATES OF 7075-T6 AND 2024-T3 ALLOYS

In order to compare and contrast the nature of precipitates in the two alloys, heat treatment schedules were based on Arrhenius rate equation for diffusion related both to nucleation and growth of precipitates. Arrhenius rate equation provided two equivalent sets of reaging conditions as:

- (i) Underaged 7075-T6 aluminum alloy reaged at 107°C for 300 hours equivalent to 2024-T3 aluminum alloy reaged at 135°C for 300 hours.
- (ii) Overaged 7075-T6 aluminum alloy reaged at 135°C for 300 hours equivalent to 2024-T3 aluminum alloy reaged at 207°C for 300 hours.

Precipitate hardening behavior of the two alloys were compared through mechanical and material properties. Fatigue life response of the two alloys were also compared under these conditions. The two reaged alloys were compared to their respective original conditions and change in behavior was measured in % change.

Increase in the yield stress of reaged 7075-T6 and 2024-T3 alloys was 3.89% and 6.55% respectively. The ultimate stress of 7075-T6 alloy decreased slightly (by 2.67%) while the ultimate stress of 2024-T3 alloy remained constant. Ductility of both 7075-T6 and 2024-T3 decreased by 10.56% and 6.47% respectively. Increase in the micro-hardness of 7075-T6 and 2024-T3 was 0.68 and 3.51% while the corresponding increase in electrical conductivities of the two alloys were 3.56% and 3.85% respectively. On the basis of above similarities we can assume that 7075-T6 and 2024-T3 alloys have similar precipitation conditions. Therefore one would expect that two alloys would provide similar fatigue life behavior i.e on reaging the two underaged alloys would have pretty close fatigue lives. However, there is a sharp contrast in their fatigue life response. Fatigue life of 7075-T6 alloy increased by 126.10% while the fatigue life of 2024-T3 remained unchanged (Tables 5.1-5.2).

The precipitate hardening response of both the overaged alloys was also compared in a similar fashion. 7075-T6 alloy reaged at 135°C for 300 hours was compared to reaged 2024-T3 alloy at 207°C for 300 hours. Losses in the yield stress and ultimate stress of the two overaged alloys were quite close (Table 5.3-5.4). However overaged 2024-T3 lost ductility by 52.65% compared to only 8.10% by 7075-T6 alloy. Decrease in the micro-hardness measured in VHN was 17.14% for 7075-T6 compared to a decrease of 12.31% for 2024-T3 alloy. Increase in the electrical conductivity of 2024-T3 was almost double the increase in electrical conductivity of 7075-T6 alloy (Tables 5.2-5.3). Normalized fatigue life of overaged 7075-T6 increased by 168.48% compared to an improvement of only 49.33% for 2024-T3 alloy under an equivalent reaged condition. On the basis of qualitative changes, the two overaged alloy have similarities indicating similar nature of the precipitate of both 7075-T6 and 2024-T3 aluminum alloys. The first equivalent condition is quite good while the second condition is not so good. However, fatigue behavior is not so comparable but appears from the above analysis to be a very complex parameter.

5.3 COMPARISON OF SIMILARITIES AND DISSIMILARITIES OF 7075-T6 AND 2024-T3 ALUMINUM ALLOYS

5.3.1 SIMILARITIES BETWEEN BEHAVIORS OF 7075-T6 AND 2024-T3 ALLOYS

Some of the similarities between the two alloys have been discussed in the previous section while some others are covered in this section. The comparison of similarities is given in the order of material properties, mechanical properties and fatigue life behavior.

Material properties such as hardness and electrical conductivity behaviors show that during underaged conditions hardness and electrical conductivities of both alloys increase. The similar behaviors are likely due to growth of coherent precipitates G.P. zones (clusters of zinc) and η in 7075-T6 and G.P. zones (clusters of copper) and θ in 2024-T3 alloy respectively. During overaging both alloys have continuous softening with larger increases in their

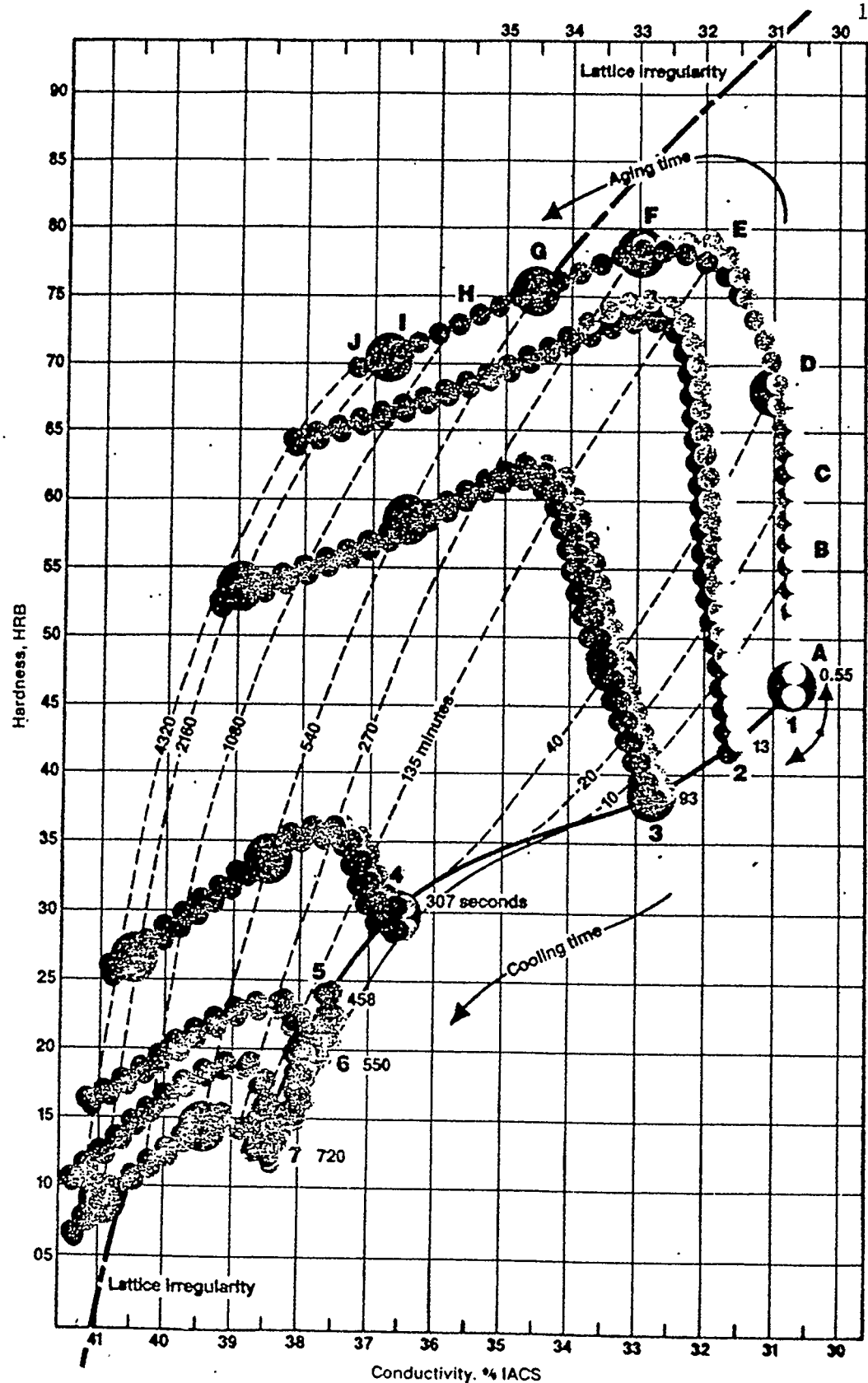


Figure 5.1: Relationship between hardness and electrical conductivity of 2219 alloy by Chihoski (23).

respective electrical conductivities. The sharp increase in electrical conductivities are likely due to drainage of zinc from the main matrix of 7075-T6 and depletion of copper from the main matrix of 2024-T3 alloy respectively. Major changes within each alloy are indicated by cut off values which are around electrical conductivity of %IACS for both the alloys (Tables 4.3 and 4.7). Both alloys have a "Sail Effect" in their hardness and electrical conductivity relationships (Fig. 5.1 to 5.3).

During earlier stages of reaging, the yield stress of each underaged alloy increased slightly while their ductilities and ultimate stresses were virtually insensitive to reaging conditions (Table 4.1 and 4.6). Since initially both alloys were slightly underaged, therefore small increases in the strengths are likely due to growth of η precipitates in 7075-T6 and θ in 2024-T3 alloy. Insensitivity in ductility can be due to large strain fields associated with the underaged conditions of both alloys (Tables 4.1 and 4.6). Yield stress and ultimate stress of both alloys decreased continuously with progressive overaging.

Fatigue lives of both alloys show somewhat complex behaviors. Normalized fatigue life of both the original alloys increase due to peakaged conditions and thereafter during overaging both have a general trend of decrease in their fatigue lives (Table 4.5 and 4.10). Increase in fatigue life can be associated with higher strength and ductility of each alloy while decrease in fatigue lives of overaged alloys are likely due to decrease in yield stress and hardness of both alloys and for the overaged 2024-T3 an additional factor may be the reduced ductility. Fatigue crack growth rate behaviors of both alloys indicate that over the intermediate range of stress intensity factors, both alloys have slower fatigue crack growth rates for the underaged conditions compared to their respective original alloys.

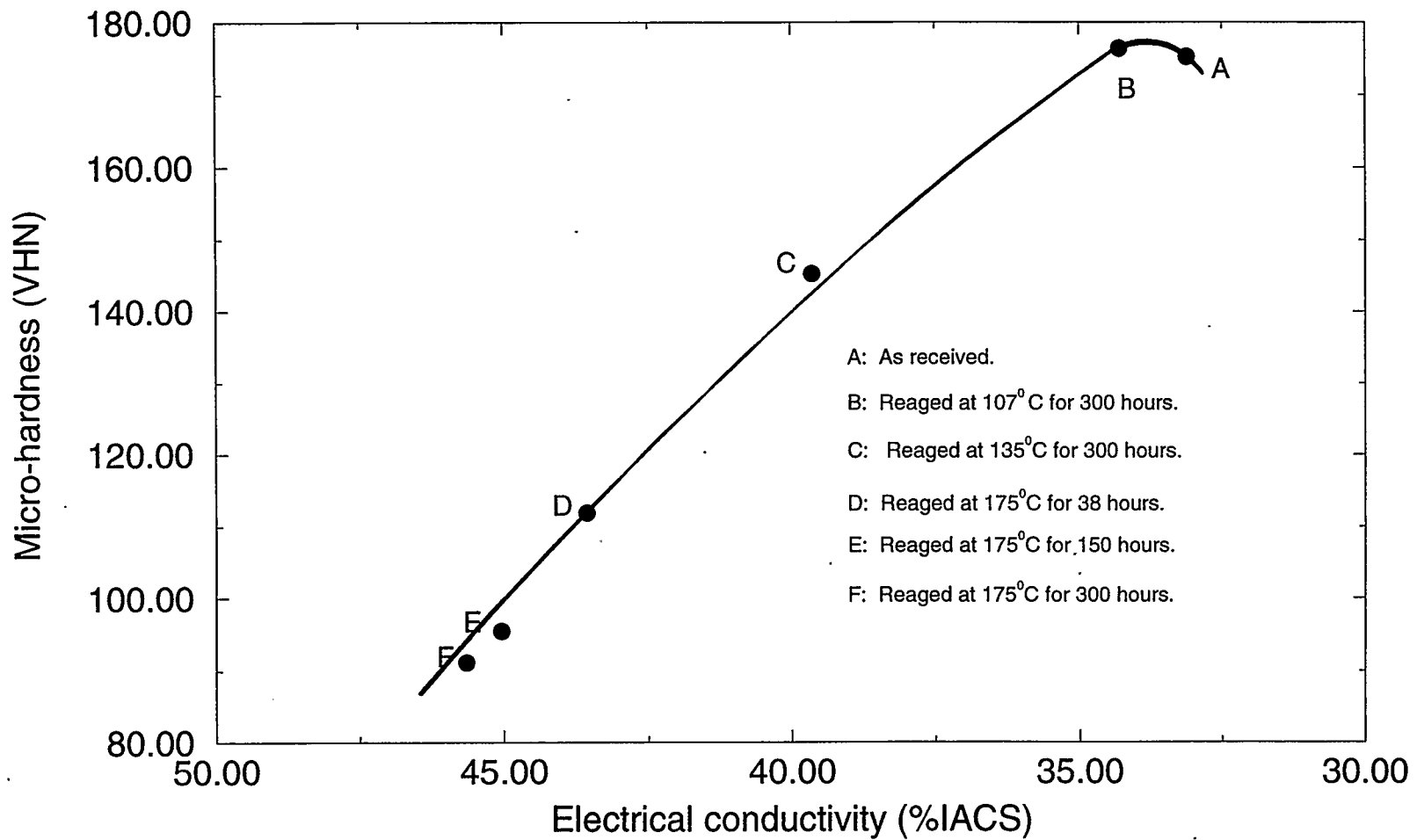


Figure 5.2: Relationship between electrical conductivity and hardness of 7075-T6 alloy; under various reaging conditions.

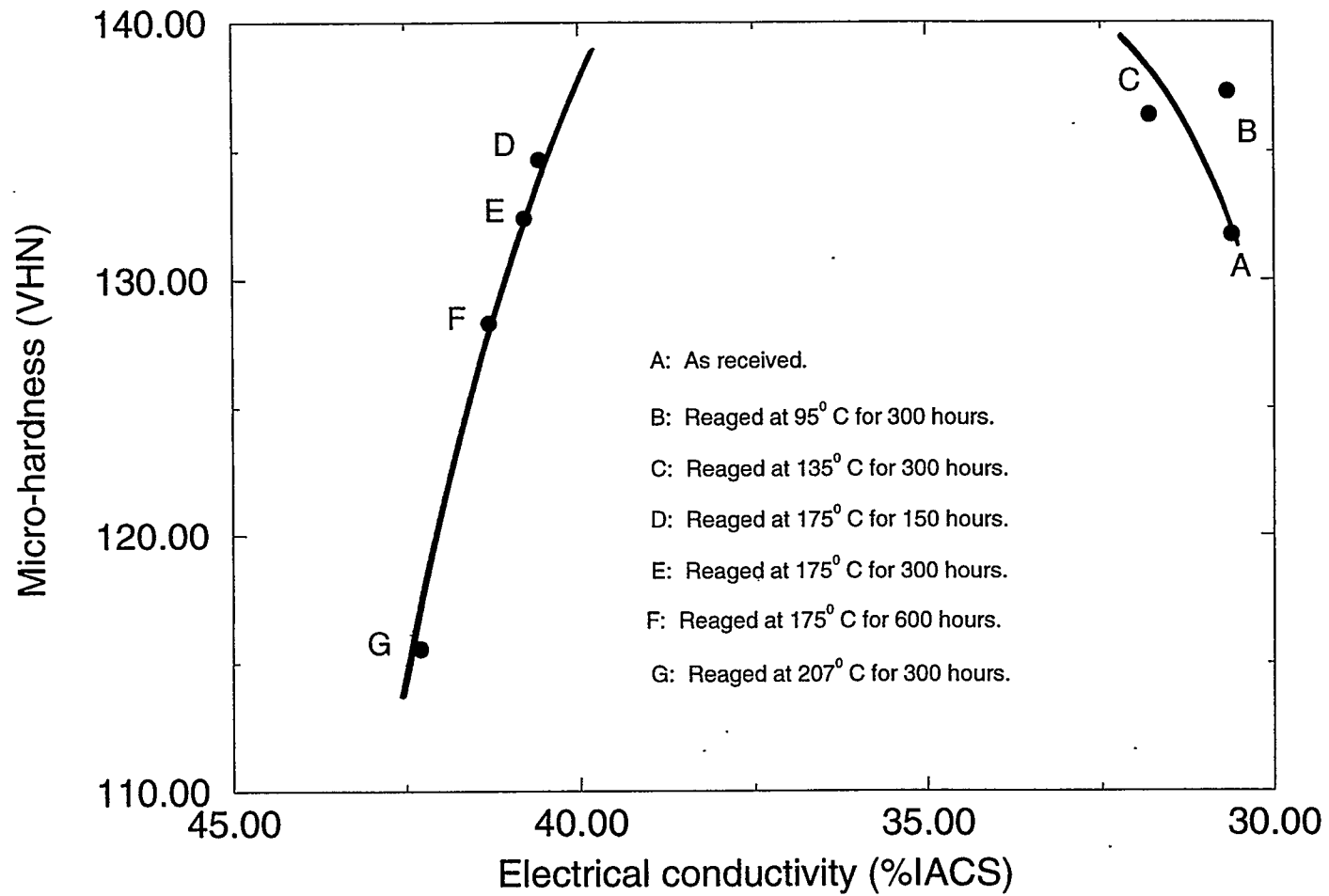


Figure 5.3: Relationship between electrical conductivity and hardness of 2024-T3 alloy; under various reaging conditions.

5.3.2 DISSIMILARITIES IN BEHAVIORS OF 7075-T6 AND 2024-T3 ALLOYS

Comparison of H-C relationships in Figures 5.1 through 5.3 indicates that 2024-T3 has a much more pronounced "Sail Effect" compared to 7075-T6. H-C relationship for 2024-T3 alloy in Figure 5.3 shows that the alloy can have same material hardness both in the underaged and overaged conditions. In contrast to 7075-T6, overaged 2024-T3 has a larger drop in hardness (Fig. 5.2 and 5.3). Changes in the hardness of overaged 7075-T6 alloy are much more gradual and uniform while the corresponding increases in the electrical conductivity are much larger compared to 2024-T3 alloy (Fig. 5.2 and 5.3).

In contrast to the H-C behavior of 7075-T6, changes in the hardness and electrical conductivity of 2024-T3 alloy are confined to two narrow regions each in the underaged and overaged condition respectively. The major changes within the alloys reflected through sharp changes in their electrical conductivities are more distinct for the 2024-T3 alloy compared to the 7075-T6 alloy (Fig. 5.2 and 5.3).

On reaging the original 7075-T6 alloy at 107°C for 300 hours, there was a slight increase in the yield stress. Beyond this condition, yield stress of 7075-T6 continuously decreased with higher degree of precipitation and the decrease is spread over a change of more than 350 MPa. While the yield stress of 2024-T3 alloy increased continuously to peakaged condition and thereafter the decrease in yield stress was gradual and limited to a change within 100 MPa.

Ultimate stress of original 7075-T6 aluminum alloy continuously decreased with higher degree of precipitation while drop in ultimate stress of 2024-T3 alloy started at the onset of the overaged condition of 175°C for 150 hours. Overall drop in the ultimate stress of 7075-T6 was more than 300 MPa compared to less than 100 MPa drop in the ultimate stress of 2024-T3 alloy (Table 4.1 and 4.6).

Ductility behavior of 7075-T6 alloy is insensitive to reaging

conditions whereas ductility of 2024-T3 alloy was unchanged up to the reaging condition of 135°C for 300 hours. Beyond this condition, the ductility of 2024-T3 alloy showed a large initial drop in the ductility and thereafter the changes in the ductility were quite minimal. At a reaging condition of 207°C for 300 hours, the alloy tended to recover some of its ductility (Table 4.1 and 4.6).

Fatigue life behavior of 2024-T3 alloy is somewhat more complex than the corresponding fatigue behavior of 7075-T6 alloy. Normalized fatigue life analysis of 2024-T3 shows an increase in the fatigue life with the degree of precipitation to a peakaged condition and thereafter the fatigue life continuously decreased until a reaging condition of 175°C for 300 hours. Beyond this, fatigue life of 2024-T3 reversed its trend and continuously increased (Fig. 4.46). While the fatigue life of 7075-T5 underaged alloy first increased to peakaged condition. Beyond this condition, the fatigue life of 7075-T6 alloy continuously decreased with higher degrees of overaging.

5.4 IDENTIFICATION OF THE UNDERAGED AND OVERAGED CONDITIONS OF 7075-T6 ALUMINUM ALLOY

The reaging conditions were examined through the effect of reaging on both the material hardness and the electrical conductivity (H-C). The original aluminum 7075-T6 alloy was solutionized, quenched and then artificially aged at 120°C for 24 hours to provide -T6 temper. Therefore the original 7075-T6 alloy was slightly underaged with respect to the optimum condition. The reaging time and temperature selections were based upon Arrhenius rate equation as mentioned in Section 3.4 of Chapter 3.

The test results for material hardness (both macro-hardness and micro-hardness) and electrical conductivity [Fig. 4.10, 4.13, and 4.16] show that the original alloy on reaging at 107°C for 300 hours is still underaged as indicated by small increase in both the material hardness and the electrical conductivity. The increase in the

macro-hardness, the micro-hardness, and the electrical conductivity are found as 1.62%, 0.68%, and 3.56% respectively. The increase in the hardness of underaged 7075-T6 alloy can be attributed to precipitate hardening due to formation and growth of G.P. zones and η'' coherent precipitates. The corresponding increase in the electrical conductivity is likely due to drainage of a small proportion of copper content from the main matrix to form η' semicoherent precipitates along the grain boundaries. Increase in both the material hardness and the electrical conductivity of the underaged alloy is consistent with the findings of Natan and Chihoski (24).

Reaging the original alloy -T6 alloy at 135°C for 300 hours resulted in a decrease in the material hardness while the corresponding electrical conductivity increased. The measured values of decrease in the macro-hardness, and micro-hardness are 6.93%, and 17.14%, respectively for the corresponding increase of 19.72% in electrical conductivity. This trend of gradual decrease in the hardness with continuous increase in the electrical conductivity indicates that the alloy is overaged (23). During the overaging condition, it is quite likely that η' incoherent precipitates were formed as well η'' are transformed into η' precipitates causing the strength and the hardness of the alloy to decrease. A sharp increase in the electrical conductivity reflects depletion of a substantial amount of copper content from the main matrix to form η' and η semicoherent and incoherent precipitates. The overaged condition of the alloy is supported by decrease in the yield stress, the ultimate stress, and micro-hardness of 7075-T6 (Table 5.3).

Beyond the reaging condition of 135°C for 300 hours, the alloy 7075-T6 is overaged. On reaging at 175°C for periods of 38, 150, 300 hours separately, the H-C relationship showed a general trend of steadily decreasing hardness and successively increasing electrical conductivity. This type of hardness-conductivity behavior of overaged 7075-T6 is consistent with the findings of Natan and Chihoski (24). It has been observed that for overaged conditions to occur, higher

reaging temperatures result in shorter reaging time periods. This is quite evident for the reaging temperature of 175°C where less than 38 hours are required for the alloy to reach an overaged condition. The macro-hardness and micro-hardness of the overaged -T6 alloy at 38 hours condition decreased by 28.87%, and 36.17% respectively while the corresponding electrical conductivity of the original alloy increased by about 31.59%.

After a reaging period of 150 hours at 175°C , the values of material properties are much less sensitive to reaging times. As the reaging time period increased from 150 hours to 300 hours, the macro-hardness, micro-hardness and electrical conductivity changed by 9.8%, 2.46%, and 1.81% respectively. It has been further observed that an increase in the electrical conductivity of the overaged 7075-T6 alloy is much larger as compared to the increase in electrical conductivity of the underaged alloy. On comparing the overaged condition at 175°C for 38 hours to an underaged condition at 107°C for 300 hours it has been observed that increase in the electrical conductivity of the overaged 7075-T6 is 31.59% for only 3.59% increase in the electrical conductivity of the underaged at 107°C for 300 hours. In contrast to the larger increase in the electrical conductivity, the decrease in the hardness of the overaged alloy has been noted to be much steadier. The decrease in the hardness of the overaged 7075-T6 alloy also is much more steady compared to the sharp increase in the hardness during underaging conditions. This is also consistent with the finding of Natan and Chihoski (24).

The increase in the material hardness of the underaged 7075-T6 alloy to its peakaged condition are likely due to formation and growth of G.P. zones and η'' precipitates. While the reduction in material hardness of the alloy is due to the transformation of coherent η'' precipitates to incoherent η' and η precipitates. During a progressive overaging the population density of η' and η increases at the expense of η'' precipitates. Some of the previous research indicates that during reaging, the precipitate hardening process is rather

complex. It is quite likely that at a specific reaging condition, formation and growth of one type of precipitates, dissolution and transformation of other type precipitates may occur simultaneously. The overall behavior is then dictated by the particles that are more predominant.

5.5 EFFECT OF AGING CONDITIONS ON MECHANICAL PROPERTIES OF 7075-T6 ALUMINUM ALLOY

5.5.1 EFFECT OF REAGING ON THE YIELD STRESS, ULTIMATE STRESS, ULTIMATE STRAIN AND FRACTURE STRAIN OF 7075-T6:

The effect of precipitate hardening on the mechanical properties of 7075-T6 alloy was measured through tensile tests by using a statistical sample of four specimens for each aging condition. Reaging the alloy below its original temperature and at 107°C for 300 hours provided interesting results. The yield stress of the underaged 7075-T6 alloy increased by about 3.89% while the ultimate stress, the ultimate strain and the fracture strain reduced by 2.67%, 12.91%, and 10.56% respectively. The small increase in the yield stress of the underaged alloy is likely due to growth of G.P. zones and η coherent precipitates, while the small drop in ductility may be due to formation of small proportion of primary η incoherent precipitates as indicated by a small increase in the electrical conductivity of the alloy (Fig. 4.18).

In the field of fracture mechanics of aluminum alloys, yield stress of 7xxx series alloys is known as one of the most important parameters to assess the fracture toughness. During the progressive reaging of 7075-T6 alloy to peakaged condition its yield stress increases and the corresponding fracture toughness decreases (43).

The combined effect of the increase in the material strength but small decrease in the plastic strain (as indicated by fracture strain) of the underaged -T6 alloy at 107°C is likely to improve the fatigue resistance of the alloy. Improved strength can be attributed to a more

homogeneous microstructure of a precipitate hardening alloy and absence of precipitate free zones (PFZ). These homogeneous precipitates strengthen the matrix to higher stability and improve the strength of the alloy (19,27). Finely dispersed η'' precipitates are homogeneously distributed with average size 35 \AA Guinier radius that provides improved strength (14). G.P. zones of $< 75 \text{ \AA}$ along with 5% of η'' precipitates of average Guinier radius $< 100 \text{ \AA}$ provide highest strength in 7xxx alloys (15). Higher fatigue life can also be associated to reversible slip at the crack tip that provides comparatively lower crack growth rates.

The measured values of mechanical properties for overaged conditions at 135°C for 300 hours, at 175°C for 38, 150, and 300 hours shows a general trend of continuous decrease in the mechanical properties with an exception of fracture strain of the overaged alloy. After a reaging condition of 175°C for 150 hours a small increase in the fracture strain occurred. The alloy overaged at 175°C for 300 hours showed an increase of 14.22% with respect to the overaging condition at 175°C for 150 hours. During the overaged conditions the decrease in the mechanical properties of yield stress, ultimate stress, ultimate strain, and fracture strain can be attributed to (i) the transformation of η'' coherent precipitates to partially coherent or incoherent secondary η' and η precipitates and (ii) the formation of primary η' and η precipitates causing the alloy to soften and lose its strength. The overaged 7075-T6 has η' precipitates localizing the strain fields causing the ultimate and the fracture strains to fall (1,22). According to Reimann and Brisbane overaged 7075 still has η'' precipitates ranging from $50\text{-}200 \text{ \AA}$ having mean value of 140 \AA along with η' incoherent precipitates (45).

On reaging at 135°C for 300 hours, the yield stress, ultimate stress, ultimate strain and fracture strain decreased by about 15.99%, 14.77%, 5.68%, and 8.10% respectively. The decrease in material properties can be attributed to the formation and growth of η' incoherent precipitates. As the density of η' precipitates increases

the strength of the alloy reduces. Transformation of η'' to η' precipitates results in a localized field as reflected by comparatively smaller values of the ultimate and fracture strains.

During progressive overaging, it has been observed that as the yield stress of 7075-T7 decreases, its corresponding fracture toughness increases. Fracture toughness increases rather sharply and continues to do so until the alloy reaches a highly overaged condition. At an overaged condition wavy dislocation movements loop around the incoherent precipitates as a result fatigue behavior of the alloy changes. Wavy dislocations are responsible for the development of persistent slip band, at the grain boundaries of overaged 7075-T7 alloy (43).

The reaging conditions at 175°C for a 38 hour period caused the yield stress to drop sharply while both the ultimate and fracture strain are insensitive to this reaging condition. The alloy is partially overaged where a good proportion of η'' coherent precipitates are transformed into η' semicoherent and incoherent precipitates causing the 7075-T6 alloy to lose its strength. While insensitivity of fracture strain is likely due to a balance between the large strain field associated with η'' and a very small proportion of localized strain fields associated with fine η' precipitates having minimal growth under this condition. It is quite possible that the overaged condition is close to the peakaged condition as indicated by the highest fracture strain compared to the rest of the reaged conditions.

On changing the reaging time from 38 hours to 150 hours, the decrease in the yield stress was recorded at 24.67% while the corresponding decrease in fracture strain was only 14.22%. This can be attributed to an increase in both the η' precipitate density and growth of η' precipitates. The decrease in strength is due to an increase in the η' precipitation density while growth of η' precipitates is likely responsible for the localized smaller strain fields. The lower strength can also be attributed to an independent heterogen-

eous nucleation of η' precipitates that can alter the relative proportion of G.P. zones, η'' and η' precipitates that affects the strength of the aluminum alloy (1). Size and spacing between the precipitates are the critical parameters of precipitation hardening, size and nature of precipitates control the strength of the alloy while the interparticle distance affects the strain fields (19,20,43).

Reaging at 175°C for 300 hours provides decreasing values of yield stress, ultimate stress, and ultimate strain while the fracture strain showed a small improvement. This small improvement in the fracture strain for this reaging condition is likely due to formation of intermetallic particles and stable θ particles causing the ductility of the material to improve and hence increase its ultimate and fracture strain. However, lower strength of the overaged alloy is likely due to size and distribution of stable particles in the aluminum matrix.

Highly overaged 7075-T6 alloy gradually tends to loose fatigue resistance and is likely due to larger precipitate free zones as PFZ are detrimental to fracture behavior of high strength aluminum alloys (43).

5.6 EFFECT OF PRECIPITATE HARDENING ON FATIGUE LIFE OF 7075-T6 ALUMINUM ALLOY

5.6.1 GENERAL

The effect of reaging condition on the fatigue life of the 7075-T6 alloy was examined through a fatigue test program. The experiment was conducted with SEN (single edge notch) specimens with clamped ends. The fatigue test data was analyzed using computer programs, providing comparison between the fatigue life of the original 7075-T6 alloy and the fatigue life of material reaged to different underaged and overaged conditions. The fatigue life under different reaged conditions was assessed through (i) comparison of the total fatigue life. (ii) comparison of the fatigue crack propagation rates from the

crack propagation test. (iii) comparison of normalized fatigue life at different reaged conditions.

5.6.2 EFFECT OF UNDERAGED 7075-T6 ALLOY ON ITS FATIGUE LIFE

The normalized fatigue cycles analysis indicated that 7075-T6 alloy reaged both at temperatures below and above the original temperature has a complex fatigue life behavior. The fatigue life of underaged 7075-T6 alloy improves continuously as the alloy is reaged to peakaged condition. Thereafter the fatigue life of the overaged alloy continuously reduces with progressive overaging conditions.

The fatigue crack propagation rate of the underaged 7075-T6 alloy reaged at 107°C for 300 hours is lower compared to the original 7075-T6 aluminum alloy. Therefore the underaged 7075-T6 alloy provides improved fatigue life (Fig. 4.22). In the crack propagation analysis, the fatigue crack propagation rates both at low stress intensity factor range and at high stress intensity factor range also shows that the rate of crack propagation for the underaged alloy is slower compared to that of the original alloy providing improved fatigue life (Fig. 4.25). The increase in normalized fatigue life of 7075-T6 alloy reaged at 107°C for 300 hours is 126.10% (Fig. 4.23). This drastic increase in the fatigue life is due to higher material strength and lower plastic damage (reflected by higher fracture strain) which leads to a very high fatigue life. Higher fatigue life under this reaging condition is also likely due to homogeneous underaged microstructure that could provide more homogeneous dislocations or dispersed slip distribution. Homogeneous dislocation distribution provides higher fatigue resistance (26,44). This is also supported by the fact that the underaged 107°C condition is comparatively closer to the optimum aging condition. Therefore, it is quite likely that small amounts of incoherent precipitates were formed along the grain boundaries. These η incoherent precipitates may be small enough to adversely affect the behavior of mechanical properties, however they may act as small barriers to reversible plane dislocati-

ons to retard them somewhat and thus provide slower crack propagation rates.

5.6.3 EFFECT OF OVERAGED 7075-T6 ALLOY ON ITS FATIGUE LIFE:

The fatigue crack propagation rates for overaged 7075-T6 alloy reaged at 135°C for 300 hours, reaged at 175°C for 38 hours have successively decreasing crack propagation rates, therefore fatigue life continuously improves with overaging until the greatest density of η' particles occurs. This is consistent with the findings of Sanders and Starke (14). The overaging gives a better fatigue life and increases as the density of η' precipitates increases. However the above results contradict the normalized fatigue cycles analysis according to which the fatigue life at 175°C for 38 hours is higher compared to the fatigue life for the alloy reaged at 135°C for 300 hours. The comparison of the fatigue life behavior of the alloy under these two conditions can be explained on the basis of fracture toughness and yield stress relations-hip. According to Lutjering and associates (43), during progressive overaging, as the yield stress of 7075-T735 aluminum alloy decreases its corresponding fracture toughness increases to a certain limit. The 7075-T6 alloy reaged to 175°C for 38 hours has higher fracture toughness by about 25%, it is literary that this can provide a comparatively better fatigue life. This improved fatigue life can also be explained on the basis that size and population density of metastable precipitates dictate the fatigue behavior of 7075-T6 alloy (44).

The one positive observation that underlines this fact is that fatigue crack growth rates of all the overaged conditions have lower rates compared to those of the original alloy. This is also supported by the crack propagation test analysis both at the low stress intensity factor range and at the high stress intensity factor range for all overaging conditions. The 7075-T6 alloy overaged at 175°C for 300 hours has higher crack propagation rates compared to those of the previous overaged conditions. This is consistent with the normalized

fatigue cycle analysis and indicates a trend of decreasing fatigue life with progressive overaging and after η' precipitates have attained maximum density. This is also consistent with the finding of Sanders and Starke (14) according to whom overaging gives a better fatigue life when the greatest density of η' precipitation occurs. Thereafter with progressive overaging, the precipitate density of η' particles reduces due to transformation of η' precipitates to η particles, then the overaged alloy has a lower fatigue resistance hence lower fatigue life. According to Park and associates, poor fatigue life of an aluminum alloy have been ascribed to soft grain boundaries which are believed to be sites at which damage takes place preferentially. The formation of these soft regions are either attributed to overaging or resolution of metastable precipitates. The fatigue crack will initiate in the soft PFZ inevitably produced during heat treatment (15).

However, overall precipitation hardening improves the fatigue life of this aircraft alloy. It is further observed that at the aircraft engine shutdown condition of 177°C , the 7075-T6 alloy takes as little as 38 hours to enter the overaging conditions. Thereafter up to 300 hours of service, the skin of the aircraft near the engine area should have at least the same resistance to the fatigue damage as that of the original 7075-T6 alloy. The peak temperature of 177°C occurs only for few minutes during each shutdown. Therefore an accumulated time at the peak shutdown condition should provide one of the guidelines for the repairs and maintenance schedule of the aircraft.

5.7 IDENTIFICATION OF UNDER AGED AND OVERAGED CONDITIONS OF 2024-T3 ALUMINUM ALLOY

The original 2024-T3 aluminum alloy was slightly under aged, therefore a raging schedule for the alloy was based upon Arrhenius rate equation, to provide two or more underaged and likewise two or more successively increasing overaged conditions. In order to establish the reaging condition, each alloy was tested using the

material hardness (both macro-hardness and micro-hardness) and electrical conductivity tests. The under aged and over aged conditions of the alloy were established by combining the changes in the material hardness to the corresponding changes in the electrical conductivity of the alloy. The experimental results as recorded in Table 4.7 through 4.9 are discussed as follows:

Measured values of macro-hardness, micro-hardness, and electrical conductivity of the original 2024-T3 were found as 70.78 ± 0.21 Rockwell B, 131.77 ± 3.76 VHN, and 30.61 ± 0.06 % IACS units respectively [Tables 4.7- 4.9]. On reaging the alloy at 95°C for 300 hours, the macro-hardness and micro-hardness increased only by 1.85% and 4.20% respectively while the corresponding electrical conductivity increased by 0.16%. At a higher temperature of 135°C , as expected, the values of material hardness were lower compared to the reaging condition of 95°C while the corresponding electrical conductivity was proportionally higher. On reaging at 135°C for 300 hours, the macro-hardness and micro-hardness increased by about 1.17% and 3.51% respectively while the electrical conductivity of the original alloy increased by 3.86%. Although the measured values of hardness and electrical conductivity are somewhat insensitive to the reaging conditions, there is a general trend of increase in both hardness and conductivity. These results are consistent with the findings of Natan & Chihoski (24) and indicate that for the reaging conditions of 95°C and 135°C , the 2024-T3 alloy is underaged. The increase in both the hardness and the electrical conductivity can be attributed to the formation and growth of zones and phases of G.P(1). zones and Θ'' precipitates both along the grain boundaries and the main matrix of the alloy. These precipitates being fully coherent with the matrix and as the Θ'' precipitates grow both in size and in number, the strength and toughness (ductility) of the alloy improves. This has been supported by both the yield stress (σ_y) and the fracture strain (ϵ_f) of the alloy reaged at 95°C and 135°C . The yield stress (σ_y) of the original 2024-T3 alloy on reaging at 95°C and 135°C increases by 6.54% and 0.50% respectively while the corresponding fracture strains (ϵ_f) increased by 11.53% and 0.58%

respectively. Qualitative analysis of the material properties on reaging at 95°C and 135°C for 300 hours confirms that under these conditions, the alloy was still underaged and that likely the matrix precipitates were predominantly Θ'' with very little amount of primary Θ' and Θ precipitates formed as indicated by a small change in the electrical conductivity.

On reaging at 175°C for 150 hours, the measured values of macro-hardness and the micro-hardness did not show appreciable changes with respect to the reaging condition. However there is a general trend of gradual decrease in the hardness of the alloy while the electrical conductivity of the original alloy increased from 30.61 % IACS to 40.57% IACS units, an increase of 32.54%. These results are also consistent with the findings of Natan and Chihoski (24) and correspond to the overaged condition of the 2024-T3 alloy. The much larger increase in electrical conductivity can be attributed to microstructural changes brought about by depletion of copper from the main matrix of the alloy to form Θ' incoherent precipitates and Θ stable particles (23,24). The decrease in hardness of the alloy is associated with (i) the transformation of Θ'' to Θ' precipitates and (ii) the formation and growth of primary Θ' precipitates. The Θ' precipitates are incoherent with the α -Al matrix of the alloy. These intermediate incoherent Θ' precipitates nucleate along (001), (010), and (100) planes having misfit in the (001) direction. This causes the hardness of the alloy to reduce. As the Θ' precipitates grow in size and number, the strength and the strain fields in the overaging alloy also reduce. This is supported by the fact that both the yield stress (σ_y) and the ductility (ϵ_f) of the alloy reduce in value. This also reflects that reduction in ductility to a much lower level is likely due to size and the spacing between them those may localize the strain fields. It has been further observed from the comparison of H-C relationships that the two reaging conditions of 135°C for 300 hours and 175°C for 150 hours are on either side of the peakaged condition and the two conditions are underaged and overaged respectively.

The above results also provide important information that after as little as 150 hours of the aircraft engine operation at its fuselage shutdown temperature of 175°C, the aircraft skin that surrounds the engine is overaged or it takes less than 150 hours of engine running time for aircraft skin to reach the peakaged condition. During overaging conditions, 2024-T3 alloy goes through complex microstructural changes. Primary incoherent precipitates Θ' and Θ particles are formed along with the transformation of Θ'' precipitates to Θ' precipitates. Thus beyond the reaging condition of 175°C for 150 hours, the alloy is overaged and the overaging condition progresses both with longer reaging periods and higher temperatures combined with shorter reaging periods.

The measured values of hardness (H) and electrical conductivity (C) for reaging conditions of 175°C for 300 hours and 600 hours respectively are within the statistical variation of the as received material and reflect very gradual changes both in the material hardness and the electrical conductivity with the higher reaging conditions. This is likely due to slow growth of Θ' and Θ precipitates with higher overaging conditions. The Θ particles are stable particles and as the transformation of incoherent Θ' precipitates progresses, the material tends to regain or recover its ductility.

At higher temperatures such as 207°C for 300 hours, as expected, the alloy has much lower hardness and a corresponding higher electrical conductivity. As before this is attributed to Θ' and Θ particles. However the density of Θ' precipitates is likely lower than the density of Θ particles, consequently the alloy is expected to regain some of its ductility. This is apparent from the fact that at this highly overaged condition, the ultimate and fracture strains are a bit higher compared to the reaging condition of 175°C for 600 hours.

5.8 EFFECT OF AGING CONDITION ON THE MECHANICAL PROPERTIES OF 2024-T3 ALLOY

5.8.1 EFFECT OF REAGING ON THE YIELD STRESS, ULTIMATE STRESS, ULTIMATE STRAIN AND FRACTURE STRAIN OF 2024-T3 ALLOY

The original 2024-T3 alloy was slightly underaged with respect to an optimum condition, therefore as expected, on reaging at 95°C for 300 hours, the underaged alloy due to its progressive precipitate hardening showed a very small improvement of 0.53% in its yield stress. However it showed a comparatively much larger increase of 24.86% and 11.53% in its ultimate and fracture strains respectively. These changes can likely be attributed to a small change in the population density of metastable coherent Θ precipitates. These Θ precipitates are approximately of the dimensions of 20 to 30 nm in diameter and 1.5 to 2.5 nm thickness lying on two {100} planes (24). These precipitates are coherent with α -Al matrix, therefore with an increase in both density and size, the strength of the alloy also increases. This is reflected by the small increase in the yield stress while a substantial growth in the size of the primary Θ particles occurs providing reasonably higher strain fields. Thus the original alloy reaged at 95°C for 300 hours with reasonably high ductility should provide improved fatigue life.

On reaging at 135°C for 300 hours, yield stress of the original 2024-T3 alloy increased from 351.80±1.17 MPa to 374.83±2.07 MPa, an increase of about 6.55% while the strain values were insensitive to this reaging condition. This increase in the yield stress is larger than the yield stress in the previous case of reaging at 95°C and is likely due to higher population density of formation of Θ precipitates of the underaged alloy. However a comparatively lower fracture strain may be due to the resultant effect of size, shape, spacing and distribution of Θ precipitates. Lebo and Grant (47) associated improved strength along with poorer ductility to dispersion of intermetallic particles. Sanders and Starke (14) associated the

radius of Θ'' precipitates to the strength and ductility of 2xxx and 7xxx series alloys. Therefore partial incoherent particles resulting from a certain size of Θ'' precipitates might have effected the ductility of the 2024-T3 alloy. Lindigkeit and Gysler (26) related larger size shearable Θ'' precipitates of underaged aluminum alloys to decreased ductility.

Reaging at 175°C for 150 hours provided slightly overaged 2024-T3 aluminum alloy. The original alloy is reaged closer to the peakaged condition as indicated by the yield stress of 400.40±1.65 MPa of the overaged alloy. There is a drastic reduction in the ultimate stress, ultimate strain and fracture strain. The experimental values of the ultimate strain and fracture strain under this reaging condition were found to be 3.78±0.32% and 4.77±0.34% respectively. These low values of strain are attributed to (i) formation of primary Θ' and Θ'' incoherent precipitates and (ii) transformation of some Θ'' precipitates to Θ' precipitates. These incoherent precipitates have only localized strain fields associated with them. Thus the overaged alloy has reduced ductility. However the combined effect of a much higher yield stress and reduced ductility is likely to provide the overaged alloy with comparatively higher fracture toughness (fatigue resistance) particularly when considering stress-life and fatigue crack initiation.

As expected, on reaging at 175°C for longer time periods of 300 and 600 hours respectively, the alloy has a general trend of continuous decrease in all mechanical properties. This can be attributed to both Θ' precipitate density and the size and distribution density of Θ' precipitates. The continuous decrease in strength of the alloy may be due to dissolution or redistribution of Θ' precipitates to increase the precipitate free zones (PFZ) along the grain boundaries. The larger size density of the PFZ causes the alloy to lose strength. During progressive overaging conditions, some small change in density of Θ' incoherent precipitates could cause the resultant strain field to reduce. The combined effect of both the low

strength and lower ductility is likely to provide lower fatigue resistance.

On reaging at 207°C for 300 hours, the alloy showed some recovery in its ductility. This can be attributed to transformation of some Θ' precipitates into more stable intermetallic Θ particles. As the density of Θ' incoherent precipitates reduces, the strain field associated with the incoherency reduces and consequently the ductility of the alloy improves. This would likely improve the fatigue resistance.

5.9 EFFECT OF PRECIPITATION HARDENING ON THE FATIGUE LIFE OF 2024-T3 ALUMINUM ALLOY

5.9.1 GENERAL

The overall fatigue life behavior of 2024-T3 aluminum alloy is somewhat complex. The fatigue life of the alloy first increases with the underaged reaging conditions. Beyond the reaging condition of 175°C for 150 hours the fatigue life of the overaged 2024-T3 alloy first decreases with the higher overaging conditions and then at highly overaged reaging conditions beyond 175°C for 300 hours the fatigue of the alloy continuously increases with overaging conditions. The detailed analysis of the effect of precipitate hardening of 2024-T3 on its fatigue life both during the underaged and the overaged conditions has been discussed separately in the following sections.

5.9.2 EFFECT OF UNDERAGED 2024-T3 ALLOY ON ITS FATIGUE LIFE

The effect of aging condition on the fatigue life of 2024-T3 aluminum alloy was measured by using SEN (single edge notched) test specimens. The experimental data was analyzed through computerized graphical analysis and by comparing the normalized fatigue life cycles. The normalized fatigue life of the original alloy on reaging to an underaged condition at 95°C for 300 hours increased dramatically by about 44.82% (Fig. 4.47). The qualitative analysis of the fatigue

test results as reflected by graphs between the number of fatigue cycles (N) and the corresponding fatigue crack length (a) are consistent with the above results (Figure 4.44). The rate of fatigue crack growth of the underaged alloy was found to be lower as compared to the original alloy. The crack propagation analysis of the fatigue test data also showed that da/dN of the underaged alloy both at low stress intensity factor range and high stress intensity factor range (ΔK) was lower than da/dN for the corresponding original alloy (Fig. 4.49). The increase in fatigue life of the underaged alloy can be attributed to the increase in both yield stress and ductility. The precipitate hardening at 95°C for 300 hours increases both the population density and the size of G.P. zones and Θ'' coherent precipitates. The resultant effect provides aluminum alloy of higher mechanical properties of yield stress and material ductility and hence higher fatigue resistance of the underaged alloy. Thompson and Levy related the fine size of G.P. zones and Θ'' precipitates of the underaged -T3 temper aluminum alloys to more effective blocking of the localized irreversible slip at the crack tip and hence a smaller crack extension or improved fatigue life (42). Thus underaged or optimum aged 2024-T3 aluminum alloy provides improved fatigue life compared to the original alloy. An increase in the fatigue life is likely due to the ease of reversible dislocation motion that depends upon the planarity of slip leading to superior behavior.

The normalized fatigue life of material underaged at 135°C for 300 hours was found unchanged from the fatigue life of the original alloy. On comparing the two underaged conditions at 95°C and 130°C , one would expect that reaging at 135°C provides a higher underaged condition and higher fatigue life. However, results from the graphical analysis of (i) the fatigue life cycles versus crack length and (ii) the da/dN versus $\log(\Delta K)$, shows that rates of fatigue crack growth for both the original alloy and the underaged at 135°C are almost the same. It is also observed that the rate of crack growth for underaged at 135°C is higher compared to the one at 95°C , hence lower fatigue life. This can be attributed to a comparatively larger size of G.P. zones and Θ''

precipitates. This is somewhat consistent with the findings of Thompson and Levy (42). According to Thompson and Levy as the size of G.P. zones and Θ'' becomes large, these particles become less effective in blocking the localized irreversible slip at the crack tip. Therefore comparatively larger localized slip causes higher crack extension at the crack tip and hence lower fatigue life. Thus a reversal in the trend of fatigue life with respect to the previous reaging condition of 95°C is likely due to growth of G.P. zones and Θ'' precipitates. It is also likely that near the peakaged condition due to formation of Θ' incoherent precipitates and limiting size of Θ'' coherent precipitates, the reversible dislocation becomes less effective that can change the fatigue life behavior.

However one encouraging sign reflected by the crack propagation test is that at least there is no detrimental effect on the fatigue life of the overaged alloy at 135°C . When the ductility of the original alloy was compared to the ductility of the overaged alloy at 135°C it was observed that their ductilities measured in terms of total fracture strains were very close while their yield stresses differed. Therefore the plastic damage for these two conditions being so close means that the conditions have nearly identical fatigue lives. Overall the overaged 2024-T3 alloy reaged at 135°C for 300 hours has a fatigue life comparable to the fatigue of the original alloy.

5.9.3 EFFECT OF OVERAGED 2024-T3 ALUMINUM ALLOY ON ITS FATIGUE LIFE:

Using the normalized fatigue life, and evaluating the life to failure for different overaged conditions and the crack propagation test analysis both at low stress intensity range and high stress intensity range showed that overaged 2024-T3 aluminum alloy provide improved fatigue life with an exception of a reaging condition of 175°C for 300 hours. The analysis also reflects that after peakaged condition there is a trend of decrease in fatigue life with the progressive overaging. This trend reverses beyond the reaging

condition of 175°C for 300 hours and thereafter the fatigue life of the overaged 2024-T3 continuously increases with progressive reaging.

The decrease in fatigue life beyond the peakaged condition occurs when 2024-T3 was reaged at 175°C for 150 to 300 hours. This can be attributed to increase in the plastic strain that causes both the hardness and the fatigue life of 2024-T3 alloy to decrease. The trend of decrease in fatigue life of the alloy is consistent with the research work by Sudarshan, Louthan, and Mabie (48). Sudarshan and associates conducted fatigue tests on aluminum alloys after overaging at temperatures between 100°C and 190°C. Their findings underline the results that hardness and fatigue life of overaged aluminum alloys 2xxx and 7xxx series change in the similar fashion. According to which, increase in the plastic strain, causes the hardness and the fatigue life to decrease.

Higher fatigue crack propagation rates associated with lower fatigue life is also likely due to semicoherent metastable particles which are unable to provide higher resistance to wavy dislocation movements or to the reversible slip.

The continuous improvement in the fatigue life of the highly overaged 2024-T3 aluminum alloy beyond an aging condition of 175°C for 300 hours is consistent with the finding of Pica, Hidayetoglu and Haworth (41) and is related to smaller hysteresis loops that occur when strain cycling the overaged aluminum alloy. This was found to occur in highly overaged aluminum alloy as a result of transformation of θ' incoherent precipitates to comparatively more stable θ intermetallic particles. Suresh, Vasudevan, and Bretz (49) revealed that these intermetallic particles are Al_7Cu_2Fe , Mg_2Si , $Al_{12}Mg_2Cr$, and Al_2CuMg . They also compared the precipitate free zones of the underaged, peakaged and overaged aluminum alloys and observed that the size of PFZ of aluminum alloys increase continuously and the PFZ of the overaged alloy are much larger compared to the underaged conditions. Therefore increase in the PFZ may have some bearing on

the decrease in the plastic strain that could cause the fatigue life of the alloy to improve. Thus the microstructure of the highly overaged alloy is controlled by θ stable particles and results in a smaller amount of plastic damage which leads to a longer fatigue life of 2024-T3 alloy. It is also likely that due to higher proportion of θ stable particles, a more homogeneous dislocation distribution leads to improved life or it could be that under the conditions crack branching within the plastic zone of a propagating fatigue crack leads to slower crack growth rates.

CHAPTER 6

CONCLUSIONS AND RECOMMENDATIONS

6.1 CONCLUSIONS

6.2 GENERAL

This Chapter concludes the experimental investigation of 2024-T3 and 7075-T6 aluminum alloys. Based on the observations in this project some recommendations have also been made for future research work. The conclusions regarding precipitate hardening and the fatigue of 7075-T6 and 2024-T3 alloys are given separately in the following sections.

6.2.1 PRECIPITATION BEHAVIOR OF 7075-T6 ALUMINUM ALLOY

The following conclusions can be drawn from the experimental results.

1. The yield stress, and material hardness show the original 7075-T6 was slightly underaged compared to the optimum (peakaged) condition.
2. Aging conditions; underaged, peakaged and overaged conditions can be explained fully by combining the hardness (H) and the electrical conductivity (C). Neither H nor C alone would completely specify the state of aging in a reaged alloy. Some of the other H-C related observations for 7075-T6 alloy follow as:
 - (a) H-C relationship shows on reaging the original alloy at 107°C for 300 hours, both the material hardness and its electrical conductivity increased during this progressively increased underaged condition. However the increase in the electrical conductivity was very minimal.
 - (b) H-C relationship for the overaged conditions shows that the material hardness decreases very gradually while the corresponding electrical conductivity increases quite rapidly.

(c) On reaging at 175°C for 38 hours, the hardness and the electrical conductivity both changed faster. Beyond this reaging condition, reaging time periods have comparatively much smaller effect both on H and C. Therefore major microstructural changes had occurred within 38 hours of the shutdown temperature of 175°C.

(d) Both the micro-hardness and the regular hardness can be used to correlate changes that are occurring within the reaged alloy as affecting its mechanical properties.

(e) The results of material hardness indicate that substantial damage has occurred in the material at the reaging condition of 175°C for 38 hours. Beyond this point further reaging times do not have anywhere near as large an effect on the material hardness values of the overaged alloy although they do continue to decrease.

3. On reaging the original 7075-T6 alloy at 107°C, that is at a temperature lower than its original temper, the alloy gains some strength as indicated by increase in its yield stress and hardness. However, there is small loss in its ultimate strength and ductility. The change in ductility is very small and it is fair to say that ductility of the reaged alloy is insensitive to reaging condition. Behavior of the ultimate stress shows that loss in ultimate stress level is within 5% compared to the original -T6 material.
4. Ductility of 7075-T6 alloy measured as a function of ultimate and fracture strain is insensitive (fairly constant) to almost all the reaging conditions. While beyond the reaging condition of 107°C, both the yield stress and the ultimate stress decrease continuously.
5. Beyond the reaging conditions 107°C for 300 hours, there are large changes in the mechanical properties of yield strength and the ultimate strength as well as similar changes in the material hardness and the electrical conductivity of 7075-T6. These changes very likely reflect the changes that occur within the alloy.

6. At the reaging condition of 175°C, micro-hardness showed more sensitivity to the reaging conditions compared to macro-hardness.
7. During the early stages of reaging at temperature higher than the original temperature, changes within the alloy occur much faster and thereafter, the changes are rather slow. This fact is reflected by both the mechanical properties and material properties behavior of 7075-T6 alloy.
8. A very substantial decrease in yield stress occurs when the alloy is reaged at 175°C for as short as 38 hours. This drop off in yield stress is more than 40% of the original -T6 material. Further reaging at 175°C for longer time periods results in only slightly lower losses occurring compared to this reaging condition.
9. As compared to losses in yield stress of overaged 7075-T6 alloy, the corresponding losses in the ultimate stress are smaller. reaging at 175°C for 38 hours results in a loss of approximately 33% of the original -T6 alloy.

6.2.2 FATIGUE LIFE BEHAVIOR OF 7075-T6 ALUMINUM ALLOY

These conclusions regarding the fatigue life behavior are based upon the actual da/dN test results and different graphical analysis such as: effect of aging conditions on normalized fatigue life, comparison of crack growth rates through relationship between crack length and fatigue life cycles, and comparison of crack growth rates under different stress intensity ranges. Some of the conclusions are focused to relate the effect of reaging on the fatigue life of the alloy.

1. The fatigue life behavior of 7075-T6 alloy as measured through normalized fatigue life and crack propagation rates indicate that considerable effect is occurring in the material for conditions of reaging as low as 107°C for 300 hours.
2. The fatigue life behavior of 7075-T6 shows a complex relationship to the reaging conditions. There is a continuous increase in the fatigue life as the alloy is reaged to peakaged condition

and thereafter, during overaging a gradual but continuous decrease in the fatigue life of the alloy. However, there is a considerable improvement in the fatigue life of the alloy for nearly all reaging conditions. After nearly 300 hours, the overaged alloy tend to loose its superiority over the original -T6 alloy.

3. With an exception reaging condition of highly overaged 7075-T6 at 175°C for 300 hours, all the reaged conditions shows more than 100% improvement in their fatigue life.
4. The material strength (both the yield stress and the ultimate stress bear direct relationship to the fatigue life response of the alloy during progressive reaging to peakaged condition. However this trend reverses once the yield stress of the alloy reaches its maximum value.
5. As compared to the original alloy, up to 300 accumulated hours operating life of the aircraft, reaging improves the overall fatigue life of the aircraft.
6. With respect to the fatigue behavior, the inspection schedules of aircraft repairs are not affected until 400 accumulated operating hours.
7. Around the optimum aging condition, 7075-T6 alloy provides much improved life compared to underaged or highly overaged.
8. Fatigue behavior of highly overaged alloy is not consistent with the fracture toughness-yield strength relationship.

6.2.3 PRECIPITATION HARDENING BEHAVIOR OF 2024-T3 ALLOY

6.2.3.1 GENERAL

The original alloy was slightly underaged compared to the optimum condition. A comparable heat treatment would be a -T861 condition which is solution treated, cold worked and artificially aged at a temperature of 190°C for a period of 12 hours. This does suggest that the alloy should not be highly susceptible to reaging at the shutdown temperature of 175°C. Most of the super saturated phases might have been diffused after the original temper, therefore fairly stable precipitates are expected in the material. However, the actual

behavior of 2024-T3 reflects actual changes occurred during reaging.

The following conclusions are based upon the experimental results and their graphical analysis.

1. 2024-T3 alloy on reaging up to 135°C for 300 hours provided higher strength and ductility. Thereafter, the alloy retained the higher level of strength, and hardness but its ductility reduced to a much lower level.
2. Beyond the reaging condition of 135°C, losses in the ultimate strength, the material hardness, and ductility occurred. However, the yield strength continuously increased to reaging condition at 175°C for 150 hours. Increase in the yield strength of reaged alloy at 175°C for 150 hours is close to 14% compared to the original -T3 material.
3. Reaging the alloy at 175°C and beyond the time period of 150 hours, results in decrease in yield strength and indicates overaged conditions. However, even after 600 hours of reaging, the yield strength of the alloy is still slightly better than it was in the the original -T3 alloy.
4. The ultimate stress level is fairly constant up to a reaging condition of 135°C for 300 hours. Beyond this condition, the ultimate stress starts to drop off and at 175°C for 150 hours reaging there is only 6% loss in the ultimate stress level over that of the original -T3 alloy. On reaging to higher conditions, the successive losses are comparatively much smaller.
5. Beyond the reaging condition of 135°C for 300 hours, there is a drastic change in the material ductility. On reaging at 175°C for 150 hours, ductility of the alloy drops off by more than 60% from its original value. After this initial drop off at 175°C for 150 hours, the ductility has a fairly constant value.
6. Highly overaged at 207°C for 300 hours, the alloy tends to recover its ductility. This is likely due to transformation of metastable precipitates to stable particles of the alloy.
7. The material hardness initially increases slightly at 95°C, thereafter both the macro-hardness and micro-hardness are insensitive up to reaging condition of 175°C for 300 hours.

Beyond this condition, the material hardness is comparatively more sensitive. With higher reaging conditions, the material hardness of overaged 2024-T3 alloy gradually falls off.

8. Reaging conditions up to 135°C for 300 hours show very slight increase in the electrical conductivity values. It is likely that under these conditions, the electrical conductivity of the alloy has not been affected.
9. On reaging the 2024-T3 alloy at 175°C for 150 hours, the electrical conductivity of the alloy increases quite sharply and the increase is about 33% of its original value. Further reaging at 175°C for longer reaging time periods, the conductivity does not appreciably change.
10. Large changes in the mechanical properties of ultimate strength and ductility at a reaging condition of 175°C for 150 hours were followed by very gradual but continuous changes during the higher overaged conditions.
11. Mechanical properties of 2024-T3 alloy show a complex behavior. At the reaging condition of 175°C for 150 hours. While the yield stress increased, values of both the ultimate stress and ductility dropped off.
12. Material hardness is fairly constant up to reaging condition of 175°C for 300 hours and thereafter values of both the macro-hardness and micro-hardness gradually dropped off.

6.2.4 FATIGUE LIFE BEHAVIOR OF 2024-T3 ALLOY

The conclusions regarding the fatigue life behavior of the alloy are based upon the actual da/dN test results and follow as:

1. The aluminum 2024-T3 alloy showed a complex fatigue life behavior.
 - (a) Looking both at the crack growth life and at the crack propagation rate relationships, fatigue of the underaged alloy reaged at 95°C for 300 hours improved. Thereafter, the fatigue life reversed its fatigue trend and continuously decreased up to the reaging condition of 175°C for 150 hours. At

this point fatigue life of the alloy was still better than the original alloy. On further reaging for higher reaging condition, first much higher crack growth rate provided a much lower fatigue life for reaging condition of 175°C for 300 hours. There after, for highly overaged conditions at 175°C and 207°C, subsequent decrease in the crack growth rates provided continuously increasing fatigue life. The fatigue life of the highly overaged alloy had much higher fatigur life compared to the original -T3 alloy.

(b) Fatigue behavior bears no direct relationship to any one of the mechanical properties of the alloy. This complex behavior can only be explained by combining the fatigue properties to precipitate hardening behavior of metastable precipitates.

(c) The fatigue life behavior of 2024-T3 shows that up to and including the reaging condition of 175°C for 150 hours, there is no detrimental effect on the fatigue life of the alloy.

(e) Beyond the reaging condition of 175°C for 150 hours, the alloy shows a complex fatigue behavior. At the reaging condition of 175°C for 300 hours, fatigue life response is very poor. However, thereafter highly overaged alloy shows an improved fatigue life. This complex behavior can be associated to microstructural changes.

2. The conventional fracture toughness-yield stress relationship alone does not completely explain the complex fatigue behavior of 2024-T3 alloy.

6.3 RECOMMENDATIONS FOR FUTURE WORK

6.3.1 RECOMMENDATIONS FOR FUTURE WORK FOR 7075-T6 ALLOY

1. Since in the aircraft industry, the aircraft skin invariably is precipitate hardened at temperatures below 200°C and as most of the work by others has been conducted at temperatures above 200°C, therefore, more research work is needed at temperatures between 100°C and 200°C.

2. In order to cut the cost of research projects, it is often observed that reaging or heat treatments are performed with much wider gaps in the temperatures and time both. This leads to inconsistency between results of various research conducted. Therefore, precipitate hardening behavior should be conducted with a spectrum of fatigue related tests with much closer successive temperature ranges and corresponding shorter reaging time periods.
3. Since size and population density of both the coherent and incoherent precipitates are critical to the fatigue life behavior of 7xxx series alloys, therefore to establish a more definite relationships between the fatigue properties and the size and population density of precipitates more research work is recommended.

6.3.2 RECOMMENDATIONS FOR FUTURE WORK FOR 2024-T3 ALLOY

1. Since an overaged 2024-T3 aluminum alloy has comparatively more complex behavior, therefore very much like 7075-T6 aluminum alloy more research work is required to know the interactive behavior of this alloy. The areas of future research of the two alloy are very common as recommended for 7075-T6 alloy.

REFERENCES:

1. Sanders, T.H., Jr., and Staley, J.T., "Review Of Fatigue And Fracture Research On High Strength Aluminum Alloys". Laboratories Alcoa Pennsylvania (U.S.A.). Fatigue and microstructure ASM 1979, pp. 467-522.
2. Truckner, W.G., "Effect of Microstructure on Fatigue Crack Growth of Al-Zn-Mg-Cu Alloys", Journal of Metals V28 issue 12, 1976, pp.A48.
3. Mondolfo, L.F., Barlock, John., "Structure of Some Aluminum-Iron-Magnesium-Manganese-Silicon Alloys", Metallkd. V66 n10 Oct. 1975, pp. 605-611.
4. Fleming, M.C., "Solidification Process", Metallurgical Transactions V5 n10 Oct., 1974, pp. 2121-2134.
5. Bucci, R.J., Thakker, A.B., Sanders, T.H., Sawtell, R.R., and Staley, J.T., "Ranking 7xxx Aluminum Alloys Fatigue Crack Growth Resistance Under Constant Amplitude And Spectrum Loading". ASTM STP 714, 1980, pp. 41-78.
6. Staley, J.T., "Influence of Microstructure on Fatigue And Fracture of Aluminum Alloys", Aluminium V 55 n4 April 1979, pp. 277-281.
7. Kung, C.Y., "Fatigue Crack Initiation And Growth Of Micro-cracks In Commercial Precipitation Hardened Al-Cu-Mg Alloys Of Ordinary And High Purity", Ph.D. Thesis, Northwestern University, Evanston, Ill., 1978, pp. 173.
8. Staley, J.T., "Microstructure and Toughness of High Strength Aluminum Alloys", ASTM STP 605, 1975, pp. 71-85.
9. El-Soudani, S.M., and Pelloux, R., "Influence of Inclusion content on Fatigue crack propagation in Aluminum Alloys", Metallurgical Transactions V44, Feb., 1973, pp. 519-531.
10. Sanders, T.H. Jr., and Otto, W.L., "Microstructure and Fatigue Resistance of 7xxx P-M Aluminum Alloys", Journal Of Metals, V31 n8 1979, pp. F19-F20.
11. Polmear, I.J., "Aging Characteristics of Complex Al-Zn-Mg Alloys", Journal of Institute Of Metals, V89 Oct., 1960, pp. 51-59.

12. Wernick, J.H., "Structure And Properties of Some Intermediate Phases", in Physical Metallurgy, American Elsevier, N.Y., 1970, pp. 229-280.
13. Thackery, P.A. Jr., "Nature and Morphology of precipitates in Al-Zn-Mg Jour. Journal of Institute of Metals V96, 1968, pp. 228.
14. Sanders, T.H. Jr., and Starke, E.A. Jr., "The relationship Of Microstructure to Monotonic and Cyclic Straining of Two Age Hardening Aluminum Alloys", Metallurgical Transactions, V7A, n9, 1976, pp. 1407-1418.
15. DeIasi, R., and Alder, P.N., "Calorimetric Studies of 7000 series Aluminum Alloys: Matrix Precipitate Characterization of 7075", Metallurgical Transactions A, Vol.8, 1977, pp. 1177-1183.
16. Papazian, J.M., "Calorimetric Studies of Precipitation and Dissolution Kinetics In Aluminum Alloys 2219 And 7075", Metallurgical Transactions, Vol.13A, 1982, pp.761-769.
17. Fu-shing Lin, "Low Cycle Corrosion Fatigue Crack Propagation Of High Strength 7xxx Aluminum Alloys", Ph.D. Thesis, Georgia Institute of Technology, Atlanata, Ga., 1978, pp. 173.
18. A.C. Zettlemoyer(ed), Nucleation, E. Hornbogen, " Nucleation of precipitates in Defect Solid Solutions", Marcel Dekker, Inc., N.Y., 1969, pp. 309-378.
19. Starke, E.A., "The causes and Effects of "Denuded" or Precipitate Free zones at Grain Boundaries in Aluminum Base Alloys", Journal of Metals, Jan., 1970, pp. 54-63.
20. Shercliff, H.R., and Ashby, M.F., "A Process Model For Age Hardening Of Aluminum Alloys-I", Acta Metall. Mater, Vol.38, No 10, 1990, pp. 1789-1802.
21. Kenawy, M.A., Nagy, M.R., Sakr, M.S., and Mostafa, M.T., "The effect Of Precipitation on The Electrical Resistivity In Al-2.5 Wt% Cu", Phy. Stat. Sol., Vol.97A, N1, 1986, pp.K73-K78.
22. Hull, S., Messoloras, S., and Stewart, R.J., "Study Of θ' Precipitates In An Al-1.56 at% Cu Single Crystal Using Electrical Resistivity, small-angle neutron scattering and Hardness Measurements", Philosophical Magazine A, Vol.57, N2, 1988, pp.261-276.

23. Chihoski, R.A., "Conductivity-Hardness Reveal Heat Treat History Of Aluminum Alloys-Part I", Metal Progress, May 1983, pp. 27-32.
24. Natan, M., and Chihoski, R.A., "Relationship between Microstructure, Hardness and Electrical Conductivity of 2219 Aluminum", Journal Of Material Science, Vol.18, 1983, pp. 3288-3298.
25. Pettit, J., Renaud, P. and Violan, P., "Effect of Microstructure on Crack Growth in a High Strength Aluminum Alloy", Fracture and the Role of Microstructure, V2, EMAS, 1982, pp. 426-433.
26. Lindigkeit, J., Gysler, A., and Lutjering, G., "The effect of Microstructure on the Fatigue Crack Propagation Behavior of an Al-Zn-Mg-Cu Alloy", Metallurgical Transactions, V12A, 1981, pp. 1613-1619.
27. Carter, R.D., Lee, E.W., Starke, E.A.Jr., and Breebers, C.J., "The Effect of Microstructure and Environment on Fatigue Crack Closure of 7475 Through Thermomechanical Processing", Metallurgical Transactions, V15A, 1984, pp. 555-563.
28. Forsyth, P.J.E., and Bowen, A.W., "The Relationship Between Fatigue Crack Behavior and Microstructure in 7178 Aluminum Alloy", Int. J. Fatigue V3, N1, 1981, pp. 17-25.
29. Ramusat, G., and Vidal, G., "Influence D'un Surrevenu a 175°C Sur La Vitesse de Fissuration par Fatigue d'un Alliage d'Aluminum 7075", La Recherche Aerospatiale, Jan.-Feb. 1977, N1, pp. 63-66.
30. Wei, R.P., Gao, M., and Pao, P.S., "The Role of Magnesium in CF and SCC of 7xxx Series Aluminum Alloys", Scripta Metallurgical, V18, 1984, pp. 1195-1198.
31. Dubost, B., Bouvaist, J., Mace, R. and Charue, M.O., "7075-101-T73: Tough Plates and Forging with Improved Fatigue Strength for Airframe Applications", Aluminum Technology, V86, 1986, pp. 459-467.
32. Kelly, A., and Nicholson, R.B. "Precipitate Hardening ", Progress in Material Science, Vol 10, pp. 149-391. Pergamon Press, Oxford, 1954.
33. Silcock, J.M., Heal, T.J., and Hardy, H.K., "Structural Aging Characteristics of Ternary Aluminum-Copper Alloys with Cadmium, Indium or Tin", Journal of Institute of Metals V 84 Sept. 1955, pp. 23-31

34. Rosen, M., and Horowitz, E., Fick, S., Reno, C. and Mehrabian, R., "An Investigation of the Precipitation-hardening Process in Aluminum Alloys 2219 by Means Of Sound Wave and Ultrasonic Attenuation," *Material Science and Engineering*, V53, 1982, pp. 163-177.
35. Turnbull, D., "Kinetics of clustering in some Aluminum Alloys", *Acta Metallurgica* 8 (1960) pp. 277-295.
36. Hardy, H.K., and Heal, T.J.: *Progress in Metal Physics*, V.5, pp. 143-278, Pergamon Press, Oxford, 1954.
37. Hirano, K. and Iwasaki, H., "Calori- and Resistometric Analysis of Aging and Precipitation in Aluminum -Copper Alloys" *Japan Institute of Metals.*, 1964, Vol.5, n3 pp. 162-170.
38. Zahra, A.M., and Laffitte, M., "Precipitation after reversion in Al-Cu 4% Alloy", *Scripta Metallurgica* V8, 1974, pp. 165-168.
39. Hillel, A.J., Edward, J.T., and Wilkes, "Theory of resistivity and Hull Effect in Alloys During Guiner-Preston Zone Formation", *Philosophical Magazine* V32 n1, July 1975, pp. 189-209.
40. Park, B.K., Lutjering, G. and Weissmann, S., "Influence of precipitation structure on Fatigue Life for an Aluminum 3 Wt% Cu Alloy", *Zeitschrift fur Metallkunde*, V62, N10, 1971, pp. 721-726.
41. Hidayetoglu, T.K., Pica, P.N., and Haworth, W.L., "Aging Dependence of the Bauschinger Effect in Aluminum Alloy 2024", *Materials Science and Engineering*, V73, N1-2, 1985, pp. 65-76.
42. Thompson, D.S., and Levy, S.A., "Special processing of Al-Cu-Mg Aircraft Alloys", *Aluminum Alloys in the Aircraft Industry*, Turin, Italy, 1-2 Oct. 1976, pp. 95-103.
43. Lutjering, G. and Gysler, A., "Fatigue And Fracture Of Aluminum Alloys", *Aluminum Transformation Technology and Applications*, ASM, 1978. pp. 171-210.
44. Ostermann, F., "Improved Fatigue Resistance of Al-Zn-Mg-Cu (7075) Alloys Through Thermomechanical Processing", *Metallurgical Transactions*, V2, 1971, pp. 2897-2902.
45. Reimann, W.H., and Brisbane, A.W., "Improved Fracture Resistance of 7075 Through Thermomechanical Processing", *Eng. Fracture Mech.*, V5, 1973, pp.67-78.

46. Porter, Samuel, "Stress Intensity Factors Of Unsymmetric Edge Crack", M.sc thesis, 1983, pp.51-56.
47. Lebo, Michael and Grant, N.J., "Structure and Properties of a splat cooled 2024 Aluminum Alloy", Metallurgical Transactions, V5, 1974, pp. 1547-1554.
48. Sudarshan, T.S., Place, T.A., Louthan, M.R. Jr., and Mabie, H.H., "Torsional Fatigue Fracture of Aged Aluminum Alloy 2024 in Dry Argon", Microstructural Science v13, 1986, pp. 111-129.
49. Suresh, S., Vasudevan, A.K., and Bretz, P.E., "Mechanisms of slow Fatigue Crack Growth in High Strength Aluminum Alloys: Role of Microstructure and Environment", Metallurgical Transactions, V15A, 1984, pp. 369-379.